STRATIGRAPHY OF THE PALO DURO BASIN
- A STATUS REPORT

by

S. C. Ruppel, R. D. Conti, S. P. Dutton,
M. A. Fracasso, M. J. Herron, S. D. Hovorka,
D. A. Johns, A. Kolker

CAUTION

This report describes research carried out by staff members of the Bureau of Economic Geology that advances the feasibility of the Palo Duro Basin for isolation of high-level nuclear wastes. The report describes the progress and current status of research and tentative conclusions reached. Interpretations and conclusions are based on available data and state-of-the-art concepts, and hence, may be modified by more information and further application of the involved sciences.

Prepared for the
U.S. Department of Energy
Office of Nuclear Waste Isolation
under contract no. DE-AC-97-83WM46615

Bureau of Economic Geology
W.L. Fisher, Director
The University of Texas at Austin
University Station, P.O. Box X
Austin, Texas 78713

1984

TABLE OF CONTENTS

INTRODUCTION

Since the beginning of Bureau research into the Palo Duro Basin area in 1979, more than 150 geologic reports have been completed and published. Approximately 30 are currently in press. Because of continuing research in the area, however, a great deal of additional work still remains unpublished. This report is an update of ongoing, as yet unpublished research into the stratigraphy of the Palo Duro Basin (fig. 1).

Although investigations on some scale are being carried out on essentially all of the stratigraphic horizons in the Palo Duro Basin area (fig. 2), only those units which have recently been the focus of relatively concentrated research efforts are reported on herein. This necessarily includes those units being analyzed for hydrocarbon potential (Mississippian and Pennsylvanian Systems), those that are the focus of hydrologic studies (Permian Wolfcamp Series and Permo-Triassic Dockum Group and Dewey Lake Formation), and the proposed waste repository horizon (Permian San Andres Formation). Work on other stratigraphic units is lower priority and is being carried out peripherally. Table 1 indicates researchers responsible for contributions to this report and those who are continuing to study various stratigraphic units in the area.

MISSISSIPPIAN SYSTEM

(Ruppel)

Age and Depositional History

The Mississippian System of North America is subdivided into four time-stratigraphic units: Chester, Meramec, Osage, and Kinderhook (Dott, 1941; Cheney and others, 1945). Proper correlation of these units requires biostratigraphic or chronostratigraphic control. In the mid-continent region, however, especially in the subsurface where paleontologic data are generally lacking, these units have been extended primarily by lithologic correlation. Local biostratigraphic studies (Thompson and Goebel, 1969) have tended to confirm the time-

stratigraphic accuracy of these correlations and to suggest that Mississippian lithologies are synchronous throughout large areas of the mid-continent. A necessary corollary of this assumption is the idea that depositional conditions were relatively uniform during the Mississippian over widespread geographic areas. Biostratigraphic studies of the Palo Duro Basin based on conodonts, however, do not support this model.

The accepted stratigraphic subdivision of the Mississippian in the Palo Duro Basin is presented in figure 3. This is based on correlatable lithologies recognized throughout the Texas Panhandle and surrounding areas of Oklahoma and Kansas (Cunningham, 1969).

Conodonts have been recovered from cores taken in 4 wells in the Texas Panhandle area (fig. 4): one in the northern part of the Palo Duro Basin (Donley 3), one in the area between the Palo Duro and Hardeman Basins (Childress 10), and two in the Hardeman Basin (Hardeman 42 and 44). Specimens recovered from the upper part of the Chappel Formation in the Hardeman Basin (Hardeman 42 and 44) are representative of the Apatognathus scalenus - Cavusgnathus Zone of Collinson and others (1962, 1971) and of the Cavusgnathus Zone of Dutro and others (1979) and Sandburg (1979). This indicates at least a middle to late Meramecian age for these rocks, which is generally consistent with previous interpretations that have suggested that the Chappel contains an upper Meramec part and a lower Osage part (Mapel and others, 1979). However, the presence of these middle to late Meramecian conodonts near the base of the upper Chappel may indicate that the lower Chappel is younger than previously assumed.

The most complete suite of conodont samples was obtained in Childress County (fig. 4). Conodonts were recovered from 12 samples representing both the "Meramec" as well as the "Osage" (equivalent to the upper and lower parts of the Chappel in the Hardeman Basin). Conodonts obtained from the "Meramec" are essentially the same as those in the Hardeman Basin cores. The fauna recovered from the lower ("Osage") Mississippian in Childress County differs slightly (it contains Taphrognathus as well as Cavusgnathus) but nevertheless also implies a middle Meramecian age (Collinson and others, 1971; Dutro and others, 1979). This indicates that true Osage rocks are either totally absent in the area or represented by a very

2

thin layer (about 40 feet of Mississippian at the base of the Childress County well was not cored). Correlations of this well with those in the Hardeman Basin based both on lithologies and conodont faunas suggest that most of the Chappel is also of Meramecian age (fig. 5).

Because of erosion, only the lower ("Osage") part of the Mississippian section is present in northern Donley County. Conodont samples were taken from 36 feet (11 meters) of core taken in the upper part of the section (fig. 5). Conodont faunas obtained in well are significantly older than any of the others studied. They represent the Taphrognathus Zone of Dutro and others (1979) and Sandburg (1979). Because this zone spans the Osage-Meramec boundary, it is impossible to accurately date these rocks. However, the abundance of Taphrognathus favors a Meramec age (Collinson and others, 1971). Since nearly 200 feet (61 meters) of Mississippian section is present below the studied interval, it is quite likely that Osage rocks are present at this locality (fig. 5). In any case, the Mississippian rocks in the Donley County area are the oldest based on the conodont faunas.

The implications of the conodont biostratigraphic studies of the Mississippian are complex. The faunas clearly indicate that the earliest major Mississippian deposition in the area began in the northern part of the Palo Duro Basin (Donley County). Although minor deposition may have occurred to the east during the Osagean, most sediments were not formed until later during the Meramecian. Based on these relationships it might be concluded that the Palo Duro and Hardeman Basins were flooded (transgressed) progressively from north to south. This is consistent with thicknesses and lithologies of supposed early Mississippian rocks in the Anadarko Basin. As was the case through much of the Paleozoic, the Anadarko Basin was a site of relatively greater subsidence than surrounding areas. Therefore it would be expected that the first Mississippian sediments would be deposited in that area. The relatively old Mississippian deposits in Donley County may represent the southern margin of the Anadarko Basin during the Osage. Arguing against this north to south transgression, however, is the pattern of depositional environments inferred for the Mississippian in the area. Regional (Mapel and others, 1979) as well as local (Ruppel, 1983) lithologic studies indicate an eastwardly

3

deepening sequence of environments in the Texas Panhandle area. Biostratigraphic data presented herein, however, illustrate that the rocks upon which this environmental interpretation is based are probably Meramec in age. Thus, it may well be that Mississippian deposition in the Texas Panhandle was controlled by two distinct tectonic events. First, at the beginning of the Mississippian (Osage time) deposition was concentrated along the area of the Anadarko Basin. During this time most of the Palo Duro and Hardeman Basin area remained emergent or received only minor amounts of sediment. Later (in the Meramec), subsidence in the Hardeman Basin (and southward and eastward), possibly associated with the formation of the Ouachita geosyncline at about this time (Mapel and others, 1979) was responsible for the inundation of the remainder of the area.

PENNSYLVANIAN SYSTEM

(S. Dutton)

General

A significant number of new electric logs have been acquired by the project since the initial work was done on the stratigraphy of the Pennsylvanian section (Dutton, 1980). Data from the new logs were incorporated into the existing Pennsylvanian data base this year. During this process, correlations of all the older logs were re-evaluated, particularly in areas with new sample logs. There are now a sufficient number of sample logs to pick the top of the Strawn throughout the Palo Duro Basin. This horizon is now being used to subdivide the Pennsylvanian. This replaces the "lower 45%/upper 55%" subdivision. The lower Pennsylvanian interval extends from the top of the Mississippian to the top of the Strawn; the upper Pennsylvanian is from the top of the Strawn to the top of the Pennsylvanian (Table 5).

Maps were prepared with the new data for lower Pennsylvanian facies (fig. 6) and net carbonate (fig. 7), and upper Pennsylvanian facies (fig. 8) and net carbonate (fig. 9). The new subdivision of the Pennsylvanian did not change maps of the upper Pennsylvanian interval

4

significantly. However, the lower Pennsylvanian is now portrayed more accurately because areas with no strata from the lower Pennsylvanian interval (Bend and Strawn groups) are delineated. Using the old subdivision, if there were any Pennsylvanian strata present, 45% would be assigned to the lower Pennsylvanian. In some areas, particularly near the Amarillo Uplift and over the Matador Arch, this resulted in Canyon or Cisco strata being placed in the lower Pennsylvanian. Now these areas are shown as having no lower Pennsylvanian strata.

Lower Pennsylvanian strata probably are missing from areas near the uplifts because of nondeposition. However, it is possible that lower Pennsylvanian sediments were deposited, and subsequently eroded, before deposition of the upper Pennsylvanian.

Petrographic Studies

Limited core samples of granite wash from the Stone and Webster #1 J. Friemel well in Deaf Smith County were available for study. These samples are 1-inch plugs of lower Pennsylvanian granite wash that were used for porosity and permeability measurements. The grain size of the samples varies from granular, very coarse sandstone to sandy, pebble conglomerate. The samples are poorly to moderately sorted, with subangular grains. The framework grains are mainly quartz, feldspar, and micrographic granite fragments, so the sandstones are classified as arkoses (Folk, 1974). The abundant micrographic granite indicates that the source area was the Bravo Dome in Oldham County (Flawn, 1956). Quartz overgrowths, ankerite, and kaolinite cements are common, and they reduce porosity and permeability within the granite wash.

Porosity in samples of Deaf Smith granite wash was measured by porosimeter as 16.1 to 17.9 percent. Porosity measured in thin sections made from the same samples ranged from 12.0 to 17.5 percent. The difference probably is caused by microporosity within clay cements and elsewhere that cannot be seen in thin section but can be measured by a porosimeter. Porosity determinations in thin sections also tend to be lower than by porosimeter because the thickness of a thin section causes a petrographer to overemphasize grain volume at the expense of pore

5

space (Jonas and McBride, 1977). Permeability to water in these same samples was 21 md vertically and 54 to 420 md horizontally.

Oil Reservoirs

Numerous oil discoveries have been made recently in Pennsylvanian granite wash and carbonates (Table 2) in east-central Oldham and western Potter Counties (fig. 10). Granite wash is the most important reservoir facies, but no core from Oldham County granite wash was available for study. However, granite wash from the J. Friemel well in Deaf Smith County is probably similar to, although older than, the productive granite wash in Oldham County.

Calculations of oil-in-place indicate that the largest fields in Oldham County contained about 10 million bbl of oil initially (Table 2). The amount of oil that ultimately can be recovered is less. An estimated 1,560,000 bbl of oil are recoverable from Hryhor Field assuming a rather low, 17-percent recovery factor (Railroad Commission of Texas, 1982). Cumulative oil production from the 12 fields in this area was 6,078,283 bbl of oil by January 1, 1983 (Table 2).

Traps in the fields are simple or faulted anticlines (fig. 11). Manarte (Granite Wash, Upper) Field is formed by a combination structural and stratigraphic trap. Oil is trapped on the eastern side of the field by granite-wash pinch-out at the margin of a north-south trending channel (Railroad Commission of Texas, 1969). Oil is trapped on the other three sides of the field by a southwest-plunging anticline.

PERMIAN SYSTEM

Wolfcamp Series

Porosity Studies (Conti)

Handford and Fredericks (1980) and Dutton, Goldstein and Ruppel (1982) have presented interpretations of the Palo Duro Basin's sedimentary evolution during Wolfcampian time. The

Wolfcamp Series, which was recognized by Bassett and Bentley (1983) as a deep-basin brine aquifer within the Palo Duro Basin, lies beneath bedded Permian salt which is currently being studied for its ability to contain and isolate high-level nuclear-waste materials. Due to its stratigraphic position below the potential-host salt beds of the San Andres, the Wolfcamp is a potential hydrologic medium for transporting radionuclides, if they were to leak from overlying salt beds. "Failure of the containment of deeply buried radioactive waste, if it occurs, would most likely involve some transport of radionuclides by ground water. The prediction of future ground-water motion is therefore of prime importance" (Davis, 1980). Discernment of the distribution of porous zones is integral to the evaluation of the amount of movable water contained in the Wolfcamp, and ultimately to the estimating deep-brine travel times and frequency of aquifer flushing.

Porosity values are obtainable from a variety of individual petrophysical logs, either directly or through calculations, but for the best data resolution, crossplotting one response against another is generally recommended (Keys and Brown, 1973). Study of porosity distributions in the Wolfcamp deep-basin aquifer was initiated to attempt to discern the distribution of lithofacies, their effective porosities, and ultimately their collective influence on ground-water dynamics of the Palo Duro Basin.

Previous Studies

To date, studies of Wolfcamp subsurface stratigraphy within the Palo Duro Basin have relied almost entirely on correlations of electric logs (resistivity and self-potential curves), gamma logs, and sample logs (Handford and Fredericks, 1980; Handford, Dutton and Fredericks, 1981). Such studies have yielded more or less generalized indications of porosity and lithology distributions. In order to better understand the vertical and lateral variations in lithology and porosity, however, more-detailed quantitative determinations of permutations of these two parameters (viz., lithology and porosity) are required.

Predicting Porosity Distributions

Because carbonate grains tend to accumulate where they are generated, the texture of many carbonate rocks depends more on the size of the in situ skeletal-grain contributions than on components that were transported in from proximate and distant environments (Wilson, 1975). Such in situ accumulations yield primary porosity, the preservation of which is subject to post-depositional diagenetic alterations which ultimately enhance or reduce the size of the interstices formed during deposition. This, added to the fact that shallow-water carbonate depositional environments generally exhibit a high degree of lateral variability, increases the complexity of predicting porosity distributions within the predominantly carbonate rock sequences (Scholle, 1979) such as those of the Wolfcamp.

Another consideration which further complicates the prediction of porosity trends in shallow-water carbonates deals with their potentially variable water chemistry at the time of deposition. Not only might the chemistry of the pore fluids have varied due to temporal chemical anisotropies in the ambient waters of sedimentation, but they might also have varied as a result of vertical sedimentary accretion to sea level or above. Such an event would ultimately allow the introduction of meteoric fluids through the (chemically) metastable sediments, initiating penecontemporaneous alteration of primary porosity systems (Scholle, 1979).

Prediction of porosity distributions in shallow-water carbonates, such as those of the Wolfcamp, is therefore assisted by the utilization of data generated from analyzing specific suites of petrophysical responses. For this study, neutron-porosity and density-porosity logs were simultaneously analyzed, by crossplotting, to delineate Wolfcamp-strata porosity distributions. Crossplotting two porosity-log responses is a frequently used method of identifying lithology and making accurate porosity estimates (Burke, Schmidt and Campbell, 1969). The values read from neutron, density or sonic logs reflect lithology, fluid content and porosity, so that porosity values can be calculated in intervals of simple (i.e., monomineralic) lithology, if only one log is available and the lithology is known. However, for Wolfcamp lithologies, which

8

are often complex, noncorrelatable, and unpredictable in extent across the Palo Duro Basin, crossplotting was employed to ascertain complex lithologies and their corresponding porosities.

Average-Porosity Distributions

Brown Dolomite.--The Brown Dolomite, which is generally regarded as the top of the Wolfcamp (Dutton, Goldstein and Ruppel, 1982) in the Palo Duro Basin is characterized by being predominantly dolomite, and having relatively high porosity (as compared with the superjacent Wichita and subjacent Wolfcamp strata). Such a distinctive lithology and porosity signature allows for the easy delineation of this interval in lithology/porosity columns constructed (not included in this report) from analyses of neutron-density logs, thus facilitating analyses of porosity distribution (figs. 12-16).

Determining weighted-average porosities yielded average-porosity trends for the Brown Dolomite interval (fig. 17). Generally, the highest average porosities in the Brown Dolomite are found in the southeast and northwest areas of the basin along the Lower Wolfcampian shelf margin (Handford and Fredericks, 1980). In the southeastern part of the basin, the axis of highest-porosity is oriented north-northwest along the southeastern shelf margin, passing through Motley and Briscoe Counties. In the northwestern part of the basin the highly porous Brown Dolomite is found in north-central Deaf Smith County. The lowest average-porosity trend in the Brown Dolomite is found in the southern part of the basin, along the Matador Arch, in south-central Hale and southeastern Lamb Counties.

Wolfcamp Strata Subjacent to the Brown Dolomite.--Effective porosity within the Lower Permian Wolfcamp strata of the Palo Duro Basin is distributed throughout arkosic sands and granite-wash clastic sediments and non-stratal-dolomite and limestone carbonate sediments. Volumetrically, the carbonate rocks are of much greater significance than the coarse-grained clastic sediments. Noneffective porosity is generally significant, especially in the lower Wolfcamp strata along the shelf margin.

Vertical distributions of rock type and void-space systems were characterized in the lithology/porosity columns constructed from analyses of neutron-porosity and density-porosity

9

data. From such columns, net thicknesses of seven porosity ranges were determined and mapped (figs. 18-24).

Weighted-average-porosity determinations yield average-porosity trends for the Wolfcamp strata underlying the Brown Dolomite (fig. 25). Average-porosities were not determined for specific lithologies, but rather for the entire stratigraphic interval, between the bottom of the Brown Dolomite and the top of Pennsylvanian strata. The highest-average-porosity trend is found in the northern part of the basin, with the axis of highest porosity oriented east-southeast, and passing through Oldham, Deaf Smith, Randall and Armstrong Counties. The highest-average-porosity trends are generally associated with alternating clastic and carbonate sediments that were deposited in shelf-margin and back shelf environments during their basinward progradation.

The lowest-average-porosity manifestations, which are found along the east, west and south basin margins, are due mostly to the presence of interpreted shales and sandy shales which have assigned effective-porosity values of 0.00 and consequently, greatly reduced (calculated) average-porosity values. The shales and sandy shales found near or landward of the basin margins are probably associated with prodelta or interdeltaic, fine-grained clastic sedimentation.

Entire Wolfcamp Interval.--The average-porosity distributions for the entire Wolfcamp interval (fig. 26) vary very little from the average-porosity distributions of the Wolfcamp strata lying beneath the Brown Dolomite (fig. 25). Essentially, the highest and lowest average porosities are found, respectively, in the northern part of the basin and the eastern, western and southern parts of the basin, as explained above. The high-porosity and low-porosity areas are similarly distributed geographically (figs. 25 and 26) due to the relatively minor influence of the Brown Dolomite in affecting the average-porosity values for each well.

10

Stratigraphic Studies (Herron and Conti)

Wolfcampian/Pennsylvanian Boundary

The Wolfcampian/Pennsylvanian contact is difficult to pick in subsurface-stratigraphy studies of the Palo Duro Basin because of lateral facies changes, scarcity of paleontological data, and lack of a correlatable contact in surrounding regions. Variances in the conformability of the contact, which reflect concomitant (regional) tectonic events add to the difficulty. Unconformities at the Wolfcampian/Pennsylvanian contact have been recognized in West Texas, on the Central Basin Platform, in eastern New Mexico, in eastern Colorado and western Kansas (San Angelo Geological Society, 1958; Meyer, 1966; Maher, 1953), whereas the contact is conformable in the Anadarko Basin and Eastern Shelf areas of the Midland Basin (Rascoe, 1978; Galloway and Brown, 1972; Gupta, 1977). In the Palo Duro Basin, the contact is represented partly by unconformities or hiatuses, and partly by apparently continuous deposition. Angular unconformities which reflect tectonic activity have been identified in two areas of the southwest part of the basin and just south of the Amarillo Uplift in the northern part of the basin (fig. 27). There is also evidence which supports depositional hiatuses or unconformities not associated with tectonic features. Wolfcampian/Pennsylvanian unconformities occur principally in Bailey, southwestern Castro, southeastern Parmer, Lamb, Hale, and Donley Counties (fig. 27).

Due to the absence of a precise definition of the lower boundary of Permian sediments and lack of paleontological control, correlation of the Wolfcampian/Pennsylvanian conformable contact in the Palo Duro Basin is uncertain. In many areas within the alternating basinal shales and thin carbonate units, a physical stratigraphic marker is not apparent. Sample-log descriptions which contain paleontological data may be useful in bracketing the contact. However, the boundary must usually be projected from the shelf areas where it is better defined, and from areas near the basin-bounding uplifts where it is marked by an unconformity through Upper Pennsylvanian?/Lower Permian strata.

11

Figure 28 shows the lithologies on top of which the Upper Pennsylvanian boundary was placed. Figure 29 shows the lower Wolfcampian lithologies which immediately overlie the contact. Figures 28 and 29 show the lateral facies changes across the basin, and the paleotectonic and depositional-environment changes which took place during Late Pennsylvanian to Early Permian time. An increase in the rate of subsidence and subsequent marine transgression in the earliest Wolfcampian caused basin enlargement. This resulted in a marked increase in the areal extent of the basinal facies (viz., shale) and landward movement of both eastern and western shelf-margins.

Wolfcampian/Wichita Boundary

The Wolfcampian/Wichita boundary is picked on top of the Brown Dolomite in the Palo Duro Basin by using distinctive geophysical-log signatures. There is a characteristic kick in neutron- and density-porosity responses and a corresponding drop in resistivity at the contact (fig. 30). These responses are due to the fairly rapid downward change in lithology and porosity from low-porosity anhydrite and anhydritic dolomite in the Wichita Group to highly-porous dolomite in the upper Wolfcampian. In general, the contact is log-correlatable across the basin. However, the lack of anhydrite in the western and some of the southern parts of the basin (fig. 31) reduces the effectiveness of using the log signature to pick the Wolfcampian/Wichita contact.

Brown Dolomite

The Brown Dolomite in the Palo Duro Basin has been described as a "porous, coarsely-crystalline, buff dolomite" (Dutton and others, 1982). In the nearby Panhandle Field of Texas, Pippin (1970) described it as "a buff, cherty, sacchroidal dolomite." In this study it has been most useful to define the Brown Dolomite by log responses and derived lithology/porosity variations. The top of the Brown Dolomite is equivalent to the top of the Wolfcampian, and is indicated by the log signatures described above throughout most of the basin. In some areas, these log-signature characteristics can be correlated with a distinct (negative) SP shoulder (fig. 30). The Brown Dolomite is massive, cross-cutting apparent bedding and facies in some areas

12

and consequently has a base which is not well-defined. Generally, an upward change in dominant lithology from limestone to dolomite accompanied by an increase in porosity best indicates the base of the Brown Dolomite.

The Brown Dolomite is present throughout the Palo Duro Basin, except in the southern parts of Floyd, Lamb, and Hale Counties, and occurs all over the Texas and Oklahoma Panhandles except in the northwest Texas Panhandle in Dallam, Hartley and Sherman Counties, and in the westernmost Oklahoma Panhandle in Cimarron and western Texas Counties (fig. 32). It is a time-transgressive unit which appears to be equivalent to the Herington Dolomite to the north (over the Amarillo Uplift and northward); it is correlative with a shelf limestone and slope system to the south in the Midland Basin (Handford and others, 1981). Correlations to the east and west have not been worked out, to date.

A Brown Dolomite isopach map (fig. 33) which was prepared from sample-logs and geophysical logs shows trends of thickening where original carbonate buildups were concentrated, such as over vertically-aggraded shelf margins in Lamb and Castro Counties, and over prograded shelf-margin systems in Briscoe, western Armstrong and Potter Counties. Thinning trends occur in the central-basin area, where few carbonate sediments were deposited until very late Wolfcampian time. The unit also thins over the Amarillo Uplift and other structurally positive features that were buried during Wolfcampian deposition. Sedimentation from the still-exposed Sierra Grande Uplift precluded Brown Dolomite deposition in the northwest in the Dalhart Basin (western Hartley, Dallam, and northwest Sherman Counties.)

The Brown Dolomite consists primarily of porous carbonate rocks that are 50-100% dolomite. Chert replacement and anhydrite nodules or pore fillings also are commonly indicated in sample logs and core description, especially at the top of the unit.

Underlying the Brown Dolomite is an unnamed, typically limestone unit, within the Palo Duro Basin, which may be correlative with the Coleman Junction Limestone of the Eastern Shelf, North Central Texas. Over the Amarillo Uplift and the Bravo Dome, granite wash or Precambrian basement rocks underlie the Brown Dolomite. In parts of the central basin area,

13

the underlying lithology is mostly shale. In a few areas a lower dolomite underlies the unit, and is nearly indistinguishable from the Brown Dolomite. A generalized map of lithologies subjacent to the Brown Dolomite is shown in figure 34.

San Andres Formation

The San Andres Formation contains the thickest and most extensive evaporite units in the Palo Duro Basin. It is of special interest because the San Andres unit 4 halite is under consideration as a potential repository horizon.

The name San Andres Formation was carried from the Central Basin Platform to the Palo Duro Basin by Nicholson (1960). The San Andres Formation was divided into a lower informal unit with five numbered cycles and an upper unnumbered unit by Presley (1979a, 1979b, 1980a, 1980b, 1981a, 1981b). Presley prepared cross sections and isopachs of selected intervals. Bein and Land (1982) investigated the geochemistry of the San Andres Formation along a generally north-south transect through the Palo Duro Basin, including information from the first two test wells drilled by DOE. The bromide geochemistry of the San Andres unit 4 was studied by Handford (1981). Ruppel and Ramondetta (1982) reported on the salt purity of the formation. Carbonate beds in the San Andres Formation in the southern Palo Duro Basin and their relationships with oil reservoir rocks in the northern shelf of the Midland Basin have been investigated by Ramondetta (1981, 1982a) and Presley and Ramondetta (1981). San Andres facies in one core were documented by Hovorka (1983).

Cyclicity (Hovorka and Fracasso)

Four regional cross sections have been prepared through the San Andres Formation (figs. 35-39). Individual wells have been projected onto each transect line along perpendiculars to the transect which passes through the wells. Wells are distributed unevenly over the Texas Panhandle. Most are concentrated along the Amarillo Uplift and Matador Arch. Lower well density inside the basin (average well spacing along transect lines is 6.31 miles), however, has

14

still proven adequate to establish precise correlation within the San Andres across the entire basin. Gamma ray logs are particularly useful for regional correlation in this predominantly carbonate-evaporite sequence because relatively thin siliciclastic and dolomitic beds produce characteristic sharply defined peaks well above the gamma baseline. Available sample logs, borehole compensated sonic logs, and density logs have also been examined to help distinguish between lithologies.

An intraformational horizon--the "pi marker" (Dunlap, 1967; Ramondetta, 1982b, fig. 39)-- is used as a horizontal datum in the correlation sections. The pi-marker is a high, sharp gamma peak situated in the middle San Andres (new informal division, see below) that can be recognized throughout the Palo Duro Basin and some distance beyond (northwestern Midland Basin, northern Northwest Shelf of the Delaware Basin, Dalhart Basin, and northern Eastern Platform of the Midland Basin). The primary advantage of using an intraformational horizon as a datum in constructing regional cross sections is that it compensates for the effects of postdepositional structural deformation on the geometry of the preserved sequence, thus restoring original depositional stratigraphy and facilitating well-to-well correlation.

Sequences of continuous core representing most or all of the San Andres Formation have been recovered from eight stratigraphic test wells drilled by DOE in the Palo Duro Basin (fig. 35). Textural, petrographic and geochemical analyses of core allow interpretation of the sequence of depositional and diagenetic environments in the San Andres Formation. At least one cored well has been incorporated in each cross section.

Ideal Vertical Sequence

An idealized San Andres cycle, based on examination of continuous DOE core intervals, is an asymmetric carbonate-evaporite vertical sequence (fig. 40). A typical cycle is composed of (1) a basal anhydritic dark-colored mudstone (10 cm to 2 m thick), (2) skeletal limestone, (3) dolomite, (4) nodular anhydrite, (5) bedded anhydrite, and (6) halite. This sequence forms as the result of gradually increasing salinity of the depositing water body (fig. 40). Halite members are interrupted by thin red bed units that become more common and thicker in the

15

upper San Andres. These represent minor episodes of clastic progradation across the shelf that probably presage the major progradational event represented by the overlying Queen-Grayburg red bed formation. The occurrence of these units appears to be extrinsically controlled and is partially independent of the typical San Andres salinity-controlled cyclicity.

Dark Mudstone.--Transgressive sediments deposited at the beginning of San Andres cycles are thin (0.1 to 3 m thick) anhydritic and pyritic, black mudstone. These are regionally extensive throughout the Palo Duro Basin and occur between the halite at the top of one cycle and the base of the next cycle. The black mudstone units are intensely disrupted at the base by soft sediment faults and folds. The upper part of some mudstone beds exhibits primary structures, including ripple lamination and fissility, and may be organic-rich.

The black mudstones formed as water depth increased, providing better circulation. This caused salinity to decrease to normal or nearly normal marine. Anhydrite beds were not precipitated at this time, suggesting that the change occurred rapidly. The black mudstone is at least in part a residue of the insoluble components of the underlying halite, which was partially dissolved by interaction with normal or near-normal marine waters. Mudstone and anhydrite interbeds and disseminated impurities within the fabrics in the mudstone are a result of removal of the underlying halite by solution. The ripple lamination in the upper part of the mudstones resulted from reworking of the residue, and probably other fine terrigenous clastics transported by dust storms or other mechanisms. The dark color of the mudstone is due to reducing conditions within the sediment and is similar to the conditions in the overlying limestone, dolomite and anhydrite.

Carbonate.--The dominant carbonate in a complete cycle is limestone, comprising skeletal grainstone, packstone, and wackestone. Up to 15 m of skeletal carbonate is present in San Andres unit 4, in most cores, where it represents a prolonged episode of widespread, near-normal marine salinity. Although the predominant allochems are transported grains, the presence of some large brachiopod shells with intact spines is evidence that skeletal carbonate was produced locally in the northern Palo Duro Basin. The diverse faunal assemblage,

16

abundance of large burrows, and normal early diagenetic history of the carbonate, including neomorphism of aragonitic shells and possible bladed aragonitic cements is further evidence of near-normal marine conditions during limestone deposition.

Facies variations within the limestone are due to migration of high energy bar sediments across lower energy interbar sediments (fig. 41). Unlike other parts of the San Andres cycle, the limestone shows no evidence of increasing salinity during deposition. Limestone fabrics indicative of interaction with evaporites are interpreted to have formed during burial diagenesis, based on textural features and the apparent normal marine character of the sediment. These fabrics include partial or complete dolomitization and cementation of all pores throughout the limestone interval with halite. Aragonitic grains were replaced by halite, and aragonite, calcite and dolomite were replaced by anhydrite in the upper part of the carbonate intervals. The diagenetic fluids causing these replacements were probably provided when carbonate environments were replaced by sulfate and halite-saturated brine pools and higher salinity waters invaded the permeable carbonates. This pattern of diagenetic alteration of preexisting sediments by fluids derived from overlying parts of the cycle is repeated for other lithologies.

The laminated or rippled dolomite in the upper part of the carbonate unit shows evidence of deposition at the start of hypersaline conditions. Skeletal grains are sparse or absent. Rippled ooid or coated particle grainstone and carbonate mudstone are the most typical sediments. The predominant allochems are micritic intraclasts, pellets, and coated grains. Many grains have internal concentric lamination resembling that of ooids, except they have been compressed against each other and deformed. This indicates that they were soft at the time of deposition. The origin of these grains is unknown. Ostracods, bivalves, and gastropod shell fragments are rare. Both packstones and interbedded dolomicrite are ripple-laminated and sparsely burrowed. The low faunal diversity, dolomitization, and sparseness of burrows reflect the hypersaline depositional environment. Evidence of exposure and supratidal sedimentation is present locally especially near the top of unit 4 carbonate but is not common, suggesting that

17

abundance of large burrows, and normal early diagenetic history of the carbonate, including neomorphism of aragonitic shells and possible bladed aragonitic cements is further evidence of near-normal marine conditions during limestone deposition.

Facies variations within the limestone are due to migration of high energy bar sediments across lower energy interbar sediments (fig. 41). Unlike other parts of the San Andres cycle, the limestone shows no evidence of increasing salinity during deposition. Limestone fabrics indicative of interaction with evaporites are interpreted to have formed during burial diagenesis, based on textural features and the apparent normal marine character of the sediment. These fabrics include partial or complete dolomitization and cementation of all pores throughout the limestone interval with halite. Aragonitic grains were replaced by halite, and aragonite, calcite and dolomite were replaced by anhydrite in the upper part of the carbonate intervals. The diagenetic fluids causing these replacements were probably provided when carbonate environments were replaced by sulfate and halite-saturated brine pools and higher salinity waters invaded the permeable carbonates. This pattern of diagenetic alteration of preexisting sediments by fluids derived from overlying parts of the cycle is repeated for other lithologies.

The laminated or rippled dolomite in the upper part of the carbonate unit shows evidence of deposition at the start of hypersaline conditions. Skeletal grains are sparse or absent. Rippled ooid or coated particle grainstone and carbonate mudstone are the most typical sediments. The predominant allochems are micritic intraclasts, pellets, and coated grains. Many grains have internal concentric lamination resembling that of ooids, except they have been compressed against each other and deformed. This indicates that they were soft at the time of deposition. The origin of these grains is unknown. Ostracods, bivalves, and gastropod shell fragments are rare. Both packstones and interbedded dolomicrite are ripple-laminated and sparsely burrowed. The low faunal diversity, dolomitization, and sparseness of burrows reflect the hypersaline depositional environment. Evidence of exposure and supratidal sedimentation is present locally especially near the top of unit 4 carbonate but is not common, suggesting that

17

the depositional environment was an extremely broad, shallow, and mostly subaqueous hyper-saline marine shelf. A small amount of siliciclastic silt within dolomite may have been wind-borne from adjacent land areas into the hypersaline marine environment.

Anhydrite.--The anhydrite part of the cycle displays a well developed vertical sequence, including from base to top: (1) anhydrite nodules in dolomite matrix, (2) nodular mosaic anhydrite, (3) laminated anhydrite with or without pseudomorphs after bottom-nucleated gypsum crystal; and (4) anhydrite-halite transition. The contact between anhydrite and dolomite is gradational over a few tens of centimeters consisting of anhydrite nodules in dolomite mudstone. The relationship between the dolomite and anhydrite is most visible where the dolomite is well laminated. It appears to be replacement of dolomite mud by anhydrite, followed by compaction of the dolomite mud around the nodules. Displacive growth of anhydrite nodules may have occurred but has not yet been documented in San Andres anhydrite.

Nodular mosaic anhydrite with and without inter-nodular dolomite makes up the lower part of the anhydrite unit. Nodular anhydrite and nodular mosaic anhydrite have been considered textures characteristic of sabkhas, based on modern Persian Gulf examples. In the Persian Gulf, sulfate nodules are formed within subaerially exposed sediment when marine and terrestrially-derived waters reach anhydrite saturation due to evaporation. However, nodular anhydrite has been observed in numerous other environments, including laminated, deep-water sediments (Dean and others, 1975). Nodular textures also result from metamorphism of secondary sulfates (Schreiber and others, 1982). Some San Andres nodular anhydrite-carbonate mixtures may have been formed in sabkha-like subaerial environments, especially where they overlie possible supratidal carbonates. However, most of the nodular anhydrite is interpreted as the result of diagenetic remobilization of subaqueously-deposited laminae of anhydrite and dolomite. Evidence for a subaqueous brine pool origin for most of the San Andres nodular mosaic anhydrite includes: (1) absence of the typical sabkha cycle (Shearman, 1971), (2) typical position of the nodular anhydrite overlying apparently subaqueously deposited carbonate and beneath subaqueously deposited laminated anhydrite, (3) common gradation between nodular and

18

laminated fabrics by occurrence of deformed and altered laminae and pseudomorphs after gypsum crystals within poorly formed nodular anhydrite, and (4) occurrence of poorly formed anhydrite pseudomorphs after bottom nucleated gypsum crystals in dolomite.

Overlying the nodular anhydrite is laminated anhydrite with pseudomorphs of halite and, less commonly, anhydrite after vertically oriented gypsum crystals. Gypsum formed single or twinned crystals exhibiting growth bands and sediment laminae entrapped during crystal growth. Hardie and Eugster (1971) and Schreiber and Kinsman (1975) have described similar vertically oriented gypsum and interpreted it as indicating growth in a shallow pond environment. The absence of truncation surfaces across the crystals suggests that the pond was deep enough so that the significant episodes of exposure did not occur. Large gypsum crystals in the San Andres have been replaced by halite, and fine gypsum sediment between crystals has been replaced by anhydrite.

At the top of the anhydrite unit is a transition to halite. The transition interval is a mixture of halite in anhydrite and, in some cases, contains a minor amount of red siliciclastic mudstone. The textures in this interval are complex and variable, including contorted beds, coarse, randomly oriented blades of anhydrite in halite cement, and partially destroyed pseudomorphs after gypsum. These textures reflect diagenetic alteration as geochemical conditions alternated between gypsum and halite saturation. In some cycles the first episodes of subaerial exposure, typical of the bedded halite unit, occurred during this transition and produced more complex diagenetic textures.

The main distinction between nodular and bedded anhydrite may be differences in timing of the influx of more saline diagenetic fluids (fig. 42). Nodular anhydrite underlies bedded anhydrite and therefore underwent initial diagenesis in fluids derived from gypsum-precipitating ponds. Nodular textures also have been observed in the upper few centimeters of bedded anhydrite beneath dolomite beds or black mudstone insoluble residue, indicating that formation of nodular fabrics can occur under the influence of lower salinity normal marine to carbonate saturated waters. Good preservation of fabrics, including pseudomorphs after gypsum crystals,

19

appears to be associated with a stage of diagenesis in halite saturated waters. This is shown by the replacement of large gypsum crystals by halite. However, the uppermost anhydrite bed in the cycle, which was subjected to halite-saturated waters shortly after deposition, has poorly preserved fabrics. The optimum conditions for preservation of primary fabrics, based on observed location in the cycle, appear to be an initial episode of diagenesis beneath the gypsum-precipitating brine pool followed, after burial of 1-3 meters, by introduction of waters derived from a halite-saturated brine pool. Textural evidence suggests that the first phase of diagenesis dehydrated the initial gypsum sand or mud matrix around the large gypsum crystals to anhydrite, but the centers of the large crystals did not have time to react. These remained gypsum until halite saturation was reached in the overlying water body and were then replaced by halite. The preservation of the fine laminae that formed along gypsum-crystal growth surfaces within the poikilotopic halite is evidence that halite replaced gypsum without formation of void space. The uppermost anhydrite was immersed in halite saturated brine before much dehydration of gypsum occurred. Therefore, dehydration of gypsum and replacement of gypsum by halite occurred simultaneously. Some primary fabrics are preserved by anhydrite rims, whereas others were too completely altered by halite replacement to be recognizable. Intermittent subaerial exposure accompanied by accumulation of clastic mudstone also disrupted fabrics in the uppermost anhydrite.

In a few sites no halite is present and anhydrite forms well preserved pseudomorphs after gypsum, usually small gypsum blades. The difference between the conditions that formed this fabric and the conditions that formed nodular mosaic fabric is not yet understood.

Halite.--Bedded halite containing interbedded anhydrite and mudstone and disseminated impurities forms the upper part of each cycle. Complex textures in halite result from its high solubility and reactivity during early diagenesis. Many textures in halite were formed during deposition as crusts of crystals on the floor of extensive, shallow brine pools. Fabrics in halite interpreted to result from brine-pool precipitation include: (1) vertically elongated halite crystals with relict growth surfaces defined by variations in abundance of minute fluid

20

inclusions (chevron zoning), (2) vertically elongated halite crystals lacking zoned fluid inclusions, and (3) halite bedding defined by color changes or by interbeds of mudstone or anhydrite.

Vertically-oriented halite crystals and crystals with upward-pointing chevron-shaped zones of fluid inclusions are abundant. Similar features have been observed in modern sediments forming by bottom-nucleated growth in shallow brine pools (Arthurton, 1973).

The regular zonation of fluid inclusions in the chevron halite of the San Andres Formation is interpreted by Roedder (1982) as the result of diurnal variation in the rate of brine evaporation in extremely shallow (less than a few feet deep) brine pools. Halite with abundant chevrons is typically white because of the fluid inclusions and presence of anhydrite as the dominant impurity. Halite with vertical crystals but lacking abundant chevron structures is typically dark colored. This is caused by the presence of minor amounts of reduced gray clay and/or traces of organic materials as well as anhydrite. It may also represent slower halite precipitation in slightly deeper water.

Horizontal red, white, and black bands in halite formed as a result of introduction of impurities such as organic material, air- or water-borne dust or anhydrite into the brine pool. Thin seams of anhydrite formed during brief pauses in halite precipitation, resulting from periodic dilution of the water within the brine pool by the introduction of meteoric? and/or marine-derived water concentrated only to gypsum saturation. The underlying halite was corroded and pitted on a centimeter scale, and chevron fabrics were truncated. Gypsum was precipitated, and as evaporation continued halite saturation was reached and halite precipitation resumed. The effect of continued input of marine-derived brine is that the Br concentration in halite with chevron fabrics is 55 to 82 ppm (average 70 ppm) (Fisher and Hovorka, in press), which is about the composition of the first halite precipitated from marine-derived brine.

Other halite brine-pool fabrics described by Arthurton (1973), such as accumulations of hoppers and rafts that formed at the water/air interface, may have been present. However, all trace of them has been lost by either recrystallization or dissolution. The presence of detrital

21

halite ooids and mud has been documented in modern environments (Weiler and others, 1974) and might occur in environments were brine-pool halite and transported grains of other sorts exist. Few examples of possible detrital halite have been observed, however. The brine pools intermittently dried up and became exposed halite flats during interruptions of the marine-derived brine influx. Microenvironments on the dry flat were subjected to either further evaporative concentration of the brine, or to partial dissolution and recrystallization of halite in contact with fresh water. This produced highly variable Br concentrations (28 to 163 ppm) within the affected halite (Fisher and Hovorka, in press). Low-salinity water penetrating the salt along grain boundaries and vertical fractures dissolved karstic pits and solution pipes and favored recrystallization of halite, destroying primary fabrics. Cessation of halite growth permitted accumulation of layers and cavity-fillings of red terrigenous mudstone which was transported onto the salt surface by eolian dust storms and sheetwash processes. Halite that fills shrinkage cracks in these mudstone layers has Br concentrations as high as 342 ppm, recording precipitation from the most highly concentrated brines. Repeated episodes of wetting and halite dissolution, followed by drying and precipitation of halite as cement and as displacive cubic or skeletal crystals destroyed bedding both in primary halite and in terrigenous mudstone. The resulting fabric retains little primary structure and is described as chaotic mudstone-halite.

The halite part of the cycle does not show well-developed vertical sequence in textures or geochemical profile, but is composed of 1- to 4-m thick sequences of alternating zones of clean halite with preserved primary fabrics, and zones of abundant mudstone interbeds and chaotic mudstone-halite fabrics.

Terrigenous Clastic Red Beds.--Mudstone, siltstone and very fine sandstone red beds 0.5 to 2.5 m thick occur at various intervals in the San Andres Formation. The distinction between these beds and the thinner red mudstone beds that are abundant in the halite is arbitrary. Thicker red beds represent more significant pulses of clastics into the evaporite environment and are recognizable on geophysical logs so that they can be correlated regionally. These beds

22

display ripple lamination, claystone drapes, and in some intervals, sorted coarse sand-sized clay rip-up clasts. Fine sandstone or siltstone-filled casts of halite crystals are abundant in some intervals. Anhydrite nodules and displacive halite cubes and skeletal crystals are abundant. Soft-sediment microfaulting is abundant in some units. The color is usually red-brown, due to oxidized iron stains in clay, and in clay coats on sand grains. Some of the sandier red beds, such as the "pi marker," are partly reduced beneath anhydrite or carbonate beds. The resulting light-gray colors are quite different from the dark, pyritic, anhydritic mudstones at the base of cycles. The composition and sedimentary structures of the red beds in the San Andres Formation are quite similar to the thicker red bed units of the adjacent Glorieta and Queen-Grayburg Formations. These are interpreted as events of clastic progradation across the evaporite shelf. Red beds are most common within the halite part of the cycle although they may occur elsewhere in the cycle. In instances where red beds were deposited at or near the top of a cycle, the character of the black mudstone at the base of the next cycle is partially or completely imprinted on the red bed, which has become included in the insoluble residue. In such cases it is difficult to separate the sediments deposited in each setting.

Variation From The Ideal Cycle

Variations from the ideal cyclic facies pattern can be traced in individual cycles in the Palo Duro Basin. Two kinds of information can be obtained from these variations. Comparison of successive cycles in one area provides information on the temporal evolution of cyclic style. Tracing variations of a single cycle across the basin provides information about depositional environments and controls on sedimentation.

Cycles in the San Andres Formation may differ from the idealized cycle in four ways: (1) the initial transgression may not bring normal marine water into a given area, so the lower units of the ideal cycle may not be deposited. Therefore, the cycle may begin with dolomite, nodular anhydrite or bedded anhydrite above a thin residue, (2) the cycle may be truncated by a transgression before halite deposition had been reached, causing the upper units of the ideal cycle to be missing, (3) the halite at the top of the cycle may be completely removed during the

23

transcription initiating the next cycle, or (4) the cycle may be interrupted by introduction of clastics.

Correlation Of Cycles

Cycles in the San Andres Formation comprise a diverse suite of lithologies including siliciclastic, carbonate and evaporite facies, as described in detail above. These lithofacies exhibit distinctive geophysical log characters (Handford, 1980; McGillis, 1980; Presley, 1981b; Presley and Ramondetta, 1981; Ramondetta and Merritt, 1982; Ruppel and Ramondetta, 1982) and individual cycles can be correlated with confidence using gamma ray logs. Other geophysical, caliper and sample logs are also used to help discriminate lithologies.

The key to the recognition of cyclicity and correlation of the San Andres using gamma ray logs is the identification of the predominantly siliciclastic insoluble residue that defines the base of each cycle. Insoluble residues that define the bases of the complete, relatively thick cycles of the lower San Andres (units 2, 3 and 4) produce characteristic asymmetric signatures on gamma ray logs (fig. 40). The log pattern displays, from base-to-top: a high basal peak (= siliciclastic insoluble residue) sharply set off from the baseline below, topped by a gradual shift back toward the baseline.

The insoluble residue-carbonate couplets at the bases of the thin cycles that are characteristic of the middle and upper San Andres (combined thickness range approximately (0.6-6 m) produce a single sharp gamma peak which cannot be differentiated from the sharp gamma peaks produced by terrigenous red beds. The distinction between such abbreviated cycle bases and terrigenous red beds on a regional scale requires their identification in core and extrapolation to correlative gamma peaks in other wells.

Four cross sections including well logs prepared through the San Andres Formation across the Palo Duro Basin and into adjacent areas show the vertical repetition and lateral extent of cycles (fig. 35-39). The sharp peaks on gamma ray logs that correspond to the bases of cycles can be traced on geophysical logs over the entire present structural limits of the Palo Duro Basin over areas of approximately 16,000 to 26,000 km^2. Some of these base-of-cycle facies

24

are less than 1 m thick, at or below the lower limit of consistent geophysical log resolution. Subtle variations in the sequence of salinity controlled facies that are below the level of resolution of geophysical logs can also be correlated between cores across the northern Palo Duro Basin.

Extension of San Andres Formation cross sections from the Palo Duro Basin north into the Dalhart Basin and south onto the Northern Shelf of the Midland Basin (figs. 36, 37) suggests several extrabasinal correlations. The lower San Andres unit 4 carbonate equivalent to the south is the Yellowhouse Dolomite on the Northern Shelf of the Midland Basin, as noted by Ramondetta (1982). To the north, a siliciclastic unit occurs sandwiched between the San Andres unit 4 carbonate and lowest unit 5 anhydrite correlatives in the Dalhart and Anadarko Basins. This has been described by some workers as the Flowerpot shale (Jordan and Vosburg, 1963). Since the Flowerpot Formation north of the Amarillo Uplift is directly overlain by the Blaine Formation, the Blaine may be correlative with the middle San Andres and unit 5 of the lower San Andres (and possibly the upper San Andres) Formation in the Palo Duro Basin. The Flowerpot Formation would therefore be equivalent to unit 4 of the lower San Andres in the Palo Duro Basin, and the underlying units 2 and 3 as far north as they can be recognized. The transgression at the base of lower San Andres unit 4 is unquestionably the event of greatest magnitude that occurred during deposition of the San Andres sequence. Unit 4 is the thickest individual cycle in the central area of the Palo Duro Basin, and extends further laterally than the other cycles of the lower San Andres. The distribution of the lower units 2 and 3 is largely confined to the existing structurally defined limits of the Palo Duro Basin. Each appears to have been subtly influenced by the Amarillo Uplift belt to the north, and both lose their definition eastward on geophysical logs approaching the outcrop belt of the Blaine Formation (figs. 38, 39). The unit 4 siliciclastic-carbonate-anhydrite basal unit, however, continues north across the Amarillo Uplift and appears to extend east into the Blaine Formation outcrop belt, where it is probably correlative with one of the named Blaine dolomite members.

Styles Of Cyclicity

Regional continuity of cycle bases and systematic differences in the vertical distribution of completeness and thickness of cycles permit the recognition of three discrete genetic packages in the San Andres Formation within the present structural limits of the Palo Duro Basin. The San Andres Formation in the Palo Duro Basin is accordingly divided into informal lower, middle and upper units (fig. 43). The lower San Andres corresponds to the lower San Andres of previous workers, and includes the previously designated units 2-5 (figs. 36-39, 43). These cycles possess a complete vertical facies sequence from the basal insoluble residue to the upper halite. Units 2, 3 and 4 are, in core from Swisher County, the most complete cycles and are characterized by a thick burrowed normal marine limestone in their lower part and a well formed halite section in the upper part. Each unit can be considered a single genetic sequence exhibiting a simple pattern of increasing salinity: mudstone insoluble residue, limestone, dolomite, anhydrite, and halite. Examination of core allows the identification of a smaller scale salinity fluctuation during the carbonate deposition of units 3 and 4. This is expressed as lower and upper regressive (salinity increasing) sequences in cores near the structural basin center (Swisher, Randall and Deaf Smith Counties). The lower sequence culminates in anhydrite, whereas the upper sequence continues on through anhydrite into the thick halite of the upper part of the cycle. In unit 4, the carbonate of the lower regressive sequence is thin and dolomitic. Textural evidence indicates that it was deposited under hypersaline conditions that were terminated shortly after the time of gypsum saturation.by transgression of the normal marine water, initiating the upper sequence (fig. 41). The thicknesses and inferred salinities of the lower and upper regressive sequences of unit 3 are similar to each other in most cores. Unit 2 was only cored once (DOE-Gruy Federal #1 Grabbe) and appears to represent a simple, single cycle.

Unit 1 of the lower San Andres Formation, identified by Presley (1979a, figs. 27 and 29; 1980, fig. 9; 1981a, fig. 21; Presley and Ramondetta, 1981, fig. 40) is best expressed on geophysical logs near the southern margin of the Palo Duro Basin. It cannot be differentiated

26

from the Glorieta Formation style of alternation of red beds and halite in the northern part of the basin. It probably represents a minor transgression whose influence did not extend far enough north in the basin to produce a recognizable facies change in available cores.

The composite nature of the lower San Andres unit 5 is apparent throughout the northern Palo Duro Basin (fig. 44). The character of this unit is transitional between the cycles of the lower and middle San Andres genetic sequences. The thick halite bed at the top of the unit is like those of units 2, 3, and 4, whereas the composite nature of the lower non-salt facies of the unit is similar to those of the middle San Andres interval. Unit 5 is a composite of four or five incomplete cycles: an initial transgression lowered the salinity only to anhydrite saturation and produced a thin basal residue, which is often not evident on geophysical logs. This sequence was then truncated by a transgression which deposited ripple laminated dolomite in Deaf Smith County, and nodular and bedded anhydrite with halite pseudomorphs after gypsum throughout the area. This was truncated in turn by a third transgression which wavered between dolomite and nodular anhydrite deposition before producing bedded anhydrite with pseudomorphs after gypsum and finally halite. The lower two cycles probably deposited some halite which was removed in the western part of the basin by each successive transgression. Evidence for the former presence of halite is: (1) the presence of fabric similar to that characteristic of the transition between the anhydrite and overlying halite incomplete cycles, (2) the influence of halite-saturated brines on the diagenesis of the anhydrite, notably the halite pseudomorphs after gypsum, and (3) the presence of black anhydritic mudstone insoluble residue.

Cycles of the lower San Andres genetic sequence are relatively thick (units 2-5 together comprise approximately just over half of the total thickness of the San Andres in the basin center). The existence of relatively thick carbonates at the bases of these cycles implies prolonged episodes of open circulation and near-normal marine salinity at moderate water depths (several meters?). Such circumstances might be most likely to develop as carbonate production kept pace with basin subsidence during transgressive events.

The middle San Andres unit corresponds roughly to the largely anhydritic lower half of the upper San Andres recognized by previous workers (figs. 36-39, 43). Cycles of the middle San Andres are relatively thin and incomplete, compared to those of the lower San Andres. Halite is not preserved, but its former existence is inferred from the insoluble residues that define the bases of the abbreviated vertical cyclic facies sequences. The lower and middle San Andres genetic units exhibit a common fundamental cyclic pattern of vertical facies sequences, if the former existence of halite in the middle unit is assumed (fig. 45). The thin, abbreviated cycles of the middle San Andres therefore suggest a change in the tempo, rather than the mode of cyclic depositional style. This change in tempo may have been caused by a lowering of basin subsidence rate, increased frequency of eustatic sea level change, or both, as explained below.

The much thinner carbonates of the middle San Andres must have been deposited over shorter time spans than the thick carbonates of the lower San Andres, assuming that these equivalent facies accumulated at similar rates. This implies that conditions of open circulation and near-normal marine salinity were significantly shorter for the middle San Andres sequence. An increased frequency of eustatic sea level change in the middle San Andres would have shortened transgressive intervals of near-normal marine salinity, without requiring a change in regional basin subsidence rate from that of the lower San Andres. Alternatively, a regional decrease in basin subsidence rate during the middle San Andres interval could have produced the abbreviated cycles, without requiring a change in the frequency of eustatic sea level fluctuation from that of the lower San Andres. If the basin subsidence rate was less than the rate of carbonate production during normal-marine transgressive events, the seafloor would rapidly aggrade, effectively restricting circulation and promoting evaporite deposition. High carbonate production in a regime of low basin subsidence rate is thus a self-limiting process, producing a relatively thin carbonate unit before the onset of evaporite deposition. If the basin subsidence rate remained less than the rate of subsequent evaporite sedimentation, the evaporite facies presumably would also rapidly aggrade to its upper limit, at sea level. A thin halite upper unit would have been particularly susceptible to complete dissolution during the transgressive, near-

28

normal marine phase initiating the next cycle. In summary, the change in tempo of cyclicity that produced the thin abbreviated cycles of the middle San Andres could have been effected by an increased frequency of eustatic sea level change and/or a regional decrease in basin subsidence rate, both relative to conditions that produced the lower San Andres sequence.

The upper San Andres genetic sequence corresponds roughly to the halite-bearing top half of the upper San Andres division recognized by previous workers above the pi-marker bed (figs. 36-39, 43). Cycles of the upper San Andres are characterized by thin basal carbonate-anhydrite units very similar to those of the middle San Andres sequence, yet halite upper units are also preserved. Moreover, prominent, relatively thick red beds are interspersed throughout the upper San Andres interval (fig. 46). The upper 50 m of the upper San Andres contains no black mudstone, carbonate or anhydrite within the halite and red beds, so cycles are not identifiable. Again, the fundamental mode of cyclicity appears to be the same as that of the lower and middle San Andres sequences, but the tempo differs from both. A pronounced asymmetry of eustatic sea-level fluctuations relative to the lower and middle San Andres, superimposed on a relatively constant regional basin subsidence rate, might produce such cycles. A rapid transgressive pulse followed by a prolonged regressive phase would produce a cycle with thin basal non-salt units and a relatively thick halite upper unit, providing the basin subsidence rate was high enough to preserve them. Alternatively, fluctuating regional basin subsidence rates relative to those of the lower and middle San Andres, superimposed on symmetric eustatic changes in sea level, could produce the same effect. A basin subsidence rate which is slow relative to the rate of carbonate production during transgression would result in rapid vertical aggradation of thin basal carbonates, causing restricted circulation and promoting evaporite deposition. A rise in basin subsidence rate during the phase of regression and evaporite deposition could preserve relatively thick halite facies overlying relatively thin carbonate facies. However, fluctuating basin subsidence rates alone or even in combination with asymmetric eustatic changes in sea level are unlikely to have produced the upper San Andres sequence. Both circumstances require the coupling of low basin subsidence rate with

29

transgression, and high basin subsidence rate with regression. This seems unlikely to produce a repetitive sequence because of the presumed independence of these parameters.

The marked increase in thickness and frequency of red beds in the upper San Andres interval appears to be genetically unrelated to San Andres cyclicity. These clastic interbeds are lithologically very similar to the overlying Queen-Grayburg red bed sequence and are probably each minor pulses that presage the major Queen-Grayburg progradation. This clastic influx may represent a reactivation of tectonism in the source area, or a regional change of continental clastic dispersal patterns.

Lateral Facies Relationships And Depositional Systems

Lateral facies relationships in the San Andres Formation can be studied both within and between lithofacies, and at regional and local scales. Each perspective contributes to our understanding of different facets of the San Andres depositional system--an environmental complex with apparently no close modern analog.

Regional-scale lateral lithofacies changes within cycles of the San Andres Formation were largely controlled by lateral salinity gradients that developed across the broad depositional shelf during the regressive phase of each cycle. Within-cycle lateral facies changes from halite to anhydrite are evident along the southern margin of the Palo Duro Basin, just north of the Matador Arch (figs. 36, 37; Presley and Ramondetta, 1981, fig. 40). This large-scale facies change, seen in nearly all cycles, presumably reflects decreasing salinity southward in the Palo Duro Basin caused by the influx of normal marine water from the Midland Basin. Analysis of these facies changes caused by salinity gradients across the shelf are based on geophysical logs. Textural details of the nature of these changes are not available because of the lack of core data. The DOE San Andres Formation cores are in the northern part of the Palo Duro Basin and patterns of facies changes due to north-south dip-oriented salinity gradients are not evident in this region. Textural evidence pertaining to subtle differences in facies shows that sedimentary conditions were quite similar over areas spanned by available cores.

30

Tongues of terrigenous red beds increase in frequency and thickness to the north in the upper San Andres sequence, reflecting both greater proximity to the continental source area and early pulses of Queen-Grayburg sedimentation. These red beds appear to be genetically unrelated to the typical San Andres cyclic facies sequence, and their occurrence is probably extrinsically controlled. Since each red bed unit may be viewed as a virtually isochronous event independent of cyclicity, the relation of individual red beds to underlying cyclic facies allows us to evaluate the lateral and temporal distributions of the evaporite facies tracts.

The "pi-marker" at the base of the upper San Andres genetic sequence is the most regionally persistent red bed unit in the San Andres Formation and is recognizable over the entire Palo Duro Basin area. It consistently overlies an anhydrite sequence, which is visible in all cored wells and is recognizable on all examined geophysical logs. This relation shows that similar depositional conditions existed across the entire basin at that time. Within our limits of resolution, single evaporite lithofacies units appear to be virtually isochronous and replace each other in vertical, rather than lateral succession. This suggests that during the regressive phase of each cycle, environmental changes, mainly salinity, occurred nearly synchronously across the entire basin. Subtle differences between bedded anhydrite in the DOE-Stone & Webster #1 Detten core, nodular anhydrite in the DOE-Stone & Webster G. Friemel and DOE-Stone & Webster Harman cores, and dolomitic laminated anhydrite in the DOE-Stone & Webster Zeeck core beneath the pi-marker record local variations (fig. 45). These variations are attributed to temporary local environmental conditions rather than to control of the facies tract by a regional salinity gradient, because the pattern is different in each cycle. The thin cycle above the pi-marker is another example. It begins with anhydrite deposition but records an increasing normal marine influence so that dolomite was produced before regression began. The dolomite indicative of maximum transgression occurs in all wells, but varies in thickness, texture, and amount of burrowing. In the Detten core the dolomite is grainstone/packstone and is thick and burrowed; in the G. Friemel core it is a thin grainstone/mudstone couplet; in the Harman and Zeeck cores it is ripple-laminated dolomite mudstone/packstone with nodular anhydrite. The

31

maximum transgression can be interpreted as essentially a time line. The differences in sedimentary conditions at each well are again interpreted as due to temporary local conditions, and are not consistent in vertical pattern. For example, among the cored wells the Detten core showed the influence of highest salinity in the cycle below the pi-marker, yet records the apparent lowest salinity at maximum transgression in the cycle above the pi-marker.

Although such detailed studies of variation within lithofacies units cannot be traced outside of the area of core control, the lateral continuity of these lithofacies is apparent throughout the Palo Duro Basin.

The basin-wide lateral continuity of individual cyclic lithofacies has been demonstrated based on geophysical log correlation (figs. 36-39). Textural evidence for corresponding lithofacies, provided by core, documents broadly uniform, predominantly subaqueous deposition. these complementary lines of evidence both pertain to the depositional systems complex of the San Andres Formation. The depositional surface at the start of each cycle must have been an extremely broad shelf with negligible topographic relief. The cyclic lithofacies are largely subaqueous sediments, deposited in a very shallow yet regionally contiguous water body. With few exceptions, most of the evidence for intermittent subaerial exposure occurs in the halite facies deposited in the late regressive phase of each cycle. The apparent isochroneity of laterally extensive cyclic lithofacies units suggests rapid sedimentary responses to likewise rapid sequential salinity changes that affected nearly the entire depositional basin. The San Andres depositional platform appears to have been both broad enough and possessed a low enough slope so that minor changes in depth of the shallow water column exerted profound effects on circulation patterns, which in turn controlled water salinity and facies development over the entire platform.

The San Andres Formation is characterized by a depositional style perhaps best described as "uniform," both in terms of vertical cyclic repetition and lateral extent of individual units. this relative depositional uniformity suggests overall regional tectonic quiescence, particularly

32

with respect to the earlier middle Carboniferous orogenic episode that affected the Texas and Oklahoma Panhandles.

On a gross scale, patterns of sedimentation in the San Andres Formation of the Palo Duro Basin can be readily conceptualized as functions of a dynamic interplay between rates of eustatic sea level change, regional basin subsidence, and sediment aggradation on a broad, low slope, low relief depositional platform. In addition to these primary factors, increasing evidence suggests a subtle, yet active structural influence overprinted on San Andres sequences both within the Palo Duro Basin and along its margins. Several examples of possible structural influence on San Andres deposition are presented below.

As noted previously, the distribution of relative thicknesses of cycles in the three San Andres genetic intervals suggests the possibility of episodic changes in regional basin subsidence rate. Non-uniform lateral changes in the thickness of individual non-salt cyclic lithofacies (insoluble residue + carbonate + anhydrite) are repeated in successive cycles of the lower and upper San Andres genetic sequences. Most prominent is a trend of thickening over the Whittenburg Trough, which is a structural low on the Precambrian basement fronting the Amarillo Uplift. Thickenings of non-salt facies this far north in the basin are unexpected because of the (inferred) rapid development of lateral salinity gradients across the basin during each cycle. However, such thickenings might well have been accommodated by high local rates of subsidence during the transgressive phases of cycles. Many of the local thickenings occur over structural lows on basement, so it seems likely that local differential subsidence rates were controlled by recurrent motion on faults at depth.

The northern depositional edges of the non-salt facies of lower San Andres units 2 and 3 terminate against the southern margin of the Amarillo Uplift, whereas unit 4 and cycles of the middle San Andres genetic sequence continue north across the uplift. The changing depositional limits of these individual cyclic facies may represent either the relative magnitudes of eustatic sea level changes, intermittent structural activity and evolution of topographic relief along the northern basin margin or a combination of both.

33

The effect of structure on sedimentation in individual cycles can be seen by comparing the DOE-Stone & Webster #1 Mansfield core, from a structurally complex area adjacent to the Amarillo Uplift, with other cores (figs. 41 and 46). Individual cycles traced from other cores to the #1 Mansfield core often show textural features indicating either a more hypersaline or a more normal marine local depositional environment, or are similar. For example, the lower San Andres unit 4 carbonate is recognized, in most cases, as a composite. An incomplete lower cycle culminates in nodular, or less than a meter of bedded anhydrite, indicating that the salinity may have reached gypsum saturation. A complete upper cycle is also present with normal marine limestone at its base. The lower cycle in the #1 Mansfield core is thicker than elsewhere and complete, culminating in several meters of bedded anhydrite and halite. Apparently, during the most hypersaline part of this cycle, the area represented by the #1 Mansfield core was both more restricted and accumulated thicker sequences of sediment. Differential movement of isolated fault blocks might explain this apparent paradox. Relatively uplifted blocks may have acted as local barriers that restricted circulation, while adjacent, relatively downdropped blocks subsided more rapidly allowing the accumulation of a thicker sedimentary pile. Alternatively, gypsum and halite may have been deposited in the lower unit 4 cycle in the #1 Mansfield and while the transgression that initiated the overlying unit 4 cycle had begun elsewhere.

An example of lower salinity in the area of the #1 Mansfield well, as compared to other areas, is seen in the third upper San Andres cycle (fig. 46). This cycle in other cores is dominantly nodular and laminated anhydrite. In the #1 Mansfield core, it is dolomite. Burrowed grainstone in the lower part of the cycle supports the interpretation that the depositional environment of this cycle was high energy and nearly normal marine in the area represented by the Mansfield core. Elsewhere, restricted gypsum-precipitating environments existed.

Similar variability is exhibited by the halite units in the #1 Mansfield core. The cycle immediately above the pi-marker is regionally a complete cycle, but in the #1 Mansfield core

34

the halite is absent and presumably has been dissolved. This second cycle above the pi-marker exhibits the reverse trend--it possesses a thicker halite section than the correlative cycle in other cores. These variations in the thickness of correlative halite facies are more difficult to interpret than similar variations in non-salt facies. This is because it is not yet clear to what extent these differences in halite thickness are due to variations in the rate of halite deposition, dissolution of halite during subaerial exposure at the end of the cycle, or dissolution during the transgression initiating the next cycle.

Structural Influence on Deposition (Fracasso)

Given an initial variable topography of the depositional surface, non-salt facies are expected to thin over topographic highs and thicken in topographic lows. This is because depressions maintain more normal marine conditions for longer periods of time than topographic highs. Extended periods of near normal marine salinities in depressions produce greater thicknesses of sediments in two ways: (1) enhanced early post-depositional dissolution of underlying halite produced thicker basal siliciclastic insoluble residues, (2) populations of skeletonized marine organisms can be supported for longer time periods, thus producing thicker accumulations of carbonates.

An initially variable depositional topography may be static (inherited from prior events) or maintained through time by contemporaneous structural activity (recurrent movement of fault blocks). A static, topographically variable, depositional surface is expected to produce a vertical sequence in which lateral thickness changes in successive cycles gradually decrease, as the depressions fill in. Prolonged expression of depositional topography by continued structural activity will produce a vertical sequence in which lateral thickness changes are maintained between successive cycles.

Structurally controlled, areally variable subsidence rates are also expected to produce lateral thickness changes in non-salt facies, without requiring initial differential relief on the depositional surface. Short-term rates of organic carbonate production generally exceed basin

35

subsidence rates (Sadler, 1981; Wilson, 1975). Thus organic carbonate sediments tend to aggrade vertically, promoting restriction of circulation, increasing salinity, and initiating evaporite sedimentation. Local basin subsidence rates that are high enough (fault controlled?) to match or exceed the rate of carbonate production will permit vertical aggradation without shallowing. Thus equable conditions for organisms are maintained and greater thicknesses of carbonates may accumulate locally. Prolonged maintenance of differential subsidence rates will produce a vertical sequence in which significant within-cycle lateral thickness changes persist between successive cycles. Cessation of differential subsidence rates will produce a vertical sequence in which within-cycle lateral thickness changes decrease between successive cycles.

Differential compaction over preexisting structures beneath the depositional surface will complement the effect of differential subsidence rates. Greater compaction and thicker sediment accumulations will occur over structural lows. Differential compaction and differential basin subsidence rates have the same effect on sedimentation: accumulations are thicker over structural lows, and these thickenings are maintained between successive cycles as long as the structural control is active. Once structural movement ceases, within-cycle lateral thickness changes decrease between successive cycles as the structural lows fill.

The Observed Patterns

Figures 47, 48, and 49 are graphs of the thickness of selected non-salt cyclic facies units along the correlation sections B-B' (fig. 39), C-C' (fig. 36) and D-D' (fig. 37), respectively. The present structural elevations of the π-marker and the base of lower San Andres cycle 4 are also plotted for reference and comparative purposes. Several relations are readily apparent. Lower San Andres cycles 2, 3, 4 and the interval designated as upper unit 1 exhibit remarkably similar patterns of lateral thickness changes across the Palo Duro Basin. These are quite distinct from the relatively uniform interval designated as middle San Andres unit 1. This apparent separation of thickness trends at lower, middle and upper stratigraphic levels supports the

36

distinction of lower, middle and upper San Andres genetic units that were previously recognized solely by systematic vertical changes in the thickness and completeness of cycles.

Lower cycles 2, 3, 4 and upper unit 1 thin uniformly to the north across the Palo Duro Basin proper in dip section C-C' (fig. 48). Cycle 1-3 and unit u-1 then thin noticeably over the Bravo Dome, whereas cycles 1-2 and 1-4 show no appreciable change in trend over this feature. Cycles 1-2, 1-3 and unit u-1 all thicken further north in the Whittenburg Trough, whereas cycle 1-4 shows no appreciable change in trend over this feature. Cycles 1-2 and 1-3 are then abruptly truncated over the Amarillo Uplift. Cycle 1-4 shows no apparent change in trend over the Amarillo Uplift, and maintains a constant thickness to further north in the Dalhart Basin. Unit u-1 continues to thicken from the Whittenburg Trough over the Amarillo Uplift and into the Dalhart Basin, where it then reverses trend and again thins to the north. The unit m-1 maintains a relatively constant thickness across the Palo Duro Basin and over the afore-mentioned structures before thinning in the Dalhart Basin. These observations imply that along this section line the Bravo Dome influenced deposition of cycle 1-3 and unit u-1; the Whittenburg Trough influenced the deposition of cycles 1-2, 1-3, and unit u-1, and the Amarillo Uplift truncated the deposition of cycles 1-2 and 1-3.

Cycles 1-2, 1-3, 1-4 and unit u-1 all exhibit abrupt thickenings to the south that presumably mark the San Andres shelf-edges. These rapid thickenings imply that the shelf to basin transition was abrupt. The 1-2 and 1-3 thickenings are approximately 10 miles north of the 1-4 and u-1 thickenings, implying southerly progradation of the San Andres shelf margin.

In a second dip section, Transect D-D' (figs. 37, 49), cycles 1-2, 1-3, 1-4 and unit u-1 thin uniformly to the north in the southern and central portions of the Palo Duro Basin. However, cycles 1-2, 1-3 and 1-4 then thicken abruptly further north in a zone fronting the Amarillo Uplift, whereas unit u-1 is truncated in this zone. Cycle 1-3 is next truncated at the southern edge of the Amarillo Uplift, whereas 1-2 and 1-4 thin abruptly but continue over the Uplift. Cycle 1-4 displays a variable thickness trend into the Anadarko Basin, whereas 1-2 thins abruptly and disappears early. Unit m-1 maintains a near constant thickness over the entire

37

region, apparently unaffected by these structures. However, it begins to thin abruptly just north of the Amarillo Uplift in the Anadarko Basin.

All the intervals thicken abruptly in the south, presumably reflecting the positions of San Andres shelf margins. Cycle 1-3 thickens further north than cycles 1-2 and unit u-1, and cycle 1-4 and unit m-1 thicken still further to the south. Shelf margin thickenings along this transect thus exhibit an oscillatory pattern through time, rather than a single progradational trend as in Transect C-C' (fig. 48).

An E-W strike section (Transect B-B', figs. 39, 47) is more difficult to interpret. Cycles 1-2 and 1-3 show quite similar patterns of thickness change over their entire extent, whereas the other units display variable patterns. Cycles 1-2, 1-3, 1-4 and possibly unit m-1 show marked thickenings to the west in northern Deaf Smith County. Unit u-1, however, thins slightly in this area. Cycles 1-2 and 1-3 thin abruptly over a small area in northeastern Randall County, but the other intervals show no change in trend in this area. Cycles 1-2, 1-3, 1-4 and possibly unit u-1 show a distinct thinning in the area of central Armstrong County, then thicken to the east in Donley County. Cycles 1-2 and 1-3 then thin uniformly east into Collingsworth County, whereas units m-1 and u-1 appear to thicken, and cycle 1-4 maintains a constant thickness. Unit m-1 shows a marked amount of lateral thickness variation in this strike section whereas unit u-1 maintains a nearly constant thickness. This is quite different from the trends of each of these units in both dip sections.

In summary, none of the units studied show a uniform trend of thinning from south-to-north, as predicted by the no-structural influence, no-topographic relief depositional model. Moreover, the rather complex vertical patterns of successive within-cycle lateral thickness changes do not conform to the inherited, static topographic relief or static differential compaction models. These changes conform more closely to model of intermittent active structural influence on patterns of sedimentation throughout the time of deposition of the San Andres Formation. In general, the lower and upper San Andres genetic units appear to have been more strongly influenced by structural activity than the middle San Andres unit. The

38

construction of more transect lines, isopach maps for each of intervals considered, and incorporation of more stratigraphic intervals will allow a few more refined spatial and temporal segregation of active structural influences on San Andres deposition in the Texas Pannandle.

Correlation of Halite, Units 4 and 5, Deaf Smith County, Texas (Hovorka)

Recurring sequences have been observed within halite units of the San Andres Formation. Detailed logging has identified 1 to 3 meter-thick zones which are traceable among the three Deaf Smith County DOE wells (figs. 50, 51). Techniques employed include visual estimation of (1) composition, (2) sedimentary structures, (3) dominant salt type based on textural classification of halite, and (4) location, composition and thickness of all interbeds or partings within halite.

Figure 50 shows an example, from the unit 5 halite, of two thin anhydrite beds which are correlatable in the three wells. Comparison of the cores shows the continuity of thin units over large areas; it also shows that some facies variations are present. For example, the thicker, lower anhydrite bed in the #1 J. Friemel and #1 Detten cores overlies several thin mudstone partings. In G. Friemel, however, there is no mudstone below the anhydrite but three partings overlie it.

Figure 51 shows one of a number of sequences in unit 4 that contain clean, slightly anhydritic salt with good primary fabric overlain by abundant mudstone beds and zones of chaotic mudstone-halite rock. the individual mudstone and anhydrite partings are not correlatable between wells, but the zones in which they are concentrated can be correlated. This kind of correlation is possible through all of units 4 and 5 in Deaf Smith County and preliminary logging suggests that similar zones can be correlated in Swisher County. The most difficult zone to correlate is the upper 10 feet of halite in each cycle.

The observation that zones which reflect subtle variations in the halite environment can be correlated from well to well indicates that the factors controlling facies in the halite affect large areas. Halite deposition did not take place in isolated brine pools but, like the underlying

39

carbonate and sulfate parts of the cycle, were deposited in a shallow but extensive water body. Detailed logging of San Andres Formation units 4 and 5 in other cores is expected to provide information on possible causes of facies changes within the halite.

Episodes of prolonged exposure occurred periodically during halite deposition. Towards the end of deposition of some cycles (especially in the upper San Andres Formation), the chaotic mudstone-halite mixture became predominant, indicating that episodes of exposure were more frequent or more prolonged as maximum progradation occurred. Mudstone-halite mixtures are transitional upwards into fine arkosic sandstone deposited in terrestrial environments (Queen Grayburg Formation).

Textural Classification of Halite (Hovorka)

Understanding of the origin of various fabrics in bedded and diagenetic halite has allowed development of a descriptive textural classification which can be used in constructing genetic interpretations.

Halite is classified based on examination of slabbed core, however, geochemical and petrographic studies have aided in the development of this classification. Halite classification is based on crystal size, crystal shape, amount and composition of impurities, distribution of fluid inclusions, and characteristic sedimentary structures. Eight classes have been recognized. These include fabrics ranging from those that originated as primary brine-pool precipitates to those formed during diagenesis.

Fabrics used to classify halite and the resulting eight classes are shown in Table 3. Each halite type is identified by a letter symbol and a type name. Typical crystal size, shape, composition and location of impurities, and fluid inclusion distribution are given for each type. The associated halite types, a summary of identifying characteristics, and a sketch of typical fabric is shown. The first five classes (chevron-halite rock, color-banded/vertically-oriented halite rock, chaotic mudstone-halite rock, recrystallized muddy halite rock, and recrystallized anhydritic halite rock) are fabrics arranged, left to right, from those showing the most primary

40

fabrics to those showing the most altered fabrics. The remaining three classes of halite (displacive halite, cavity-filling halite cement, and fibrous fracture-filling, halite cement) are fabrics produced by halite introduced into sediments during diagenesis.

Chevron-halite rock is characterized by abundant, minute (less than 50 micron) fluid inclusions. Most crystals are elongated in a vertical direction, probably a result of competition for space. Truncation surfaces are visible as anhydrite partings. Anhydrite, in intercrystalline positions as well as in partings, is the most common impurity in chevron halite. It typically comprises 1 to 5% of the rock and, in combination with the abundant fluid inclusions, imparts a conspicuous white color to the rock.

The fabric of chevron halite, in almost all examples, has been disturbed by recrystallization along grain boundaries and by formation of karst pipes and pits. Karst pits are several centimeters wide and 10 cm to as much as two meters deep. Such pits can be recognized as areas where primary fabrics have been dissolved and the cavity filled with coarse, clear halite cement and/or concentrations of siliciclastic mudstone. The floors of pits are blanketed with anhydrite or mudstone left as a residue when the halite was dissolved. Pipes are narrow (1 cm wide), anastomosing, vertical flaws in the halite where halite was recrystallized or dissolved, presumably along fractures which have now been healed. Pits and pipes appear to have been superimposed on brine-pool fabrics during episodes of drying in which the halite was exposed to corrosion by meteoric water. Many but not all pits and pipes can be traced upward to mudstone beds which are believed to have been deposited on the surface during the formation of pits and pipes.

Color-banded/vertically oriented, halite rock resembles chevron-halite rock in the abundance of anhydritic partings and the vertical elongation of the crystals, but the minute fluid inclusions, and the chevrons they define, are absent. Dark color due to trace amounts of clay and organic material is typical; variations in the intensity of the color define bedding (color banded). Vertically oriented crystals, anhydrite partings, and color bands are commonly associated. Color-banded/vertically oriented, halite rock, like chevron-halite rock, originated

41

as a brine-pool precipitate. The difference in fabric is due to, as yet unidentified, subtly different environmental conditions. Color-banded/vertically oriented, halite rock contains abundant pits and pipes.

Chaotic mudstone-halite rock is composed of masses of siliciclastic mudstone between relatively coarse, euhedral to anhedral halite crystals. No bedding is preserved and the origin of this fabric is, in many examples, enigmatic. A model for formation of chaotic mudstone-halite rock has been developed based on examination of intervals in which some texture is preserved. The parent material was color-banded/vertically oriented or chevron-halite rock. It is believed that extensive alteration during prolonged exposure resulted in destruction of most primary fabric by the formation of pits and pipes and recrystallization of halite. Mudstone accumulation was favored by several factors. (1) The dry condition of the flat prevented precipitation of halite, but input of fine siliciclastic material, probably fallout from dust storms, continued in this environment. Siliciclastic silt and clay is present in all lithologies; it could concentrate due to the absence of evaporite formation on the dry halite flat environment. (2) The dry condition of the flat favored transportation of siliciclastics by fluvial and sheetwash processes. (3) Impurities in the halite were concentrated at the surface and on pit floors as halite dissolved. Any or all of these processes may result in accumulation of mudstone at the surface and within pits. A second process contributing to the development of chaotic disrupted fabric in chaotic mudstone-halite rock is displacive growth of halite crystals within the sediment. This kind of halite precipitates when halite-bearing waters of either marine or meteoric origin evaporate. Repetition of the sequence of pipe and pit formation followed by precipitation of displacive halite produces the chaotic fabric characteristic of chaotic mudstone-halite rock.

Recrystallized, muddy, halite rock is a catch-all class for halite with no identifiable primary fabric and no evidence of the kind of intense alteration which has affected chaotic mudstone-halite rock. A minor amount (1 to 10%) mudstone is present, but it was not concentrated in pits or in beds. The origin of this fabric is not clear, and possibly all intervals

42

identified as recrystallized, muddy, halite rock do not have the same origin. This fabric, in some cases, formed from color-banded/vertically oriented halite which recrystallized under the influence of waters penetrating along grain boundaries or along now obscure fractures. In other cases, a minor amount of claystone or gypsum co-deposited with halite may have released enough water during diagenesis to recrystallized halite. It is possible that some halite may have been deposited lacking fabrics recognized as primary, and would therefore fall in this class, even though it never underwent recrystallization.

Recrystallized anhydritic, halite rock is the equivalent of recrystallized, muddy, halite rock with mudstone lacking or concentrated in scattered spots. Much of it appears to have formed due to recrystallization of chevron-halite rock. A few scattered intervals have a salmon-pink color, suggesting that the invading waters may have altered a few percent gypsum or anhydrite to polyhalite. The mineralogy of these intervals has not been determined by petrography or geochemistry.

Displacive halite, in contrast to the halite rock types discussed previously, comprises only a minor element in nonhalite lithologies. Displacive halite is a common constituent in mudstone and siltstone beds, especially those associated with halite rock. Displacive halite also occurs in anhydrite beds within, beneath, or overlying halite rocks, and in a few locations is found within carbonate rocks close to halite. Displacive halite forms cubes, slightly skeletal crystals (hopper crystals), and extremely skeletal crystals.

Halite, cavity-filling cement is most abundant in karst pits. In these locations the crystals can be extremely coarse, in many examples larger then the 10 cm core width. In some examples, the presence of a pit is deduced from the presence of an interval of very coarse halite. The halite, cavity-filling cement is typically clear, clean halite, with large fluid and vapor-filled inclusions. Impurities associated with the halite are the insoluble residue material which typically defines the pit floor and anhydrite and mudstone which fell into the pit as cement was precipitating. Halite cement is abundant in other lithologies, especially sandstone and carbonate grainstones.

Fibrous, fracture-filling halite cement is common throughout the halite section, especially in mudstone interbeds within halite rock. It also occurs within fractures in carbonate rocks and dark anhydritic mudstone beds at the base of cycles. Halite-filled fractures do not occur in anhydrite beds, apparently because any fractures which developed were healed by anhydrite. Fibrous, fracture-filling halite is very similar in appearance in all lithologies. It characteristically has a deep orange color. All fractures have a vertical orientation and fibers are oriented normal to fractures. Most do not appear to widen upward toward paleo-surfaces, indicating that they are formed in the subsurface. A few examples examined in thin section are tentatively interpreted to have formed later than most diagenetic features such as multifaceted dolomite and anhydrite, but before precipitation of these phases ceased, timing fibrous halite precipitation as the last early diagenetic process.

Quartermaster and Dewey Lake Formations

Volcanic Ash Beds (Kolker and Fracasso)

The age of the Quartermaster and Dewey Lake Formations of the Permian Basin is problematic. Although they are generally considered Late Permian in age, the possibility of an early-to-middle Triassic age has also been raised. The discovery of volcanic ash beds in the Quartermaster and Dewey Lake Formations of the Palo Duro Basin, radiometrically dated as Late Permian, contributes to the resolution of this ambiguity.

The lithologically correlative Quartermaster (Texas and Oklahoma Panhandle outcrops), Dewey Lake (Panhandle and Midland Basin subsurface), and Pierce Canyon (Delaware Basin outcrop and subsurface) Formations (fig. 2) are progradational continental red-bed sequences that represent the culmination of a regional, cyclic trend of marine regression from the Permian Basin which had begun in the early-to-middle Permian (King, 1942). The age of these units is questionable because they are unfossiliferous--presumably because of deposition in extremely inimical (arid/evaporitic?) physical environments. They are conformably underlain by the Rustler Formation in the Delaware and Midland Basins and the presumably correlative

informal Alibates succession in the Palo Duro Basin (fig. 2). These subjacent deposits contain carbonate and evaporite beds that represent the last transgression of the Permian sea. Impoverished and poorly preserved Late Permian (Ochoan) invertebrate faunas have been reported from both units (Baker, 1915; Roth and others, 1941; Dunbar and others, 1960). The overlying Dockum Group is widely regarded as late Triassic in age, based largely on continental biostratigraphic zonation. The Quartermaster, Dewey Lake, and Pierce Canyon Formations are usually regarded as Ochoan in age because of their apparent genetic/lithologic continuity with the underlying conformable Ochoan sequence (King, 1942; Miller, 1966). Their contact with the overlying Dockum Group has been described as both unconformable and conformable. The possibility of a locally conformable relation with overlying strata of Late Triassic age has been the main basis for consideration of an Early-to-Middle Triassic age for at least part of the Quartermaster - Dewey Lake - Pierce Canyon sequence. In many instances, the question of time conformity may have been confused with the geometric property of stratal concordance. Thus the Dockum and underlying units may be locally concordant but nonetheless unconformable throughout their areal extent.

Two volcanic ash beds have recently been discovered in the Quartermaster (outcrop) and Dewey Lake (subsurface) Formations in the Palo Duro Basin. The lower ash bed ranges in stratigraphic position from 4-20 meters (13-66 feet) above the top of the uppermost Alibates non-siliciclastic unit (sulfate or carbonate). Radiometric dates of 251 ± 4 and 261 ± 9 m.y. old have been obtained for this bed by the K/Ar method. Both values are well in the range of Late Permian ages. The upper ash bed has not been dated. The contact between the Dockum and Quartermaster - Dewey Lake unit varies from concordant to discordant at the locations of ash sample sites and measured sections (figs. 52, 53, and 54); the level of the lowest Dockum biota has not yet been determined at these sites.

Stratigraphy

The depositional systems represented by the Quartermaster, Dewey Lake, and Pierce Canyon Formations have not been elaborated in detail. Genetic interpretations range from a

45

saline water body, mud flat, and eolian system in the Delaware Basin (Miller, 1966); landlocked sea and fluvio-deltaic sequence in the Palo Duro Canyon State Park area (Matthews, 1969); shallow marine, shoreline, and fluvial system in the Palo Duro Canyon area (Hood, 1977); hypersaline water body, tidal flat, and sabkha sequence in the Texas Panhandle region (McGowen and others, 1979); relict sea or lake, fan-delta, and braided stream system in the Palo Duro Canyon and Caprock Canyons State Park areas (Gustavson and others, 1981); lacustrine and prodelta sequence in the Delaware Basin (Eager, 1983); and a largely alluvial plain, overbank and ephemeral channel-fill sequence in the Texas Panhandle area. Collectively, these interpretations imply deposition in a large, restricted hypersaline water body and marginal shoreline environments, with a fluvio-deltaic clastic input. The water body may have been marginal-marine or a continental playa lake—currently available evidence does not allow a distinction. Marginal-marine or continental sabkha deposition is not obvious in outcrop, and is probably a minor component at best.

The Quartermaster and Dewey Lake Formations were measured and sampled at several outcrop and subsurface sites in the Palo Duro Basin (figs. 52, 53, and 54) to document the areal distribution and stratigraphic position of the ash beds. Figures 53 and 54 are generalized lithologic sections that document the stratigraphic positions of the ash beds and significant vertical differences in grain size distributions. The top of the uppermost Alibates carbonate or sulfate bed was used as a lower datum wherever possible. Sections were measured either to the base of the Dockum Group or to a thick, massive cliff-forming sandstone commonly present in the uppermost Quartermaster just below the Dockum.

The Dewey Lake sequence was not examined in detail in the Department of Energy (DOE)/Gruy Federal Rex White #1 core (location 1, Fig. 52), but the presence of both upper and lower ash beds was noted. The lower ash bed there is situated approximately 5.5 meters above the top of the Alibates. This ash bed was located in all sections, but the upper ash bed was only located in Caprock Canyons State Park, the DOE/Gruy Federal Grabbe #1 and Rex White #1 cores. This may be a function of differential thickness rather than a real difference in areal

46

distribution. The lower ash bed is commonly several centimeters thick (0.3-20.0 cm range) and weathers to a prominent pink-white color; the upper ash possesses a maximum observed thickness of only 2.5 cm and weathers to a light purple to maroon color, providing a lesser contrast against the surrounding brick-red Quartermaster - Dewey Lake sediments.

Several apparent trends can be discerned among the measured sections. The proportion of coarser-grained fraction decreases from E-SE to W-NW, and the interval between the top of the Alibates and the lower ash bed thins from E-SE to W-NW. These changes suggest the possibility of Quartermaster - Dewey Lake progradation from E-SE to W-NW, but a wider data distribution is necessary to substantiate this. The possibility that these thickness changes may reflect the existence of local clastic depocenters cannot be discounted. The sequences generally display a coarsening-upward pattern; both grain size and coarse-fraction set thickness increase upward. Such a pattern is typical of prograding clastic sequences. Mudstone units appear massive in outcrop, but commonly contain even to wavy, continuous, parallel laminations in core. This suggests that most of the fine-grained fraction was deposited from suspension in a low energy environment, and was not bioturbated subsequent to deposition. The coarser fraction, which ranges from siltstone to medium grained sandstone, is most commonly ripple cross-laminated over an extremely wide range of bed thickness. Climbing ripples and soft-sediment deformation structures are abundant. Most of the coarse grained fraction thus appears to have been deposited in rapid pulses by traction.

Petrology and Age

The lower ash bed is present in all examined localities. It varies in thickness from approximately 1.3 to 20.0 cm, but is generally several centimeters thick. It is cross-laminated in both outcrop and core samples. Its apparent wide areal distribution and blanket-like geometry seem to preclude deposition in restricted channels; the primary structures instead imply syndepositional reworking by gentle bottom currents. The upper ash bed is sporadically distributed and displays no internal primary structures in outcrop or core. It is present as a

47

concentration of millimeter sized intraclasts dispersed in a 5.0 cm thick intraclastic zone in the Grabbe #1 core. This implies reworking subsequent to partial induration.

Mineralogy and texture of the lower ash beds are the same in each sampled occurrence, including Palo Duro Canyon State Park (sample PD-2), lower Palo Duro Canyon (sample PD-1), Caprock Canyons State Park (sample 072982) and in the Swisher County #1 Grabbe core (sample S-915). Each sample contains varying amounts of subhedral to euhedral phenocrysts in a well-crystallized clay matrix having no distinct outlines of relict shards. Locally, the orientation of clay grains is highly random, and may be inherited from devitrified shards. Phenocrysts include sanidine, quartz, biotite, and minor amounts of apatite, zircon, and Fe-Ti oxide. A large proportion of sanidine grains are hollow, possibly due to diagenesis. Some quartz grains are embayed. The presence of euhedral biotite and apatite indicates that transport has been minimal. The upper ash at Caprock Canyons State Park contains plagioclase in addition to sanidine and has a larger proportion of phenocrysts to matrix than the lower ash beds. Phenocrysts are coarser grained and hollow sanidine is less common in the upper ash.

The matrix of each lower ash bed consists of non-expansive clay with a 10 A basal spacing, probably illite (fig. 55). A minor amount of expansive clay (smectite) that was probably derived from alteration of illite is present in Sample PD-2 (Palo Duro Canyon). The upper ash at Caprock Canyons contains only expansive clay (smectite), with basal spacings of 15.5 A after air drying, 17.1 A after glycolation, and 9.8 A after collapse upon heating to 550°C for 2 hours.

K/Ar determinations on biotite in ash beds at Caprock Canyons State Park (2 determinations) and in the Swisher County #1 Grabbe core give late Permian ages ranging from 261 ± 9 to 251 ± 4 m.y. (Table 1). All ages are within the range of overlap of experimental errors. K/Ar ages of 251 ± 4 and 257 ± 9 m.y. were determined by different labs for 2 splits of a 785 mg concentrate of biotite from Caprock Canyons. Only 110 mg of biotite were separated from tuffaceous material in the #1 Grabbe core. Sample size was limited by the lower overall biotite concentration, and limited volume of core available for processing. Duplicate analyses of

potassium and radiogenic argon[40] were performed on this material, but the second argon[40] analysis is considered less reliable due to a malfunction in an induction furnace used to reduce contamination by atmospheric argon[40]. The proportion of radiogenic argon[40]/atmospheric argon[40] is only 0.178 in this analysis, compared to 0.718 to 0.850 for previous determinations. Due to the small sample size, no biotite concentrate was left to repeat the second argon[40] analysis for S-915.0. Using the first argon[40] determination gives an age of 261 $\pm$ 9 m.y., as reported in Table 1; an age of 271 $\pm$ 9 m.y. is obtained if an average of the two argon[40] analyses is used.

Although no previous descriptions of discrete ash beds in the Dewey Lake/Quartermaster Formation have been reported, the presence of hollow sanidine in the Pierce Canyon red beds and elsewhere in the Dewey Lake Formation has been noted by Miller (1955, 1966). Local concentrations of apatite, biotite in excess of muscovite, and embayed euhedral quartz were also recognized in the Pierce Canyon Formation. The mean length of sanidine crystals in the Delaware Basin was found to be 0.12 to 0.14 mm. The mean length of sanidine for 4 samples of "lower ash" ranges from about 0.08 mm (sample PD-2) to 0.11 mm (Sample 072982), based on measurement of 20 grains per sample. Overall, the grain size of sanidine in samples from the Palo Duro Basin appears to be less than that observed in the Pierce Canyon red beds, suggesting that the Delaware Basin is closer to the source area. Some variation in grain size may be due to changes in wind velocity during transport (Williams and others, 1954).

While volcanic activity may have occurred throughout much of Dewey Lake time, the consistent stratigraphic position, similarity in mineralogy and texture, and agreement (within experimental error) of K/Ar ages indicate that the lower ash bed observed in all the localities is correlative and represents a unique event. Correlation of the "upper" ash bed(s) is more difficult to ascertain, because of their reduced thickness and sporadic exposure.

TRIASSIC SYSTEM

Dockum Group (Johns and Hovorka)

The Late Triassic age Dockum Group overlies the Permian age Dewey Lake Formation and underlies Cretaceous age rocks and the Tertiary Ogallala Formation. Recent studies have focused primarily on environments and depositional systems of Dockum outcrops with limited subsurface interpretations (Boone, 1979; Seni, 1979; McGowen and others, 1979; McGowen and others, 1980; Seni and others, 1980; Granata, 1981). Current study of the Dockum is concentrating on (1) subsurface correlations, (2) facies descriptions, environmental interpretations and diagenesis of core in DOE-Stone & Webster's wells, (3) structure and tectonics during the Triassic and (4) clay mineralogy in the Dockum versus that in the Permian.

General Correlations

Four cross sections constructed across the Palo Duro Basin display the current interpretations of stratigraphic contacts and distribution of Dockum sediments (fig. 56). These sections (figs. 57-60) show the Dockum thinnest in the north and east and thickest, over 1400 feet, to the west and south, which corresponds with the geometry of the Dockum depositional basin (McGowen and others, 1979). Evident on the north-south cross sections (figs. 58, 59) is the protection from erosion provided by the Cretaceous cover in the southern part of the basin. All of the cross sections show the Dockum to be composed of numerous sandbodies with interbedded siltstones and mudstones. While individual sandstones are very difficult to trace laterally, packages or sand-rich intervals can be correlated with a fair degree of confidence. Examination of such packages has revealed areas of possible structural activity during deposition of the lowermost Dockum sediments.

Figure 60 is a north-south cross section which intersects the Matador Arch, an east-west oriented uplift forming the southern boundary of the Palo Duro Basin in the southern Lamb County. The basal sandstone package in figure 60 thickens into a structural low defined by

50

Lamb #67. This low could have originated as a direct result of faulting or by dissolution of the underlying Salado saltbeds. The cross section shows about 80 feet less salt in Lamb #67 than in the adjacent Lamb #58. Since this is also the difference in sandstone thickness, it is possible that salt dissolution has occurred contemporaneous with sandstone deposition. However, the cross section (fig. 60) also shows a total of 250 feet of offset on top of the Alibates Formation, of which only 80 feet can be attributed to salt dissolution. This leaves 170 feet of offset to be accounted for by other means; faulting is one possible explanation. Since reactivation of old structural elements is believed to have initiated Dockum deposition (McGowen and others, 1979; McKee and others, 1959), it is likely that faulting created or recreated a structural low allowing thicker accumulation of sediment than on the surrounding structural "highs."

Additional applications of correlating sandstone packages will be used in future to help define: (1) individual river or stream systems, (2) extent of high lake level transgressions, and (3) boundaries of delta lobes during progradation.

The Dockum underlies the Ogallala Formation in most of the Palo Duro Basin. This contact can be picked on most geophysical logs with a high degree of confidence. Figures 57 and 58 show the eastward-sloping erosional contact with the Ogallala which is essentially the paleo-dip direction (Seni, 1980; TDWR, 1982). Figures 59 and 60 parallel the paleo-strike of the Ogallala and show a more uniform horizon for the contact with exceptions, presumably due to channeling by Ogallala streams.

The basal contact of the Dockum with the Dewey Lake Formation is very difficult to pick in the subsurface. McGowen and others (1979) used the occurrence of a high-gamma-ray emitting unit, interpreted to be a mudstone, in the upper part of the Dewey Lake as the base of the Dockum. In core now available (DOE-Gruy Federal #1 Rex White well [Randall County #25] and DOE-Gruy Federal #1 Grabbe well [Swisher County #17]) the contact is picked at the boundary between a mud or siltstone with a high gamma-ray response and a sandstone with a much lower gamma-ray response (fig. 61). This characteristic response can be abrupt, as in the

51

Grabbe well (fig. 61), or gradational, as in the Rex White well (fig. 61). In either case, this basal pick can be traced throughout the basin without much difficulty.

Core Studies

Dockum/Dewey Lake Contact

The base of the Dockum Group was cored in four DOE wells. These cores show that the nature of the contact is unpredictable and variable across the basin.

DOE-Gruy Federal #1 Rex White.--This is the only core in which a sharp, easily identifiable contact was found. The upper Dewey Lake consists of red-brown planar to low angle climbing ripple laminated, fine to very fine grained sandstone. This has been cut into by a reduced poorly cemented, muddy, fine to medium grained sandstone considered to be of Triassic age.

DOE-Gruy Federal #1 Grabbe.--The contact appears to be at the base of a red-brown, burrowed, bimodal, ripple laminated very fine grained sandstone with pervasive pedogenic structures. Unfortunately, there was no core recovery for the next eighteen feet until red-brown, parallel to ripple laminated siltstones and mudstones, characteristic of the Dewey Lake Formation, were encountered.

DOE-Stone & Webster #1 Mansfield.--The Dockum/Dewey Lake contact occurs between the cross-bedded, medium sandstones of the Dockum at 450 feet and the contorted, accretion-rippled, very fine-grained sandstones of the Dewey Lake below about 500 feet. The questionable interval contains very fine-grained sandstone with some bimodal sandstone beds and small scale sedimentary structures which are similar to known Permian sediments. However it also contains 20 feet of purple, green, and red claystone with thin, rippled sand units which might be correlatable with laminated mudstone beds at the base of the Dockum in outcrops. Load cast structures are abundant in this interval but are not common in most Permian sediments.

DOE-Stone & Webster #1 J. Friemel.--The contact between the Dockum Group and underlying Dewey Lake Formation is not clear-cut; two horizons are deemed possible. Our present interpretation favors the contact at 1076.6 feet, which is the base of a medium to coarse grained sandstone containing coarse grains of well-rounded and polished or frosted sand with large-scale cross stratification which fines upwards to ripple laminated sandstone. The overlying sequence consists of a succession of similar fining upward units (10-15 ft thick) dominated by large-scale cross-stratified sandstone beds.

A second possibility for the contact occurs at 1091 feet, the base of a contorted laminated, bimodal sandstone which grades upwards into ripple laminated, fine grained sandstone with thin, 1-2 grain thick lags of coarse, well-rounded, frosted and polished sand grains, overlain by laminated and desiccation crack bearing mudstone. The entire cycle is about 14 ft thick and is truncated by the above-described sequence starting at 1076.6 feet. The units below (Dewey Lake Formation) consist primarily of thin bedded units (3-5 ft thick) of ripple laminated fine grained sandstone, siltstone, and mudstone units.

The base of the unit of 1076.6 feet is where large-scale features are predominant, and is continued upwards for greater than a hundred feet, and characterizes the lower portion of that sequence. Thus, the contact at 1076.6 feet is favored for the contact between the Dockum Group and underlying Dewey Lake Formation.

Core descriptions and interpretations of the Dockum/Dewey Lake contact interval suggest that the nature of the contact is variable throughout the Palo Duro Basin. Only in the Rex White well, where fluvial sandstones of the Dockum have eroded down into the Permian strata, is the contact clear-cut. The J. Friemel well also appears to have an erosional, fluvial, basal contact, at either 1076.6 feet or 1091 feet, but the distinction between the Permian and Triassic is very subtle, if it exists at all. The basal Dockum is apparently eolian in the Grabbe well which is environmentally identical to much of the Permian sediments. The Mansfield well may also have an eolian base or possibly it may even be lacustrine. The base of the Dockum may represent eolian Triassic deposits that have been reworked by fluvial processes or

53

completely removed by eroding channel systems. These processes have produced complex and highly variable relationships between the Permian and Triassic strata.

Dockum Lithologies

Sediments of the Dockum Group were cored in four DOE wells. Three of these cores were logged early in the West Texas Waste Isolation project and were not logged in great detail. Therefore only the recently logged J. Friemel well is discussed here.

The Dockum facies in this core consist primarily of cross and ripple laminated sandstone, siltstone, and mudstone, pebble conglomerates, granule conglomerates, and intraclastic and burrowed siltstone and mudstone, most of which are calcareous. Plant fragments are found associated with the conglomerate, sandstone, and siltstone units. The contact with the overlying Ogallala Formation is a sharp unconformable contact between underlying intraclastic, blocky siltstone of the Dockum Group and overlying structureless medium grain sandstone of the Ogallala Formation. The contact with the underlying Permian Dewey Lake is also thought to be unconformable.

From the base of the Dockum Group upward, four major depositional (?) packages are observed based upon associations of units and repeated sequences of sediments.

The lowermost package can be subdivided into lower, middle and upper portions. The lower portion is 96 ft thick and consists of 5-10 ft thick cross-stratified sandstone units with basal scours, in which sequences thin upwards. These units are gradationally and sharply overlain by ripple laminated sandstone, siltstone, and mudstone units, 1-10 ft thick, which fine upwards in grain size and scale of structures. Repeated sequences of sandstone-siltstone/mudstone units range from 25 feet thick at the base to 6 feet at the top of the lower part of the interval.

The middle portion consists of 22 ft of low angle cross-stratified and ripple laminated fine grain sandstone with laminae of organic debris defining the stratification. The upper 8 ft is subhorizontally laminated, fine grain, muddy sandstone.

54

The upper portion consists of 64 ft of nearly horizontal, thinly laminated claystone and mudstone. The upper mudstone contains calcareous clasts.

The base of package 2 marks a dramatic change in deposition and can be subdivided into two portions. The lower portion is 59 ft thick and consists of sharp bounded, 2-8 ft thick, calcitic cemented pebble conglomerates with crude pebble imbrication and crude cross-stratification, in fining upwards sequences 1.5 ft to 4 inches thick. Conglomerates are interbedded with units of laminated mudstone and massive to crudely laminated sandstone 1 to 5 ft thick.

The lower portion grades upwards from a pebble conglomerate to cross-stratified sandstone of the upper portion which grades upwards from medium to fine sandstone with subhorizontal laminae at the top. The upper portion is 57 feet thick.

The change from package 2 to package 3 is gradational, but package 3 (357 ft thick) is characterized by showing a less regular association (no observed pattern) of lithologies. In general, it consists largely of ripple laminated siltstone and mudstone truncated by scour channels with sharp bases, caliche granule lags, and gradational tops; these sequences decrease in abundance and thickness upwards. Channelized regions are associated with organic debris. The thick units of ripple laminated siltstone and mudstone are also interbedded with sharply bounded, cross-stratified, fine-grain sandstones and coarse-grain siltstones which increase in thickness and abundance upwards.

Package 4, which appears to be in gradational contact with the top of package 3, is the upper 31 ft of the Dockum Group. It consists of blocky textured, bioturbated, intraclastic, calcareous, silty mudstone.

Overall the Dockum Group consists of terrigenous clastic sediments representing a variety of fluvial and lacustrine related depositional environments. It is believed that the Triassic Dockum represents a change to more humid climatic conditions from the underlying Permian evaporite sequences.

The previously described package 1 appears to represent an overall fining upwards regressive sequence. Thick sandstone units of the lower portion may represent channelized deposition. The thinner fine sandstone and associated organics of the middle portion are more representative of overbank or lacustrine associated deposition. Calcareous clasts in the upper portion may be caliche and represent soil forming processes and possibly the transition from humid to more arid climatic conditions.

The lower portion of package 2 represents deposition in an arid-type climate. The conglomerates may represent distal, braided river bar facies. The upper fining upwards sequence may represent a transition back to more humid or semi-humid climates.

Package 3 may be progradational from package 2 and represent more distal, upper deltaic facies with abundant splays or small Gilbert-type deltas in the upper portion of package 3.

The combined packages 3 and 4 represent an overall fining upwards or regressive sequence. Package 4 resembles soil textures but may represent an alternatingly wet-dry lacustrine environment.

Thin Sections Studies

Eighty-nine thin sections were examined from the interval 780 to 287 ft in the DOE-Gruy-Federal #1 Grabbe well. This encompasses all of the recovered Dockum core and includes 14 thin sections from the transitional lower part of the Dockum (780-726) which are similar in texture, composition, and sedimentary structures to Upper Permian rocks but lack halite and anhydrite cement. Upper Permian samples are very similar to each other; they are fine-grained, red, slightly muddy, with or without reduced spots, and contain small scale rippled or laminated structures. Dockum samples vary from pure clay to clean sandstone to caliche pebble conglomerate, with a corresponding variety of colors (gray, green, red, brown, pink, etc.) and a variety of sedimentary structures.

All fourteen thin sections from the transition interval (780 to 726 feet) are muddy, coarse siltstone or fine sandstone. Lithology of the contact interval was briefly described in the core

studies section. Three of them (751.8, 747.6, 740.9) are bimodal, with well-rounded, super-mature, medium-grained sand in a finer angular sand matrix. Bimodal sands with rounded coarse grains are typical of Upper Permian rocks. A plot of the ratio of quartz:feldspar:rock fragments (fig. 62) shows that samples from this transition interval plot with the Permian samples in or near the lithic arkose area of the diagram. Fine anhedral or rhombic carbonate typical of Upper Permian rocks makes up a few percent of most transition rocks. Sedimentary structures observed are small scale ripples, fine lamination, and disrupted or homogenized structures due to burrowing or fluid escape. Sediments are muddy because of clay intimately intermingled with the fine sand in the form of clay drapes, clay cutans, and squashed rock fragments. A few samples which lack clay in some areas are partially or completely cemented with calcite. There is no evidence that halite or anhydrite cement were ever present, and there is no evidence of the timing of carbonate cement precipitation. Most of the samples are red, with reduced spots or coarser beds.

This interval is above the top of the salt dissolution zone, and halite cement would not have been preserved even if initially present. Therefore, it cannot be petrographically determined whether the initial sediment was identical to Permian sediments with evaporite cements, now dissolved, or whether the absence of evaporites reflects the first evidence of change into Triassic conditions.

The samples above 726 feet are significantly different from those in the transition interval in texture, composition, and sedimentary structures, and contain minor amounts of unusual elements such as lignitized plant fragments, bone fragments, caliche, and glauconite. Most sandstones and siltstones exhibit horizontal or inclined and cross-bedded orientations to grains. Variations include lamination accentuated by placers of heavy minerals, clay intra-clasts, and flakes of mica or lignite; the composition of rock fragments varies. Mica is concentrated in some beds, making up to 10% of the rock, and is entirely absent in other beds. These variations in sandstone composition and texture cannot be correlated with any particular grain size, depositional environment or location in the section, and could probably best be

57

explained as very local variations in hydrodynamic winnowing and concentration of platy grains, or local contributions of clay chips, reworked caliche, or older sandstone.

Five thin sections from the #1 Grabbe core have features which suggest that soil processes affected their textures. Thin sections 650.0 and 289.0 have complex disrupted structures cut by vertical cracks in clay. Thin section 380.0 is partially fragmented caliche or fresh-water limestone. Thin section 413.5 contains caliche nodules and 713.0 contains hematite nodules which may be soil features.

Soil features are more common near the top of the Dockum section, where very fine sandstones and siltstones are more common than coarse sandstones (footage 441.2 to 289.0). These features indicate that more delta plain and fluvial environments are represented near the top of the formation.

Other distinctive sedimentary structures examined in thin section include clay drapes, especially in fine sandstones and siltstones, load casts, a sandstone dike (sample 576.4), and a graded bed with a contorted base (sample 574.0).

The great variety of locally derived grains contributes to the diversity of Dockum sediments. Carbonate-pebble conglomerates contain clasts of calcareous clay soils; calcite-cemented, laminated, fine sandstone pebbles; clasts of older dolomite rocks with ghosts of forams and abraded, dolomitized echinoderm plates; and abundant caliche. Caliche pebbles are calcite or dolomite microspar and are structureless, vaguely pelleted, contain floating silici-clastic silt grains or have concentric cracks or a central area filled with calcite or dolomite spar. A few grains of coarsely crystalline calcite and dolomite with radial, undulose extinction are probably caliche or travertine related to caliche. Pyrite is common within carbonate rock fragments.

Lignitized plant fragments are common in the upper middle part of the Dockum Formation, between footages 577.8 and 441.2. This corresponds to the most reduced part of the section in core, where pyrite is common both within sandstone beds and replacing plant fragments and carbonate grains. Oxydized red beds are entirely absent. In this part of the

58

section cross-bedded sandstone beds increase in scale and frequency compared to laminated beds and represent various deltaic environments.

Plant fragments are preserved as dark brown organic material. Most are elongate, structureless, and are indented, but not broken by adjacent sand grains. Some are partially replaced by pyrite. A few fragments are thicker and exhibit some woody structures partially replaced by pyrite. These fragments have been slightly compressed. Most of the plant fragments have shrunk away from adjacent sand and cracked in the elongate direction, leaving holes which are filled with epoxy. The shrinkage probably was caused by desiccation of the rock after coring.

Glauconite is found near the top of the Dockum Formation, from footage 509.0 to 455.5 in laminated or cross-laminated fine sandstones. The presence of glauconite indicates that sandstones were deposited in a marine influenced environment. The presence of slightly glauconitic sandstones directly below siltstones with soil textures discussed above suggests that the facies changes might be a result of sudden relative fall of sea level rather than deltaic progradation.

Other locally derived grains include clay chips, which are commonly included with sand-sized grains. Most clay chips have been partially squashed by postdepositional compaction and can only be distinguished from clay matrix by the assumption that cross-bedded sandstones should contain no clay matrix. A few large clasts of clay are found, indicating that transport distance was not far. Sample 505.2 contains a large clay clast with gypsum crystals growing displacively within it. Some grains identified as clay chips may actually be rock fragments derived from outside the basin rather than from ripped-up clay drapes.

Phosphatic bone fragments were identified in four thin sections (554.6, 540.3, 526.0, 505.2) and phosphate grains of questionable affinities recognized in several other thin sections. All are sand-sized fragments, well rounded and clearly transported as detrital grains.

Figure 62 shows the change in composition in the #1 Grabbe core from the Permian samples, which cluster around a lithic arkose composition with an average quartz:feldspar:rock

59

fragment ratio of 65:22:13, to the Dockum samples which are litharenites and arkosic litharenites with quartz:feldspar:rock fragment ratios averaging 55:10:35. This compositional change reflects a real change in source area, and is not due only to the increase in grain size. Coarser sandstones might be expected to contain more rock fragments than equivalent finer sediment in which rock fragments would have been disaggregated into constituent grains. The ratio of feldspar to quartz should remain about the same from coarse sediment to fine if the source materials were the same. The ratio of feldspar to quartz is significantly higher in Permian and transitional sediments than in Dockum sediments. Feldspar is slightly more weathered in Dockum sandstones than Permian sandstones, but few feldspar grains have been entirely removed; therefore, the change in composition is not due to changing climatic conditions but to a different source area that yielded angular quartz, less feldspar, and more metamorphic rock fragments.

The character of the metamorphic rock fragments is different in Upper Permian and transition rocks than in the Dockum Formation. Composite quartz-mica rock fragments are common in Permian and transition sandstones, but show little or no foliation. In Dockum sandstones quartz-mica rock fragments have well-developed foliation and are clearly derived from schist, gneiss, and phyllite. Stretched composite quartz and large fresh flakes of muscovite, chlorite, and biotite are common in Dockum sandstones and also suggest a metamorphic source. Analysis of heavy mineral suites might yield more information about source areas. No trends were observed in ratios of rock fragments, quartz types, or mica or feldspar composition.

Diagenesis has been simple in transitional and Dockum rocks. All sediments underwent a slight postdepositional compaction which squashed weight-bearing clay chips. Large mica flakes were deformed by compaction in one-third of the sandstones, but not deformed in the majority of them. Porosity before cementation averaged 18% but was higher, up to 30%, in samples with few clay intraclasts.

60

The common cement is coarse, pore filling sparry calcite which, in the average sample, fills half the available pore space. Calcite cement preferentially fills pores adjacent to carbonate rock fragments, probably because of ease of nucleation on existing crystals. Calcite cement completely fills pore spaces in only two out of twenty-seven thin sections point-counted for cement. One of these (504.2) has very coarse crystals with a poikilotopic texture. Two other thin sections (473.0, 477.0) are partially cemented with poikilotopic calcite. Two thin sections (540.3 and 588.3) have an early generation of bladed calcite cement around carbonate rock fragments. Both of these are caliche rock fragment conglomerates, in which dissolution of the carbonate rock fragments provided a local source for calcite. Most carbonate rock fragments show some evidence of dissolution, in the form of concentrations of impurities around siliciclastic sand grains imbedded in the carbonate rock fragments, or microstylolites where two carbonate rock fragments are adjacent. Five out of twenty-seven thin sections have less than 1% calcite cement, with abundant void space. Most sandstones which contain lignitized plant fragments also have sparse calcite cement, perhaps because these sandstones were isolated from fluids which cemented other sandstones and might have altered plant material.

Kaolinite occurs as a cement in six samples of the upper part of the Dockum Formation, footages 505.2 to 471.5. This corresponds to the interval where plant fragments are most common. It also corresponds to the occurrence of skeletalized plagioclase grains. Most Dockum feldspar grains are fresh or slightly sericitized or vacuolized. In this interval of kaolinite cement many plagioclase feldspar grains are intensely vacuolized. Dissolution must have occurred after deposition and compaction of the sandstone because the skeletal feldspar grains would have been crushed by transportation or pressure. The correspondence in location and amount (a few percent of each kaolinite and skeletal feldspar) suggests that dissolution of plagioclase feldspar was the source of the kaolinite. The timing of plagioclase dissolution with respect to calcite precipitation is ambiguous. Calcite does not replace or cement vacuoles in

61

feldspar. However, kaolinite occurs in spaces between calcite crystals which suggests it predated calcite cement precipitation.

Other cements include local occurrences of pyrite cementing a few sand grains and limonite cement. Limonite forms liesegang bands which cut across structure in thin section 443.0. No evidence of present or former halite or anhydrite cements were found within Dockum or transition sediments.

The variety of Dockum sediments reflects two characteristics of Dockum sedimentation: a variety of depositional environments and the presence of locally derived materials which are concentrated in some sediments and absent in others. These changes from the more uniform upper Permian deposition reflect changes in source area, depositional environment, and possibly climate during the Triassic.

Clay Mineralogy Studies

Samples for clay mineralogy were analyzed from the DOE-Gruy Federal #1 Rex White well to detect possible changes across the Permian-Triassic boundary. The Rex White well was chosen for this initial investigation because it is the only well in which the Dockum/Dewey Lake contact is clearly defined. The lithology of the contact can be found in the Core Studies section. Preliminary data show a uniform occurrence of illite (plus other clays) in the Permian section but an absence of illite in Triassic (Dockum) samples. Additional sampling is underway to determine if this change actually corresponds with the contact. If so, this method will be applied in other cores where the boundary position is in question.

REFERENCES

Ahlbrandt, T. S., 1979, Textural parameters of eolian deposits: in A study of global sand seas, U.S. Geological Survey, Professional paper 1052, p. 21-51.

Ahlbrandt, T. S., and Fryberger, S. G., 1981, Sedimentary features and significance of interdune deposits, in Ethridge, F. G., and Flores, R. M., Recent and ancient nonmarine depositional environments. Models for explanation Soc. Economic Paleontologists and Mineralogists Special Publication 31, p. 293-314.

Arthurton, R. S., 1973, Experimentally produced halite compared with Triassic layered halite-rock from Cheshire, England: Sedimentology, v. 20, p. 145-160.

Baker, C. L., 1915, Geology and underground waters of northern Llano Estacado: University of Texas at Austin, Bureau of Economic Geology, Bulletin No. 57.

Barrett, M. E., and Kirschner, C. E., 1979, Depositional systems in the Rinconada Formation (Precambrian) Taos County, New Mexico: New Mexico Geological Society Guidebook, p. 121-126.

Bassett, R. L., and Bentley, M. E., 1983, Deep Brine Aquifers in the Palo Duro Basin: Regional Flow and Geochemical Constraints, Bureau of Economic Geology Report of Investigations No. 130, The University of Texas at Austin, Austin, Texas, 59 p.

Bein, A., Land, L. S., 1982, San Andres carbonates in the Texas Panhandle: sedimentation and diagenesis associated with magnesium-calcium-chloride brines: Bureau of Economic Geology Report of Investigations No. 121, 48 p.

Boone, J. L., 1979, Lake margin depositional systems of the Dockum Group (Upper Triassic) in Tule Canyon, Texas Panhandle: Master's thesis, The University of Texas at Austin, 147 p.

Bramlette, M. N., 1929, Natural etching of detrital garnet: American Mineralogist, v. 14, p. 336-7.

Budnik, R. T., 1983, Influence of basement structure on distribution and facies of overlying strata, Palo Duro Basin, Texas Panhandle, in Gustavson, T. C., and others, Geology and

geohydrology of the Palo Duro Basin, Texas Panhandle, a report on the progress of nuclear waste isolation feasibility studies (1982): The University of Texas at Austin, Bureau of Economic Geology Geological Circular 83-4.

Burke, J. A., Schmidt, A. W., and Campbell, R. L., Jr., 1969, The Litho-Porosity Cross Plot - a method of Determining Rock Characteristics for Computation of Log Data, The Log Analyst, v. 10, # 6, November-December, 1969, p. 25-43.

Collinson, C. W., Scott, A. J., and Rexroad, C. B., 1962, Six charts showing biostratigraphic zones and correlations based on conodonts from the Devonian and Mississippian rocks of the upper Mississippi Valley: Illinois Geological Survey Circular 328, 32 p.

Collinson, C. W., Rexroad, C. B., and Thompson, T. L., 1971, Conodont zonation of the North American Mississippian: Geological Society of America Memoir 127, p. 353-394.

Cheney, M. G., Dott, R. H., Hake, B. F., Moore, R. C., Newell, N. D., Thomas, H. D., and Tomlinson, C. W., 1945, Classification of Mississippian and Pennsylvanian rocks of North America: American Association of Petroleum Geologists Bulletin, v. 29, p. 125-169.

Cunningham, B. J., 1969, Identification and division of the pre-Pennsylvanian sediments-western Anardarko Basin, in Pre-Pennsylvanian Geology of the Western Anadarko Basin: Panhandle Geological Society, Amarillo, Texas, p. 7-26.

Davis, S. N., 1980, Hydrogeologic Effects of Natural Disruptive Events on Nuclear Waste Repositories (Prepared for the Office of Nuclear Waste Isolation under its contract with the U.S. Department of Energy), Pacific Northwest Laboratory, Richland, Washington, 33 p.

Dean, W. E., and others, 1975, Sedimentological significance of nodular and laminated anhydrite: Geology, v. 3, p. 367-372.

Dott, R. H., 1941, Regional stratigraphy of mid-continent: American Association of Petroleum Geologists Bulletin, v. 25, p. 1619-1705.

Dunbar, C. O., and others, 1960, Correlation of the Permian formations of North America: Geological Society of America Bulletin, v. 71, p. 1763-1806.

Dunlap, W. H., 1967, San Andres oil exploration in the Cato-Slaughter trend of southeastern new Mexico, in The oil and gas fields of southeastern New Mexico, 1966 Supplement--A symposium: Roswell Geological Society, Roswell, New Mexico, p. 21-24.

Dutro, J. T., Jr., Gordon, M., Jr., and Huddle, J. W., 1979, Paleontological zonation of the Mississippian System, in Paleotectonic Investigations of the Mississippian System in the United States, U.S. Geological Survey Professional Paper 1010 S, p. 407-429.

Dutton, S. P., 1980, Depositional systems and hydrocarbon resource potential of the Pennsylvanian System, Palo Duro and Dalhart Basins, Texas Panhandle; The University of Texas at Austin, Bureau of Economic Geology Geological Circular 80-8, 49 p.

Dutton, S. P., Goldstein, A. G., and Ruppel, S. C., 1982, Petroleum potential of the Palo Duro Basin, Texas Panhandle: The University of Texas at Austin, Bureau of Economic Geology Report of Investigations No. 123, p. 1-87.

Eager, G. P., 1983, Core from the Dewey Lake, Rustler, and upper Salado Formations, Culberson County, Texas, in Shaw, R. L., and Pollan, B. J. (eds.), Permian Basin Cores--A Workshop, PBS-SEPM Core Workshop No. 2, Midland, Texas, 1983.

Fisher, R. S., and Hovorka, S. D., in press, Geochemical and textural evidence of primary and altered halite, Permian San Andres Formation, Texas: in Gustavson, T. C., and others, 1983, Geology and geohydrology of the Palo Duro Basin, Texas Panhandle - A report on the progress of nuclear waste isolation feasibility studies (1983): The University of Texas at Austin, Bureau of Economic Geology Geological Circular.

Flawn, P. T., 1956, Basement rocks of Texas and southeast New Mexico: University of Texas, Austin, Bureau of Economic Geology Publication 5605, 261 p.

Flawn, P. T., Goldstein, August, Jr., King, P. B., and Weaver, C. E., 1961, The Ouachita System: University of Texas, Bureau of Economic Geology Publication 6120, 401 p.

Folk, R. L., 1966, A review of grain-size parameters: Sedimentology, v. 6, p. 73-93.

Folk, R. L., 1971, Longitudinal dunes of the northwestern edge of the Simpson desert, Northern Territory, Australia, 1. Geomorphology and grain size relationships: Sedimentology, v. 16, p. 5-54.

3

Folk, R. L., 1974, Petrology of sedimentary rocks: Austin, Hemphill Publishing Company, 182 p.

Friedman, G. M., 1979, Address of the retiring president of the International Association of Sedimentologists: Differences in size distributions of populations of particles among sands of various origins: Sedimentology, v. 23, p. 3-32.

Galloway, W. E., and Brown, L. F., Jr., 1972, Depositional systems and shelf-slope relationships in Upper Pennsylvanian rocks, North-Central Texas: The University of Texas at Austin, Bureau of Economic Geology Report of Investigations No. 75, 62 p.

Gonzalez, R. A., and Woodward, C. A., 1973, Petrology and structure of Precambrian rocks of the Pedornal Hills, New Mexico: New Mexico Geological Society Guidebook, 23rd, p. 144-147.

Grambling, J. A., 1979, Precambrian geology of the Truchas Peaks region, north-central New Mexico, and some-regional implications: New Mexico Geological Society Guidebook, 30th, p. 135-143.

Granata, G. E., 1981, Regional sedimentation of the Late Triassic Dockum Group, West Texas and Eastern New Mexico: Master's thesis, The University of Texas at Austin, 198 p.

Gravenor, C. P., and Leavitt, R. K., 1981, Experimental formation and significance of etch patterns on detrital garnets: Canadian Journal of Earth Sciences, v. 18, p. 765-775.

Gupta, S., 1977, Meiofloral succession and interpretation of the base of the Permian System in the Eastern Shelf of Northcentral Texas U.S.A.: Review of Palaeobotany and Palynology, v. 24, p. 49-66.

Gustavson, T. C., and others, 1981, Selected aspects of the geology of the Palo Duro Basin, Texas Panhandle: The University of Texas at Austin, Bureau of Economic Geology, Field Trip Guidebook, 31 p.

Handford, C. R., 1980, Lithofacies and depositional environments of evaporite-bearing strata based on Randall and Swisher County cores, in Gustavson, T. C., and others, 1980, Geology and geohydrology of the Palo Duro Basin, Texas Panhandle--A report on the progress of

nuclear waste isolation feasibility studies (1979): The University of Texas at Austin, Bureau of Economic Geology Geological Circular 80-7, p. 5-7.

Handford, C. R., 1981, Bromide geochemistry of Permian Halite in the Randall County Core, in Gustavson and others, Bureau of Economic Geology Geological Circular 81-3, p. 75-80.

Handford, C. R., Dutton, S. P., and Fredericks, P. E., 1981, Regional Cross Sections of the Texas Panhandle: Precambrian to mid Permian, Bureau of Economic Geology, The University of Texas at Austin, Austin, Texas, 8 p. (text) and 7 cross sections.

Handford, C. R., and Fredericks, P. E., 1980, Lower Permian Facies of the Palo Duro Basin, Texas: Depositional systems, Shelf-margin Evolution, Paleogeography and Petroleum Potential, Bureau of Economic Geology Report of Investigations No. 102, The University of Texas at Austin, 31 p.

Hardie, L. A., and Eugster, H. P., 1971, The depositional environment of marine evaporites: a case for shallow clastic accumulation: Sedimentology, v. 16, p. 187-220.

Holdaway, M. J., 1978, Significance of chloritoid-bearing and stauvolite-bearing rocks in the Picuris Range, New Mexico: Geological Society of America Bulletin, v. 89, p. 1404-1414.

Hood, C. H., 1977, Geology of Fortress Cliff Quadrangle, Randall County, Texas: Unpublished Master's thesis, West Texas State University, 123 p.

Hovorka, S. D., 1982, Carbonate-Anhydrite-Halite Cycles, San Andres Formation (Permian), Palo Duro Basin, Texas: in Shaw, R. L., and Pollan, B. J., eds., Permian Basin Cores-A workshop. Permian Basin Section SEPM Core Workshop #2, p. 197-224.

Hovorka, S. D., Naiman, E. R., and McGowen, J. H., 1982, Petrographic summary of Permian rocks from the DOE/Gruy Federal #1 Grabbe well, Swisher County: in Gustavson, T. C., and others, Geology and geohydrology of the Palo Duro Basin, Texas Panhandle, The University of Texas at Austin, Bureau of Economic Geology Geological Circular 82-7.

Jonas, E. C., and McBride, E. F., 1977, Diagenesis of sandstone and shale: Application to exploration for hydrocarbons: Department of Geological Sciences, The University of Texas at Austin, Continuing Education Publication Number 1, 165 p.

5

Jordan, L., and Vosburg, D. L., 1963, Permian salt and associated evaporites in the Anadarko Basin of the western Oklahoma-Texas Panhandle region: Oklahoma Geological Survey Bulletin, v. 102, p. 1-76.

Keys, W. S., and Brown, R. F., 1973, Role of Borehole Geophysics in Underground Waste Storage and Artificial Recharge in Braunstein, Jules, ed., 1973, Underground Waste Management and Artificial Recharge, Volume I, Sponsored by AAPG, USGS and International Association of Hydrological Sciences, p. 147-191.

King, P. B., 1942, Permian of West Texas and southeastern New Mexico: American Association of Petroleum Geologists Bulletin, v. 26, no. 4, p. 535-763.

Maher, J. C., 1953, Permian and Pennsylvanian rocks of southeastern Colorado: American Association of Petroleum Geologists Bulletin, v. 37, no. 5, p. 913-939.

Mapel, W. J., Johnson, R. B., Bachman, G. O., and Varnes, K. L., 1979, Southern midcontinent and southern Rocky Mountains region, in Paleotectonic Investigations of the Mississippian System in the United States, U. S. Geological Survey Professional Paper 1010 J, p. 161-187.

Matthews, W. A., III, 1969, The geologic story of Palo Duro Canyon: The University of Texas at Austin, Bureau of Economic Geology, Guidebook 8, 51 p.

McGillis, K. A., 1980, Mapping of facies by well log interpretation, in Gustavson, T. C., and others, 1980, Geology and geohydrology of the Palo Duro Basin, Texas Panhandle--A report on the progress of nuclear waste isolation feasibility studies (1979): The University of Texas at Austin, Bureau of Economic Geology Geological Circular 80-7, p. 8-11.

McGowen, J. H., Granata, G. E., and Seni, S. J., 1979, Depositional framework of the lower Dockum Group (Triassic), Texas Panhandle: The University of Texas at Austin, Bureau of Economic Geology Report of Investigations No. 97, 60 p.

McGowen, J. H., Seni, S. J., Andersen, R. L., and Thurwachter, J. E., 1980, Uranium resource evaluation, Lubbock Quadrangle, Texas: Prepared for the U.S. Department of Energy, Grand Junction, Colorado, Subcontract No. 78-133-E, 51 p.

6

McKee, E. D., Oriel, S. S., Ketner, K. B., MacLacklan, M. E., Goldsmith, J. W., MacLacklan, J. C., and Mudge, M. R., 1959, Paleotectonic Maps of the Triassic System: U.S. Geological Survey Miscellaneous Geologic Investigations Map I-300.

McLaren, Patrick, 1981, An interpretation of trends in grain size analysis: Journal of Sedimentary Petrology, v. 51, p. 611-624.

Meyer, R. F., 1966, Geology of Pennsylvanian and Wolfcampian rocks in southeast New Mexico: New Mexico Bureau of Mines and Mineral Resources Memoir 17, 120 p.

Miller, D. N., Jr., 1955, Hollow sanidine grains: stratigraphic marker for the Pierce Canyon Formation, West Texas and southeastern New Mexico: Journal of Sedimentary Petrology, v. 25, no. 3, p. 235-237.

Miller, D. N., Jr., 1966, Petrology of Pierce Canyon Redbeds, Delaware Basin, Texas and New Mexico: American Association of Petroleum Geologists Bulletin, v. 52, no. 2, p. 283-307.

Miller, J. P., Montgomery, Arthur and Sutherland, P. K., 1963, Geology of part of the southern Sangre de Cristo Mountains, New Mexico: New Mexico Bureau of Mines and Mineral Resources, Memoir 11, 106 p.

Milliken, K. L., 1979, The silicified evaporite syndrome--two aspects of silicification history of former evaporite nodules from southern Kentucky and northern Tennessee: Journal of Sedimentary Petrology, v. 49, p. 245-256.

Naiman, E. R., Bein, A., and Folk, R. L., 1983, Complex polyhedral crystals of limpid dolomite associated with halite, Permian Upper Clear Fork and Glorieta Formations, Texas: Journal of Sedimentary Petrology, v. 53, no. 2, p. 549-555.

Nelson, T. A., 1976, An automated rapid sediment analyser (ARSA): Sedimentology, v. 23, p. 867-872.

Nicholas, R. L., and Rosendal, R. A., 1975, Subsurface positive elements within the Ouachita foldbelt in Texas, and their relation to paleozoic cratonic margin: American Association of Petroleum Geologists Bulletin, v. 59, no. 2, p. 193-216.

7

Nicholson, J. H., 1960, Geology of the Texas Panhandle in aspects of the geology of Texas, a symposium, The University of Texas at Austin, Austin, Texas, Bureau of Economic Geology Publication No. 6017, p. 51-64.

Nie, N. H., Hull, C. H., Jenkins, J. G., Steinbrenner, Karin, and But, D. H., 1975, Statistical package for the social sciences: New York, McGraw-Hill, 675 p.

Nielsen, K. C., and Scott, T. E., Jr., 1979, Precambrian deformation of history of the Picuris Mountains, New Mexico: New Mexico Geological Society Guidebook, 30th, p. 113-120.

Pippin, L., 1970, Panhandle-Hugston Field, Texas-Oklahoma-Kansas--the First Fifty Years, in Halbouty, M. T., Geology of Giant Petroleum Fields: American Association of Petroleum Geologists Memoir 14, p. 204-222.

Powell, B. N., and Fischer, J. F., 1976, Plutonic igneous geology of the Wichita magmatic province, Oklahoma Guidebook for field trip #2, south-central section, Geological Society of America, 1976 meeting; published by Oklahoma Geological Survey.

Powell, B. N., Gilbert, M. C., and Fischer, J. F., 1980, Lithostratigraphic classification of basement rocks of the Wichita province, Oklahoma: summary: Geological Society of America Bulletin, pt. 1, v. 91, p. 509-514.

Presley, M. W., 1979a, Upper Permian evaporites and red beds, in Dutton, S. P., and others, Geology and geohydrology of the Palo Duro Basin, a report on the progress of nuclear waste isolation feasibility studies (1978): The University of Texas at Austin, Bureau of Economic Geology Geological Circular 79-1, p. 39-49.

Presley, M. W., 1979b, Salt deposits, in Dutton, S. P., and others, Bureau of Economic Geology Geological Circular 79-1, p. 50-56.

Presley, M. W., 1980a, Upper Permian salt bearing units, in Gustavson and others, Geology and geohydrology of the Palo Duro Basin, Texas Panhandle, Bureau of Economic Geology Geological Circular 80-7, p. 12-23.

Presley, M. W., 1980b, Salt depth and thickness studies, in Gustavson and others, Geology and geohydrology of the Palo Duro Basin, Texas Panhandle, Bureau of Economic Geology Geological Circular 80-7, p. 33-40.

8

Presley, M. W., 1981a, San Andres Salt Stratigraphy and Salt Purity, in Gustavson and others, Geological Circular 81-3, p. 33-40.

Presley, M. W., 1981b, Statistical analysis of lithologic interpretations from well logs, in Gustavson, T. C., and others, Geology and Geohydrology of the Palo Duro Basin, Texas Panhandle--A report on the progress of nuclear waste isolation feasibility studies (1980): The University of Texas at Austin, Bureau of Economic Geology Geological Circular 81-3, p. 19-24.

Presley, M. W., 1981c, Middle and Upper Permian salt-bearing strata of the Texas Panhandle: Lithologic and facies cross sections, Bureau of Economic Geology Map Series.

Presley, M. W., and McGillis, K. A., 1982, Coastal evaporite and tidal-flat sediments of the upper Clear Fork and Glorieta Formations, Texas Panhandle: The University of Texas at Austin, Bureau of Economic Geology Report of Investigations No. 115, 50 p.

Presley, M. W., and Ramondetta, P. J., 1981, Hydrocarbon potential of San Andres Carbonates in the Palo Duro Basin--Stratigraphic and facies analysis, in Gustavson, T. C., and others, 1981, Geology and geohydrology of the Palo Duro Basin, Texas Panhandle--A report on the progress of nuclear waste isolation feasibility studies (1980): The University of Texas at Austin, Bureau of Economic Geology Geological Circular 81-3, p. 59-63.

Rahmani, R. A., 1973, Grain surface etching features of some heavy minerals: Journal of Sedimentary Petrology, v. 43, p. 882-888.

Railroad Commission of Texas, 1969, Docket no. 20-29, 540, application by Shell Oil company for Discovery Allowable and New Field Designation of Manarte (Granite Wash, Upper) for Shell Alamosa 315 No. 2, Oldham County, Texas.

Railroad Commission of Texas, 1982, Docket no. 10-78, 609, application by Baker & Taylor Drilling Company for discovery Allowable and New Field Designation of Hryhor (Granite Wash) for Baker & Taylor Aurora No. 1, Oldham County, Texas.

Ramondetta, P. J., 1981, Genesis and emplacement of San Andres oil in the northern shelf of the Midland Basin, Texas, in Gustavson and others, Bureau of Economic Geology Geological Circular 81-3, p. 52-58.

9

Ramondetta, P. J., 1982a, Genesis and Emplacement of oil in the San Andres formation, northern shelf of the Midland Basin, Texas: Bureau of Economic Geology Report of Investigations No. 116, 39 p.

Ramondetta, P. J., 1982b, Facies and stratigraphy of the San Andres Formation, Northern and northwestern shelves of the Midland Basin, Texas and New Mexico: The University of Texas at Austin, Bureau of Economic Geology Report of Investigations No. 128, 56 p.

Ramondetta, P. J., and Merritt, R. M., 1982, Use of geophysical well logs for the determination of mud and anhydrite content in bedded salt, in Gustavson, T. C., and others, Geology and geohydrology of the Palo Duro Basin, Texas Panhandle, A report on the progress of nuclear waste isolation feasibility studies: The University of Texas at Austin, Bureau of Economic Geology Geological Circular 82-7, p. 105-108.

Rascoe, B., 1978, Sedimentary cycles in the Virgilian Series (Upper Pennsylvanian) of the Anadarko Basin: Oklahoma Geological Society Shale Shaker, v. 28, p. 123-131 and 144-149.

Roedder, E., 1982, Possible Permian diurnal periodicity in NaCl precipitation, Palo Duro Basin, Texas, in Gustavson, T. C., and others, Geology and geohydrology of the Palo Duro Basin, A report on the progress of nuclear waste isolation feasibility studies: The University of Texas at Austin, Bureau of Economic Geology Geological Circular 82-7, p. 101-104.

Roth, R., and others, 1941, Permian pelecypods in the lower Quartermaster Formation, Texas: Journal of Paleontology, v. 15, no. 3, p. 312-317.

Ruppel, S. C., 1983, Facies and depositional setting of Mississippian rocks in the Palo Duro-Hardeman Basin area, in Shaw, R. L., and Pollan, B. J., (eds.), Permian Basin Cores--A Workshop: Permian Basin Section, Society of Economic Paleontologists and Mineralogists Core Workshop No. 2, Midland, Texas, p. 47-68.

Ruppel, S. C., and Ramondetta, P. J., 1982, Determination of salt purity using gamma-ray logs: San Andres Formation, Palo Duro Basin, in Gustavson, T. C., and others, Geology and geohydrology of the Palo Duro Basin, Texas Panhandle, A report on the progress of

nuclear waste isolation feasibility studies: The University of Texas at Austin, Bureau of Economic Geology Geological Circular 82-7, p. 183-200.

Sadler, P. M., 1981, Sediment accumulation rates and the completeness of stratigraphic sections, Journal of Geology, v. 89, no. 5, p. 569-584.

San Angelo Geological Society, 1958, The base of the Permian--a century of controversy: Guidebook, San Angelo Geological Society, 73 p.

Sandburg, C. A., 1979, Devonian and Lower Mississippian conodont zonation of the Great Basin and Rocky Mountains: Brigham Young University Studies, v. 26, pt. 3.

Seni, S. J., 1979, Genetic stratigraphy of the Dockum Group (Triassic), Palo Duro Canyon, Panhandle, Texas: Master's thesis, The University of Texas at Austin, 157 p.

Seni, S. J., 1980, Sand-body geometry and depositional systems, Ogallala Formation, Texas; University of Texas at Austin, Bureau of Economic Geology Report of Investigations #105, 36 p.

Seni, S. J., McGowen, J. H., and Risner, R. S., 1980, Uranium resource evaluation, Amarillo Quadrangle, Texas: Prepared for the U. S. Department of Energy, Grand Junction, Colorado, Subcontract No. 78-158-E, 28 p.

Schlumberger, 1972, Log Interpretation, Volume I-Principles, Schlumberger Limited, New York, N. Y., 113 p.

Scholle, P. A., 1979, Porosity Prediction in Shallow versus Deep Water Limestones-Primary Porosity Preservation Under Burial Conditions, in Geology of Carbonate Porosity, AAPG Continuing Education Course Note Series #11.

Schreiber, B. C., and Kinsman, D. J., 1975, New observations on the Pleistocene evaporites of Montallegro, Sicily and a modern analog: Journal of Sedimentary Petrology, v. 45, p. 469-479.

Schreiber, B. C., Roth, M. S., and Helman, M. L., 1982, Recognition of primary facies characteristics of evaporites and the differentiation of these forms from diagenetic overprints (1-32), in Handford, C. R., Loucks, R. G., and Davies, G. R., (eds.), Depositional

11

and Diagenetic Spectra of Evaporites--A Core Workshop: SEPM Core Workshop No. 3, Calgary, Canada.

Shearman, D. J., 1971, Marine evaporites: the calcium sulphate facies: American Society of petrology Geology Seminar, University of Calgary, Canada, 65 p.

Siedlecka, A., 1972, Length-slow chalcedony and relics of sulfates--evidences of evaporitic environments in the Upper Carboniferous and Permian beds of Bear Island, Svalbard: Journal of Sedimentary Petrology, v. 42, p. 812-816.

Simpkins, W. W., Gustavson, T. C., Alhades, A. B., and Hoadley, A. D., 1981, Impact of evaporite dissolution and collapse on highways and other cultural features: The University of Texas at Austin, Bureau of Economic Geology Geological Circular 81-4, 23 p.

Simpson, G. S., 1976, Evidence of overgrowths on and solution of detrital growths garnets: Journal of Sedimentary Petrology, v. 46, p. 689-693.

Smith, D. A., in press, Basement and lower Paleozoic structural influence on Upper Permian sedimentation over the Donley Positive; Donley County, Texas Panhandle, in Gustavson and others, Geology and geohydrology of the Palo Duro Basin, Texas Panhandle, a report on the progress of nuclear waste isolation feasibility studies (1982): The University of Texas at Austin, Bureau of Economic Geology Geological Circular.

Texas Department of Water Resources, 1982; Evaluating the ground-water resources of the High Plains of Texas, Vol. 1; Texas Department of Water Resources LP-173, 238 p.

Thompson, T. L., and Goebel, E. D., 1969, Conodonts and stratigraphy of the Meramecian Stage (Upper Mississippian) in Kansas: Kansas Geological Survey Bulletin 192, 56 p.

Tweto, Ogden, 1980, Precambrian geology of Colorado: Colorado Geology, Rocky Mountain Association of Geologists, 1980 Symposium, p. 37-46.

Weiler, Y., and others, 1974, Halite oolites and ripples in the Dead Sea, Israel: Sedimentology, v. 21, p. 623-32.

Williams, H., and others, 1954, Petrography: An Introduction to the Study of Rocks in Thin Sections: Freeman and Company, San Francisco, 406 p.

Wilson, J. L., 1975, Carbonate Facies in Geologic History, Springer-Verlag, 471 p.

12

LIST OF TABLES

FIGURE CAPTIONS

Figure 1.   Map of Texas Panhandle area showing location of Palo Duro Basin.

Figure 2.   Stratigraphic column and general lithologies for the Palo Duro and Dalhart Basins.

Figure 3.   Accepted subdivision of Mississippian rocks in the Palo Duro Basin.   Possible Kinderhook deposits (not shown) occur sporadically at the base.   Amerada Petroleum Corporation, Lafayette Hughes Trustee No. 1, Hall County, Texas (BEG No. 18).

Figure 4.   Map of the Texas Panhandle area showing location of the Palo Duro and Hardeman Basins and four cored wells.   Donley 3: Service Drilling Company, Kathleen C. Griffin No. 1.   Childress 10: Wes-Tex, Kewanee, and Coastal States Producing Co., Steve Owens No. 1-A. Hardeman 42:   Sun Oil Co., Quanah Townsite Unit No. 1. Hardeman 44: Standard Oil Co. of Texas, Coffee No. 1.

Figure 5.   Probable correlation of 4 wells for which conodonts were recovered.   No horizontal scale.   Wells and line of section shown in Figure 1.

Figure 6.   Distribution of lower Pennsylvanian facies and interpreted depositional environments.

Figure 7.   Isolith map of total carbonate in the lower part of the Pennsylvanian System.

Figure 8.   Distribution of upper Pennsylvanian facies and interpreted depositional environments.

Figure 9.   Isolith map of total carbonate in the upper part of the Pennsylvanian System.

Figure 10. Location of oil fields in Oldham and western Potter Counties.   Reservoirs in these fields are Pennsylvanian granite wash or carbonate.

Figure 11. Structure contour map on the top of the upper granite wash, the reservoir for Lambert, Hryhor, and Sundance Fields (Railroad Commission of Texas, 1982).   See figure 5 for location.

Figure 12. Net thickness of the 0-5% porosity range for the Brown Dolomite.

Figure 13. Net thickness of the 5-10% porosity range for the Brown Dolomite.

1

3

Figure 43. Stratigraphic divisions of the San Andres Formation, with reference geophysical log from Swisher County. The informal unit subdivisions of genetic sequences are working stratigraphic intervals that are recognized on geophysical logs and are mappable. Genetic cycles are smaller-scale intervals based on analysis of core, and cannot generally be distinguished individually on geophysical logs. Unit bases in all cases correspond with genetic cycle bases. The present authors find that Presley's cycle 1 cannot be traced with certainty as far north as Swisher County, and suggest that the base of the San Andres Formation in this area and north corresponds to the base of unit 2.

Figure 44. Lower San Andres unit 5, a generally northwest-southeast cross section through cored wells showing what appears to be a fairly simple carbonate/anhydrite unit overlain by a halite sequence in Deaf Smith County is a composite of four or five thinner cycles. Each cycle has a carbonate/anhydrite or anhydrite lower unit and a halite upper unit. The halite has been preserved in all the cycles in Swisher County, but has been removed from the lower cycles in Deaf Smith county.

Figure 45. Middle San Andres cycles in a generally east-west cross section through cored DOE wells. The log of each well shows, left to right, visually estimated percent lithology, sedimentary structures and a graph of interpreted facies arranged in order of decreasing salinity. Note the consistent thickness and sequence in cycles across the basin, and the intervals where textural evidence suggests the former presence of halite at the top of cycles.

Figure 46. Upper San Andres cycles in a generally east-west cross section through cored DOE wells. The log of each well shows, left to right, visually estimated percent lithology, sedimentary structures and a graph of interpreted facies arranged in order of decreasing salinity.

Figure 47. Graph of thickness of selected non-salt cyclic units following line of cross-section B-B' (Fig. 39).

4

5

Table 1. Bureau of Economic Geology stratigraphy research in the Palo Duro Basin.

Stratigraphic Unit	Contributors to this Report	Ongoing Research Interest
Dockum Group	Johns, Hovorka	Johns
Dewey Lake Fm.	Kolker, Fracasso	Fracasso
Alibates Fm.		Hovorka
Salado-Tansill Fm.		Nance, Hovorka
Yates Fm.		Nance, Hovorka
Seven Rivers Fm.		Nance, Hovorka
Queen-Grayburg Fm.		Nance, Hovorka
San Andres Fm.	Hovorka, Fracasso	Hovorka, Fracasso, Greimel, Ruppel
Glorieta Fm.		
Clear Fork Group		
Tubb Fm.		
Red Cave Fm.		
Wichita Fm.		
Wolfcamp Series	Conti, Herron	Conti, Herron, Ruppel, Hovorka
Pennsylvanian System	Dutton	Dutton
Mississippian System	Ruppel	Ruppel
Ordovician/ Cambrian System		Ruppel
Precambrian		Budnik

Table 2. Oil fields in the Northwestern Palo Duro Basin

Field Name	Discovery Date	Depth (ft)	Reservoir	Drive Mechanism	API Gravity	Porosity (%)
Alamosa (Virgil)	5/57	6,101	Lower Virgilian Limestone	--	40.0	--
Alamosa, East (Granite Wash)	9/57	7,116	Missourian granite wash	--	43.3	--
Alamosa, Southeast (Missouri)	7/59	6,664	Missourian dolomite	--	36.6	--
Hryhor (Granite wash)	3/82	7,156	Granite wash	Dissolved gas and possible water drive	43.2	18
Lambert (Granite wash, upper)	1/79	6,786	Missourian granite wash	Water drive	42.6	13
Lambert 2 (Cisco)	10/79	6,110	Virgilian algal limestone	Dissolved gas drive	42.0	4.5
Lambert 3 (Granite wash)	7/80	5,720	Granite wash	--	36.0	--
Lambert 4 (Penn)	2/81	5,942	Pennsylvanian sandstone	--	42.8	--
Manarte (Granite wash)	3/69	7,093	Granite wash	Water drive	39.7	17
Manarte (Granite wash, upper)	8/81	6,542	Granite wash	Water drive	40.4	11
Sundance (Granite wash, upper)	8/81	7,058	Granite wash	Dissolved gas and possible water drive	42.7	10
Toscosa (Granite wash)	1/58	8,524	Missourian granite wash	--	43.0	--

1983 Discoveries

Field Name	Depth (ft)	Reservoir	API Gravity
Baker & Taylor 1 Billy's Creek	7,895	Granite wash (upper)	45.6
Baker & Taylor 1 East Billy's Creek	9,956	Lower Missourian granite wash	43.2
Baker & Taylor 1 Whose Mistake	6,526	Missourian granite wash	41.8
Shell 1-47 Bivens	8,890		43.0
Baker & Taylor 1 Amy	6,368	Missourian granite wash	42.2

*Estimated oil in place = 7758 bbl x Production acres / acre-ft

Table 2. (Continued)

					Total 1982 Production		
Permeability (md)	Average net pay (ft)	Interstitial water saturation (%)	Productive acres	Estimated oil in place (bbl)[x]	Gas (Mcf)	Crude oil (bbl)	Cumulative oil production to 1-1-83 (bbl)
--	--	--	--	--	0	0	58,270
--	--	--	--	--	0	0	97,195
--	--	--	--	--	0	0	48,277
--	15	42	320	3,887,689	34,864	405,508	405,508
48	68	40	320	13,167,498	68,453	329,606	1,375,980
8	25	45	400	1,920,105	27,566	119,358	333,492
-	-	-	-	-	26	671	11,989
--	--	--	--	--	20,817	1,675	5,485
60	36	43	400	10,825,203	2,723	6,794	491,349
60	41	32	440	10,468,583	8,052	209,141	2,719,706
668	20	25	320	3,723,840	44,634	487,987	526,830
--	--	--	--	--	0	0	4,202

774 bbl/day

216 bbl/day

53 bbl/day

93 bbl/day
32 bbl/day

[x] Average net pay x Porosity x (1-water saturation)

Table 3. Textural classification of halite with genetic significance.

Symbol	A	B	C	D	E	F	G	H	I
Halite type	chevron halite rock	color banded/ vertically oriented halite rock		chaotic mud-stone-halite rock	recrystallized muddy halite rock	recrystallized anhydritic halite rock	displacive halite in other sediments	halite cavity-filling cement	fibrous fracture-filling halite cement
Halite crystal size	0.5 to 5 cm	0.5 to 5 cm		0.3 to 3 cm	1 to 5 cm	1 to 5 cm	0.5 to 3 cm	1 to 20+ cm	.3 to 1 cm
Halite crystal shape	subvertical mosaic; L:W= 3:2 to 4:1	subvertical mosaic; L:W= 3:2 to 4:1		equant anhedral to euhedral crystals	equant mosaic	equant mosaic	euhedral cubes or hopper shapes	equant mosaic	fibrous
Impurities — Composition	anhydrite common; mudstone possible	anhydrite, mudstone, organics		mudstone, minor anhydrite	mudstone, minor anhydrite	anhydrite	mudstone; also dolomite, anhydrite	cavity filling halite is clean but is associated with mudstone and anhydrite insoluble residues	trace of hema-tite present as coloring agent; otherwise, pure halite
Impurities — Percentage	<1 to 5%	1 to 5%		10 to 50%	1 to 10%	1 to 25%	50 to 99%		
Impurities — Location	anhydrite on grain boundaries, partings; mudstone only in pipe fills	within and between grains, along partings, in pipes		in masses between halite crystals; some also within grains	within grains, minor between grains	along partings, grain boundaries	matrix for halite		
Fluid Inclusions	abundant, small; define relict growth faces	varied		few	varied	varied	few	large and abundant	?
Associated with halite types	F along crystal boundaries and pipes, H and/or D in pipes	F and E, H and/or D in pipes		mudstone beds typically include remnant B halite	may contain remnant A, B, possibly H	may contain remnant A, B, possibly H	non-halite rocks	all halite types	in non-halite rocks
Identifying characteristics	minute fluid inclusions along relict halite growth faces	bedding and/or vertical orienta-tion of crystals		10 to 50% mudstone in intercrystalline masses, cha-otic texture	halite red, brown, or black, 1 to 10% impurities, no bedding	halite with 1 to 25% anhydrite, no bedding	euhedral to subhedral halite crystals in sediments	exceptionally coarse, clear crystals, fill cavity in other salt type	fibrous halite in fracture; many examples are red

C reserved for another primary fabric not yet recognized

Table 4. Stratigraphic nomenclature for Late Permian Rocks, Permian Basin and Texas Panhandle.

| System | Series | Lithologic Units | | |
		Palo Duro Basin	Midland Basin	Delaware Basin
PERMIAN	OCHOAN	Quartermaster/ (outcrop) Dewey Lake (subsurface) Fm.	Dewey Lake Fm.	Pierce Canyon Fm.
		Alibates (informal succession)	Rustler Fm.	Rustler Fm.
		Salado/Tansill Fm.	Salado Fm.	Salado Fm.

Table 5. K-Ar ages and geochemical data from biotite in volcanic ash beds, Quartermaster and Dewey Lake Formations, Texas Panhandle

Sample 072982, Caprock Canyons State Park, Briscoe County, Texas (34°24'52"N, 101°5'51"W)

Sample weight	590 mg		195 mg
%K	7.434 7.383	7.409 (ave.)	7.542
$Ar^{40}*$	0.1438 0.1402	0.1420 ppm (ave.)	0.1406 ppm
$Ar^{40}*$ Total Ar^{40}	0.823 0.850		79%
Age	257± 9 m.y.		251 ± 4 m. y.
Laboratory	Krueger Geochron Labs, Cambridge, MA		The University of Texas at Austin, Department of Geological Sciences (F. W. McDowell, analyst).

Sample S-915, DOE-Gruy Federal #1 Grabbe Core, Swisher County, Texas (34°39'44"N, 101°37'55"W)

		Microprobe analysis average of 10 analyses on 5 grains, weight percent		Ions per 24 (O,OH,F)	
Sample weight	110 mg				
%K	7.329 7.393	7.361 (ave.)	SiO_2 38.77	Si	5.844
			TiO_2 3.84	Ti	0.436
			Al_2O_3 13.15	Al	2.337
$Ar^{40}*$	0.1435		FeO^b 13.99	Fe	1.765
	0.1552[a]		MgO 14.44	Mg	3.243
			Na_2O 0.47	Na	0.139
			K_2O 8.90 (K=7.39%)	K	1.711
$Ar^{40}*$	0.718		OH^c 3.97	OH	2.000
Total Ar^{40}	0.178[a]		Total 97.53	Total	17.475
Age	261**±9 m.y.				
Laboratory	Krueger Geochron Labs, Cambridge, MA				

$Ar^{40}*$ = radiogenic Ar^{40}
a - incomplete sample decontamination
b - total Fe as FeO
c - calculated
** - see text

Constants Used:
$\lambda_\beta = 4.963 \times 10^{-10}$/yr
$\lambda_e = 0.581 \times 10^{-10}$/yr
$K^{40}/K = 1.167 \times 10^{-4}$
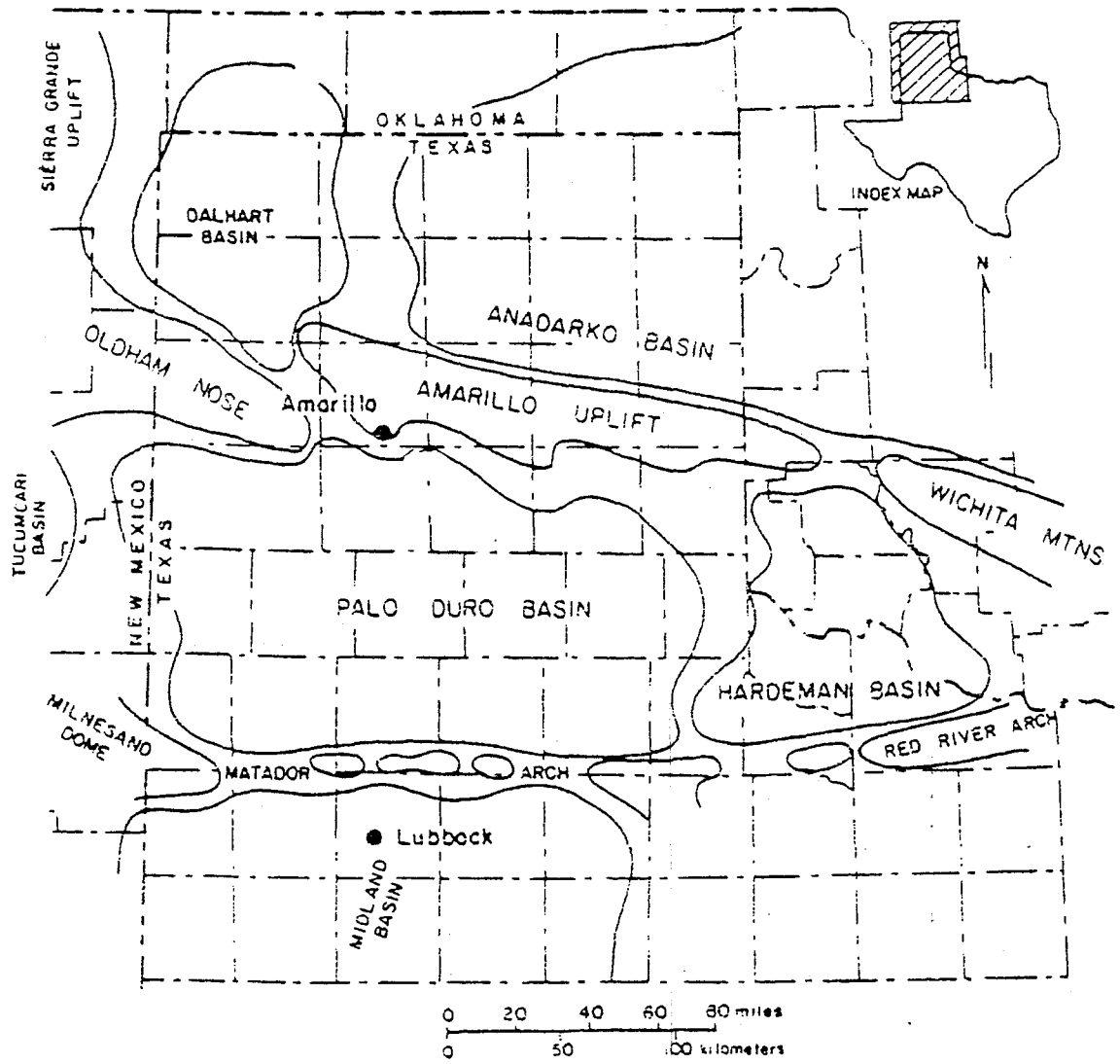
Figure 1. Map of Texas Panhandle area showing location of Palo Duro Basin.

SYSTEM	SERIES	GROUP	Palo Duro Basin FORMATION	Dalhart Basin FORMATION	General Lithology and depositional setting
QUATERNARY	HOLOCENE		alluvium, dune sand Playa	alluvium, dune sand Playa	
QUATERNARY	PLEISTOCENE		Tahoka "cover sands" Tule / "Playa" Blanco	"cover sands" "Playa"	Lacustrine clastics and windblown deposits
TERTIARY	NEOGENE		Ogallala	Ogallala	Fluvial and lacustrine clastics
CRETACEOUS			undifferentiated	undifferentiated	Marine shales and limestone
TRIASSIC		DOCKUM			Fluvial-deltaic and lacustrine clastics
PERMIAN	OCHOA		Dewey Lake	Dewey Lake	Sabkha salt, anhydrite, red beds, and peritidal dolomite
PERMIAN	OCHOA		Alibates	Alibates	Sabkha salt, anhydrite, red beds, and peritidal dolomite
PERMIAN	GUADALUPE	ARTESIA	Salado/Tansill	Artesia Group undifferentiated	Sabkha salt, anhydrite, red beds, and peritidal dolomite
PERMIAN	GUADALUPE	ARTESIA	Yates	Artesia Group undifferentiated	
PERMIAN	GUADALUPE	ARTESIA	Seven Rivers	Artesia Group undifferentiated	
PERMIAN	GUADALUPE	ARTESIA	Queen/Grayburg	Artesia Group undifferentiated	
PERMIAN	GUADALUPE		San Andres	Blaine	
PERMIAN	LEONARD	CLEAR FORK	Glorieta	Glorieta	
PERMIAN	LEONARD	CLEAR FORK	Upper Clear Fork	Clear Fork	
PERMIAN	LEONARD	CLEAR FORK	Tubb	undifferentiated Tubb-Wichita Red Beds	
PERMIAN	LEONARD	CLEAR FORK	Lower Clear Fork	undifferentiated Tubb-Wichita Red Beds	
PERMIAN	LEONARD	CLEAR FORK	Red Cave	undifferentiated Tubb-Wichita Red Beds	
PERMIAN	LEONARD	WICHITA			
PERMIAN	WOLFCAMP				Shelf and shelf-margin carbonate, basinal shale, and deltaic sandstone
PENNSYLVANIAN	VIRGIL	CISCO			Shelf and shelf-margin carbonate, basinal shale, and deltaic sandstone
PENNSYLVANIAN	MISSOURI	CANYON			Shelf and shelf-margin carbonate, basinal shale, and deltaic sandstone
PENNSYLVANIAN	DES MOINES	STRAWN			
PENNSYLVANIAN	ATOKA	BEND			
PENNSYLVANIAN	MORROW	BEND			
MISSISSIPPIAN	CHESTER				Shelf carbonate and chert
MISSISSIPPIAN	MERAMEC				Shelf carbonate and chert
MISSISSIPPIAN	OSAGE				
ORDOVICIAN		ELLENBURGER			Shelf dolomite
CAMBRIAN ?					Shallow marine(?) sandstone
PRECAMBRIAN					Igneous and metamorphic

Figure 2. Stratigraphic column and general lithologies for the Palo Duro and Dalhart Basins.

Figure 3. Accepted subdivision of Mississippian rocks in the Palo Duro Basin. Possible Kinderhook deposits (not shown) occur sporadically at the base. Amerada Petroleum Corporation, Lafayette Hughes Trustee No. 1, Hall County, Texas (BEG No. 18).

Figure 4. Map of the Texas Panhandle area showing location of the Palo Duro and Hardeman Basins and four cored wells. Donley 3: Service Drilling Company, Kathleen C. Griffin No. 1. Childress 10: Wes-Tex, Kewanee, and Coastal States Producing Co., Steve Owens No. 1-A, Hardeman 42: Sun Oil Co., Quanah Townsite Unit No. 1. Hardeman 44: Standard Oil Co. of Texas, Coffee No. 1.

Figure 5. Probable correlation of 4 wells for which conodonts were recovered. No horizontal scale. Wells and line of section shown in Figure 1.

Figure 6. Distribution of lower Pennsylvanian facies and interpreted depositional environments.

Figure 7. Isolith map of total carbonate in the lower part of the Pennsylvanian System.

Figure 8. Distribution of upper Pennsylvanian facies and interpreted depositional environments.

Figure 9.   Isolith map of total carbonate in the upper part of the Pennsylvanian
System.

Figure 10. Location of oil fields in Oldham and western Potter Counties. Reservoirs in these fields are Pennsylvanian granite wash of carbonate.

Figure 11. Structure countour map on the top of the upper granite wash, the reservoir for Lambert, Hryhor, and Sundance Fields (Railfoad Commission of Texas, 1982). See Figure 5 for location.

Figure 12. Net thickness of the 0-5% porosity range for the Brown Dolomite.

Figure 13.   Net thickness of the 5-10% porosity range for the Brown Dolomite.

Figure 14. Net thickness of the 10-15% porosity range for the Brown Dolomite.

Figure 15. Net thickness of the 15-20% porosity range for the Brown Dolomite.

Figure 16.   Net thickness of the 20-25% porosity range for the Brown Dolomite.
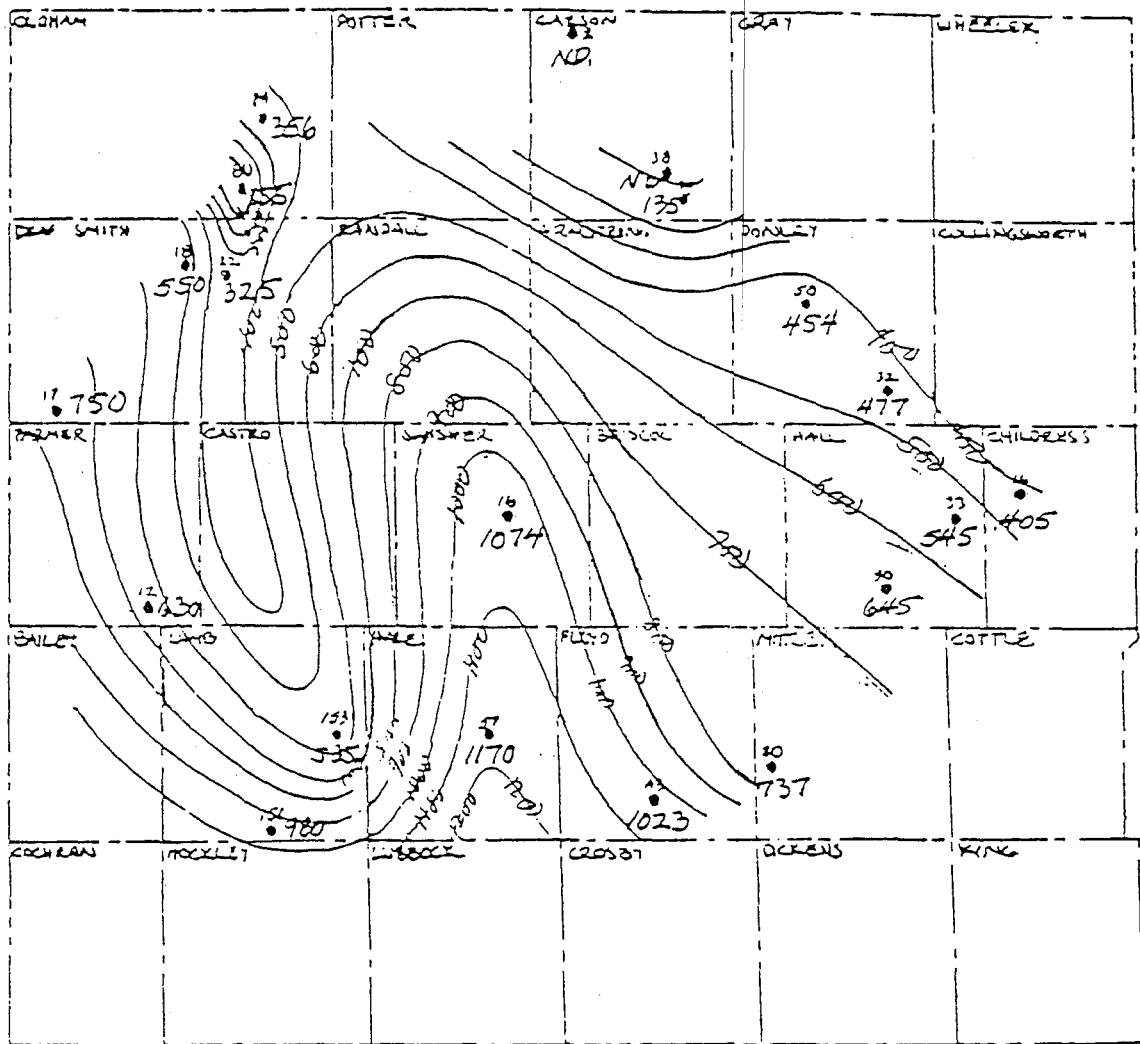
EXPLANATION

43 - BEG F
● - NEUTRON-DENSITY LOG
11.20 - WEIGHTED AVERAGE POROSITY (%)

CONTOUR INTERVAL = 1% POROSITY

N

0 _____ 40 miles
0 _____ 40 KM

———— LOWER WOLFCAMPIAN SHELF MARGIN

— — MIDDLE WOLFCAMPIAN SHELF MARGIN

•••••• UPPER WOLFCAMPIAN SHELF MARGIN

(HANDFORD, 1980)
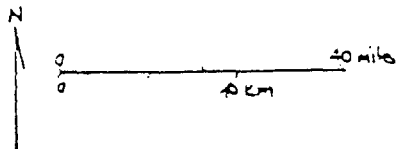
FIGURE 17.

Figure 18. Net thickness of the 0-5% porosity range for the Wolfcamp (below the Brown Dolomite).
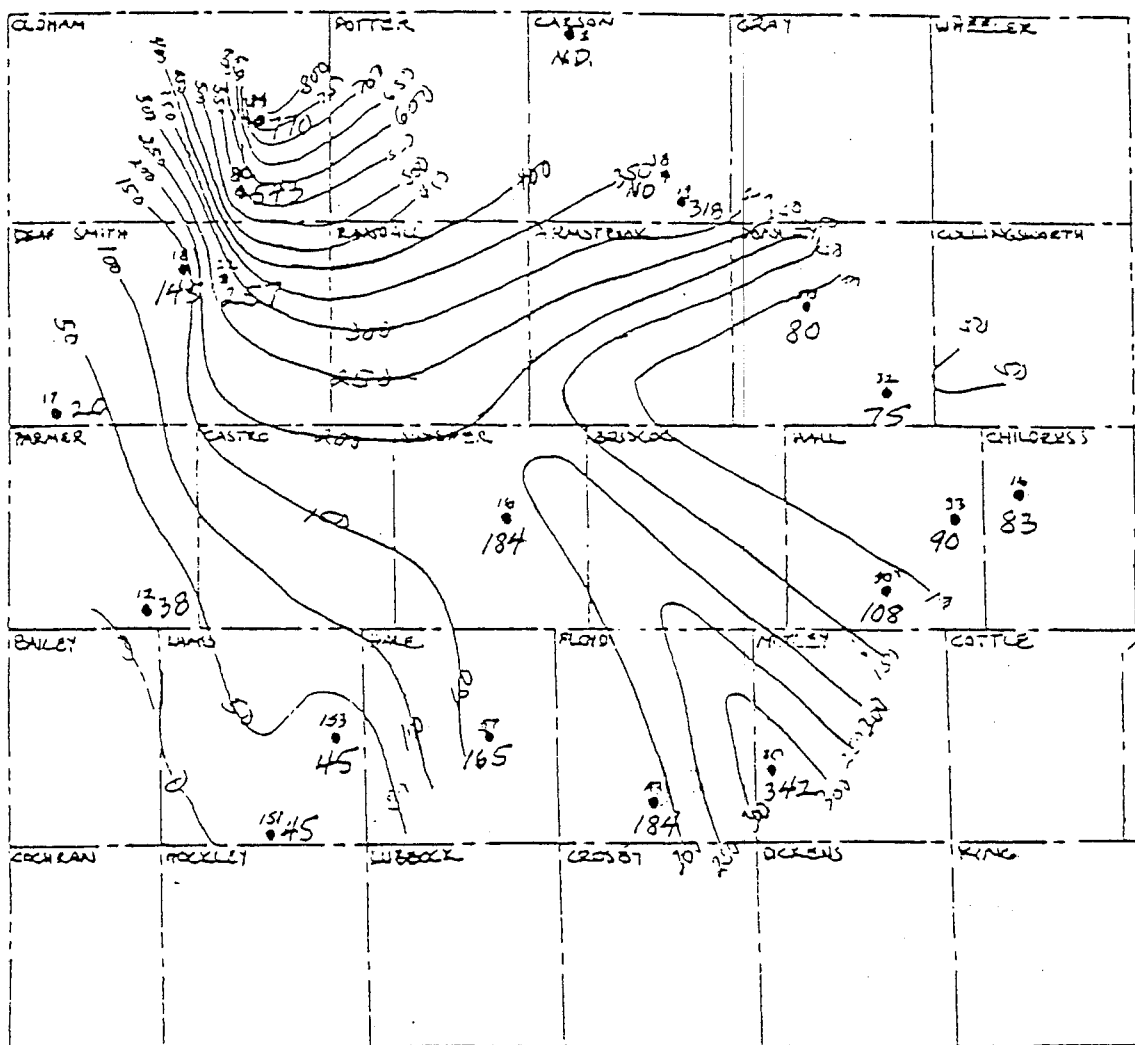
Figure 19. Net thickness of the 5-10% porosity range for the Wolfcamp (below the Brown Dolomite).

Figure 20. Net thickness of the 10-15% porosity range for the Wolfcamp (below the Brown Dolomite).
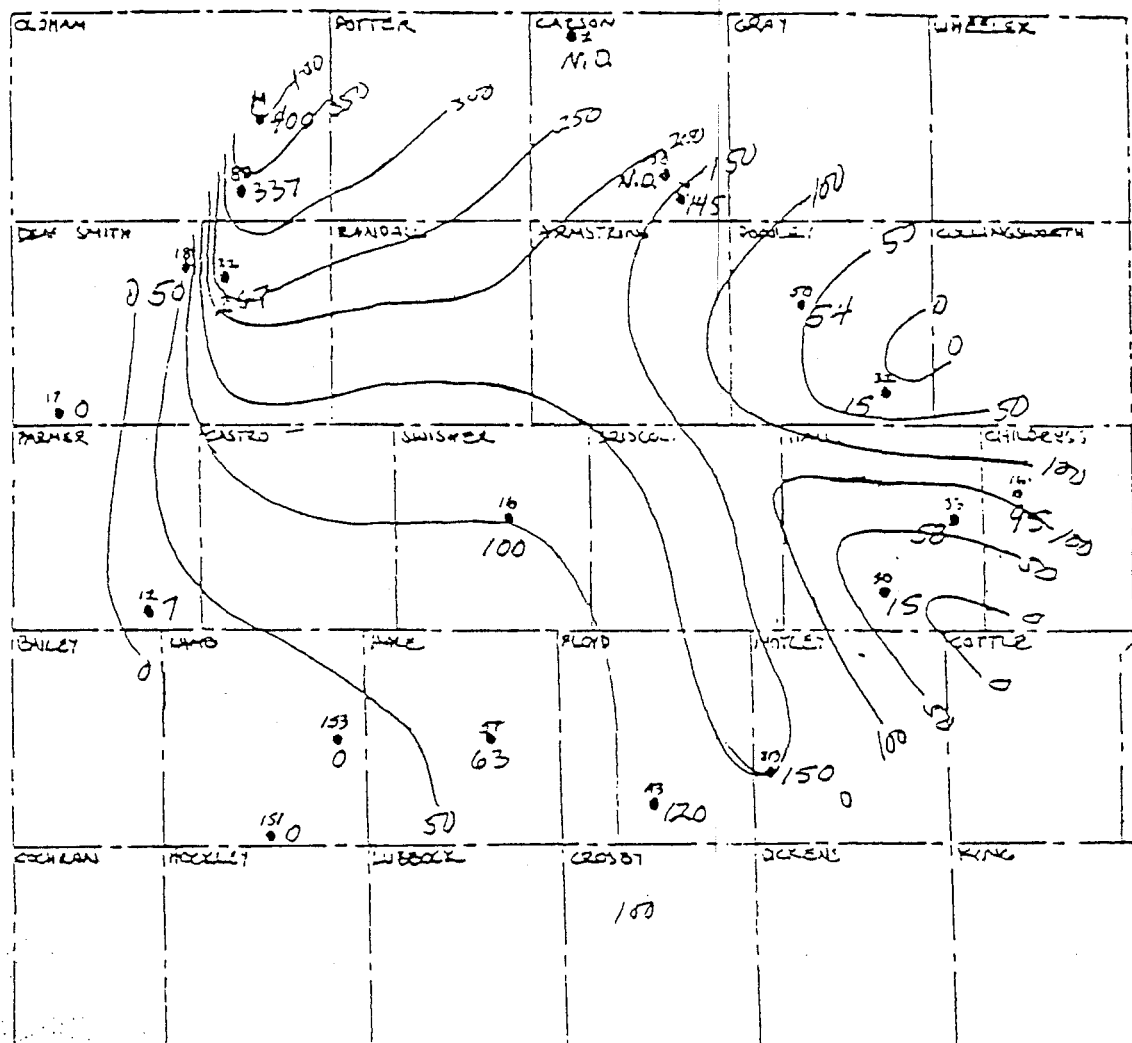
Figure 21. Net thickness of the 15-20% porosity range for the Wolfcamp (below the Brown Dolomite).
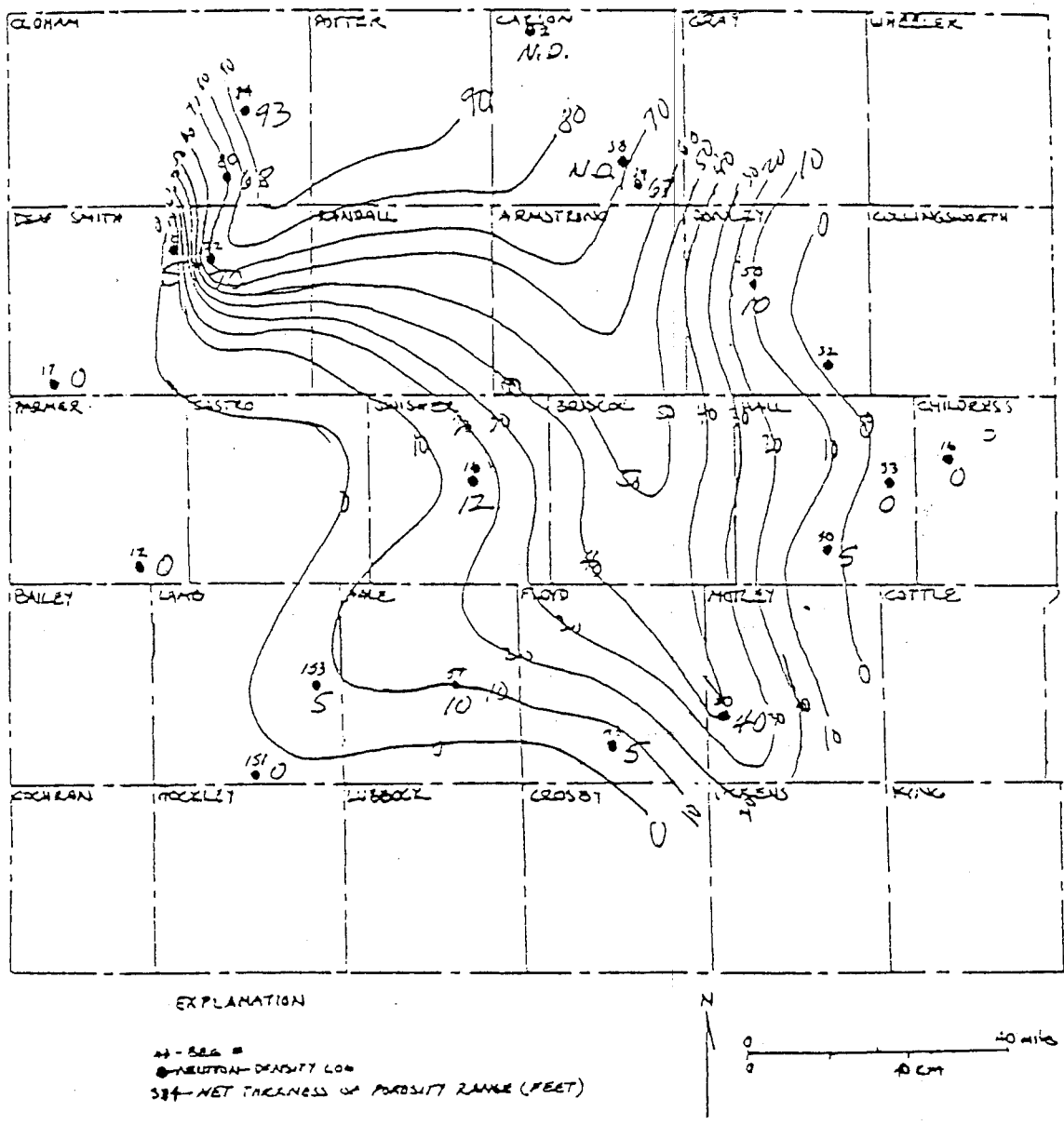
Figure 22. Net thickness of the 20-25% porosity range for the Wolfcamp (below the Brown Dolomite).

EXPLANATION

H - SEA =
●-NEUTRON-DENSITY LOG
SEA - NET THICKNESS OF POROSITY RANGE (FEET)

C. I. = 10'

Figure 23. Net thickness of the 25-30% porosity range for the Wolfcamp (below the Brown Dolomite).
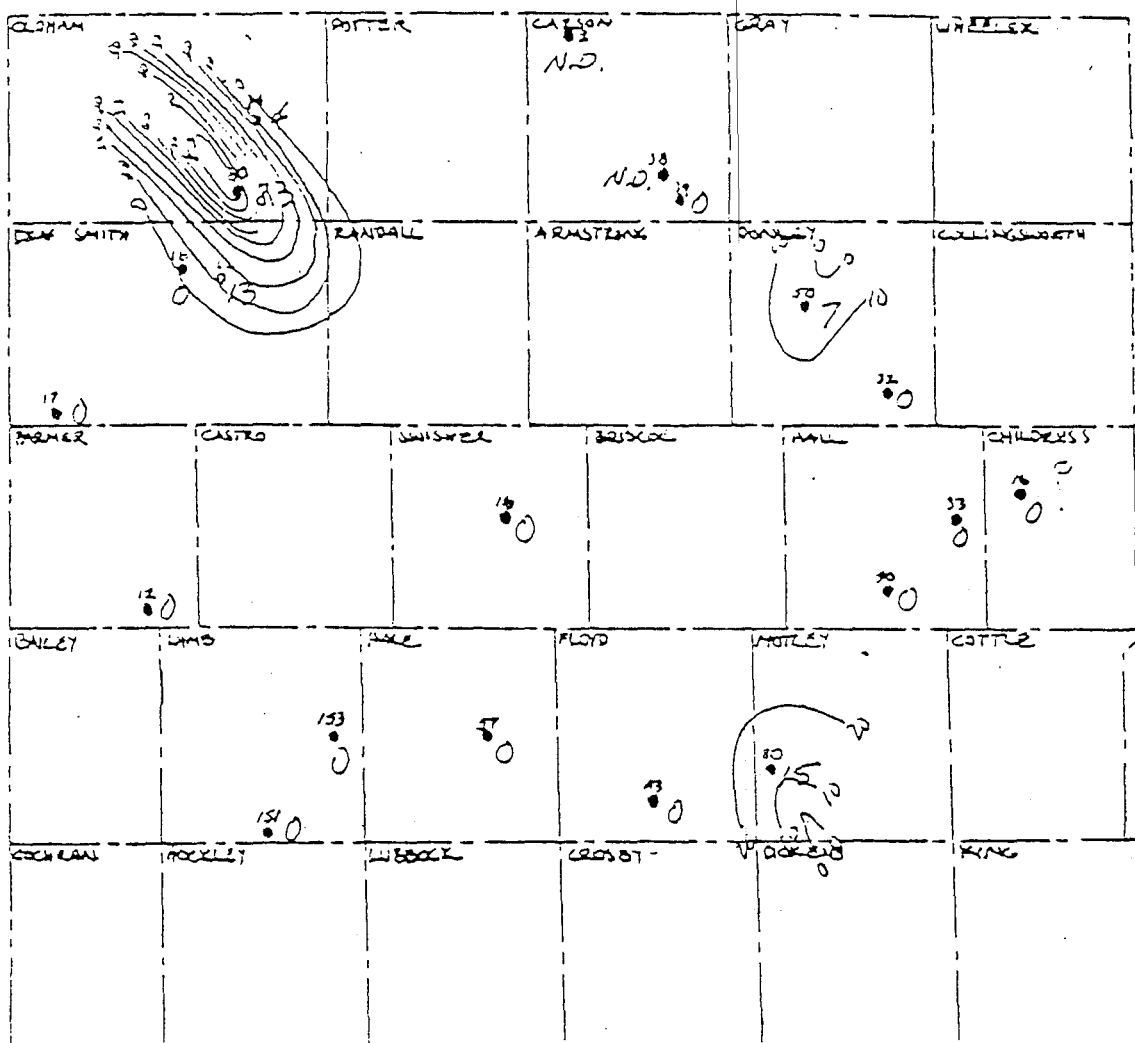
EXPLANATION

N-LOG =
●-NEUTRON-DENSITY LOG
574-NET THICKNESS OF POROSITY RANGE (FEET)

C. I. = 10'

N

0 _____ 40 miles
0   PCM
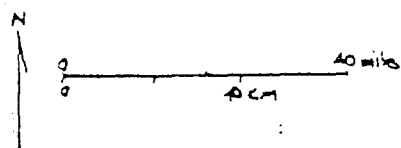
Figure 24. Net thickness of the >30% porosity range for the Wolfcamp
(below the Brown Dolomite).
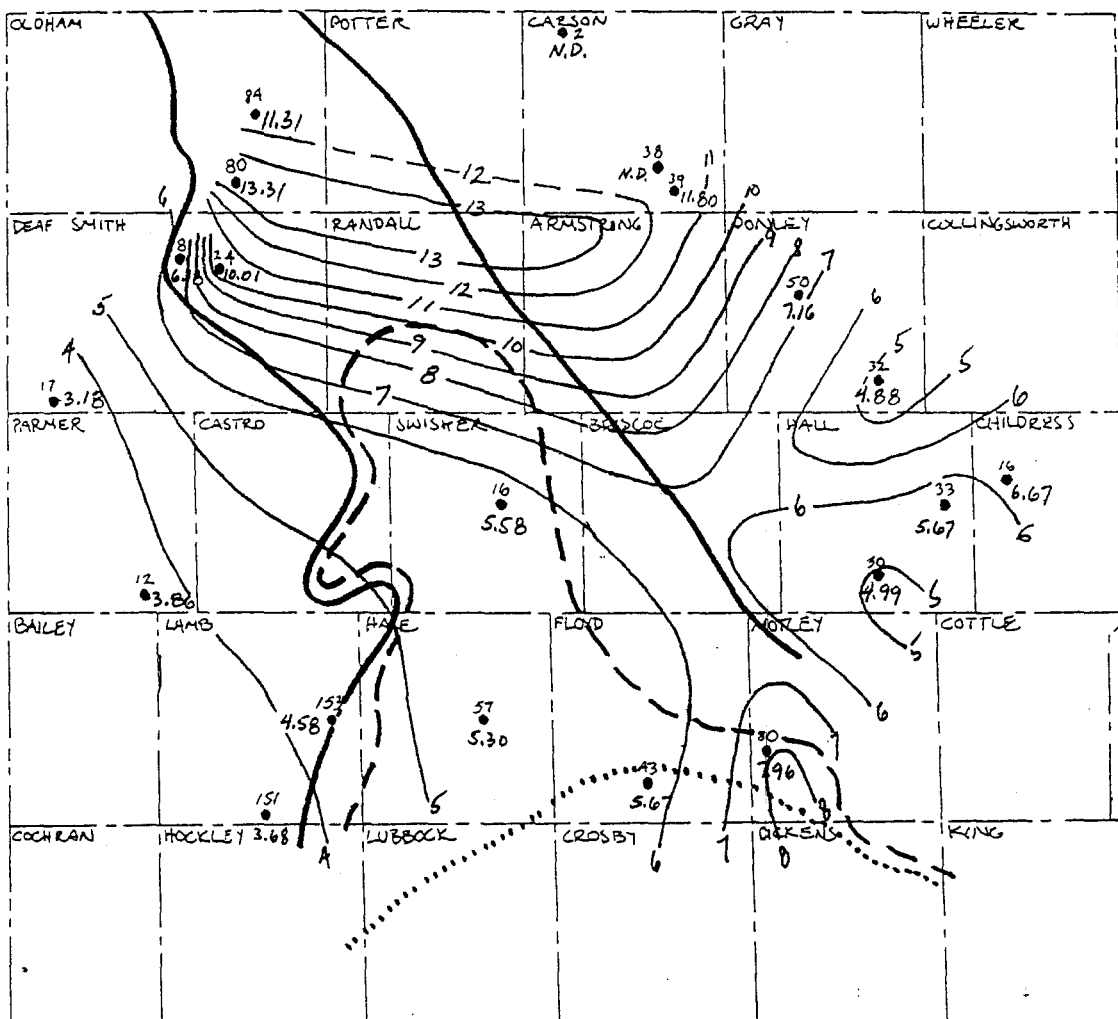
EXPLANATION

43 - BEG #
● - NEUTRON-DENSITY LOG
11.20 - WEIGHTED AVERAGE POROSITY (%)

CONTOUR INTERVAL = 1% POROSITY

N

0 _____ 40 mile
0 _____ 40 KM

———— LOWER WOLFCAMPIAN SHELF MARGIN

— — MIDDLE WOLFCAMPIAN SHELF MARGIN

• • • • • UPPER WOLFCAMPIAN SHELF MARGIN

(HANDFORD, 1980)

FIGURE 25.
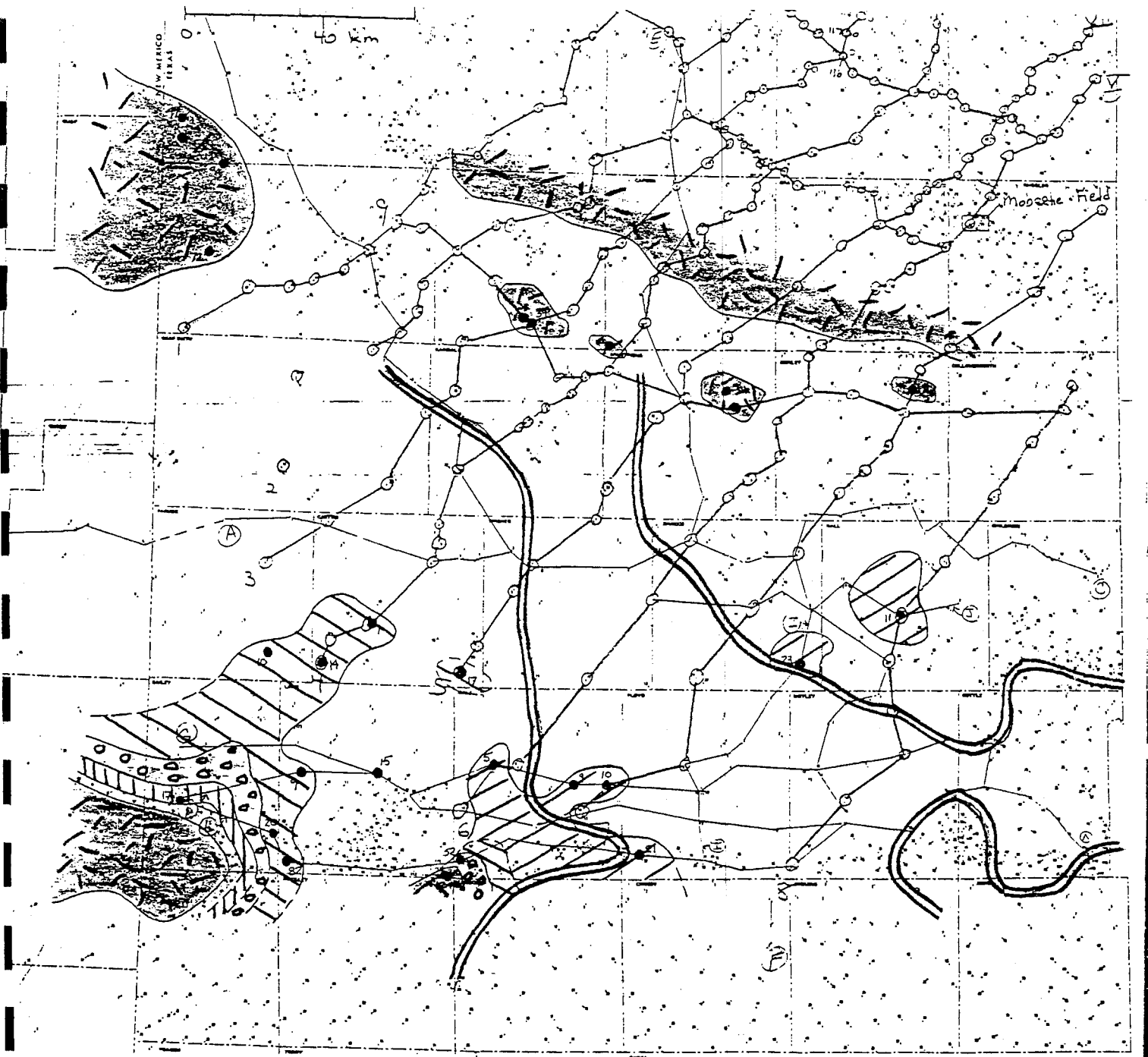
FIGURE 26

FIGURE 27, WOLFCAMPIAN SUBCROP

Legend:

- PRECAMBRIAN
- ORDOVICIAN
- MISSISSIPPIAN
- PENNSYLVANIAN (DESMOINESIAN)
- PENNSYLVANIAN (MISSOURIAN)
- PENNSYLVANIAN (VIRGILIAN – UNCONFORMABLE TOP)
- PENNSYLVANIAN (VIRGILIAN) CONTINUOUS DEPOSITION
- PENNSYLVANIAN SHELF MARGINS

FIG. 28.
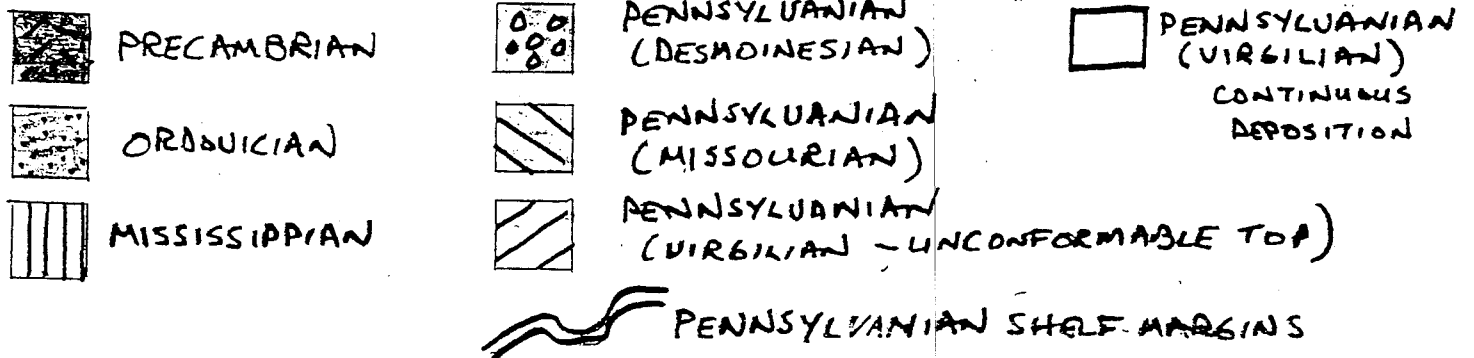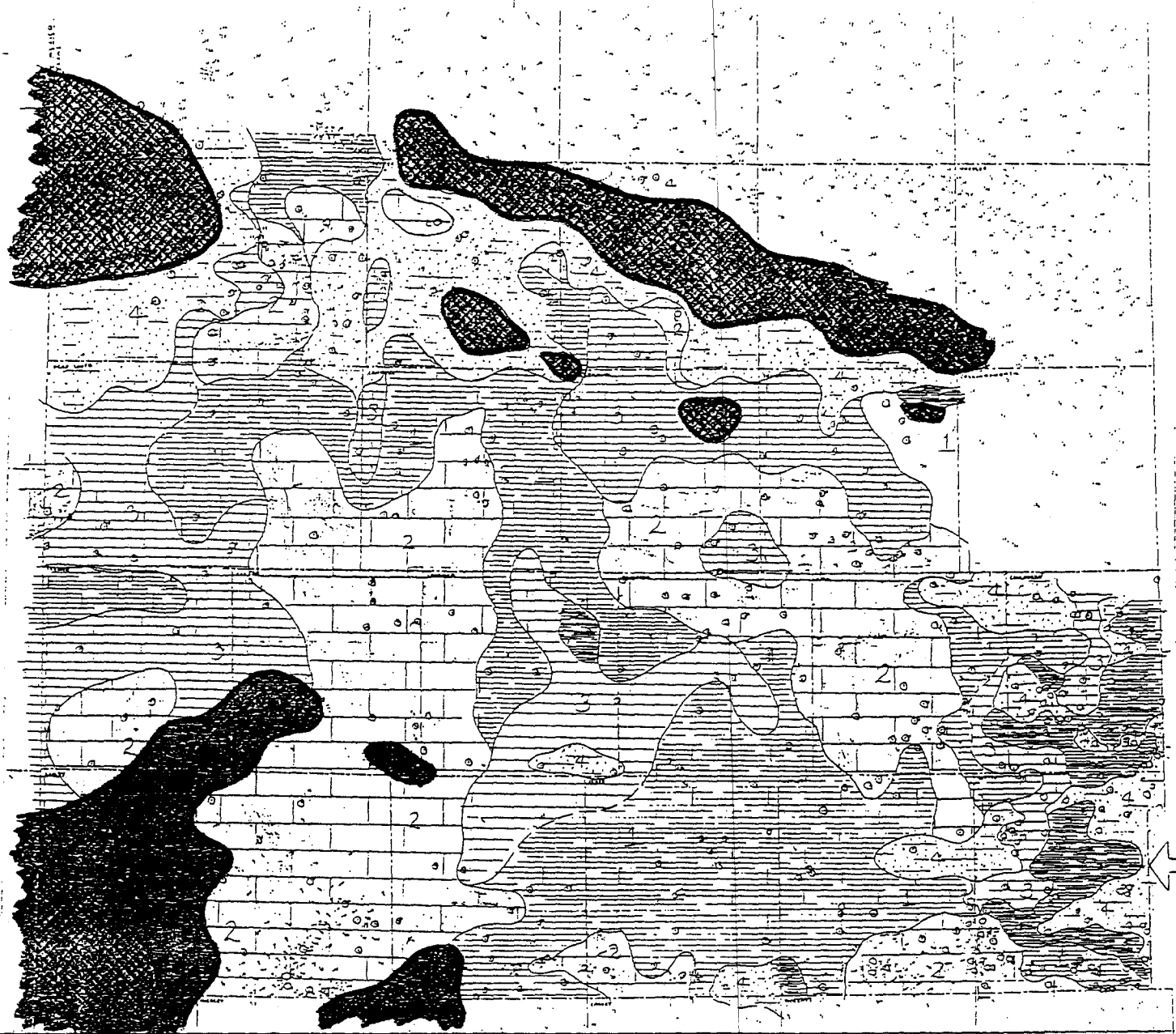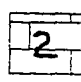
FIGURE 28. LITHOFACIES OF UPPER VIRGILIAN

1 — THIN (<100') LS OVERLYING SH

ABSENT

2 — MASSIVE LS (>100')
SHELF AND SHELF MARGIN (>75% $CaCO_3$)

3 — MIXED LS AND SHALE

4 — CLASTICS: SANDSTONE, GRANITE WASH, SHALE

5 — SHALE (>75%)

Figure 29. Lithologies of lowermost (approximately 100 ft) Wolfcampian.

Legend:
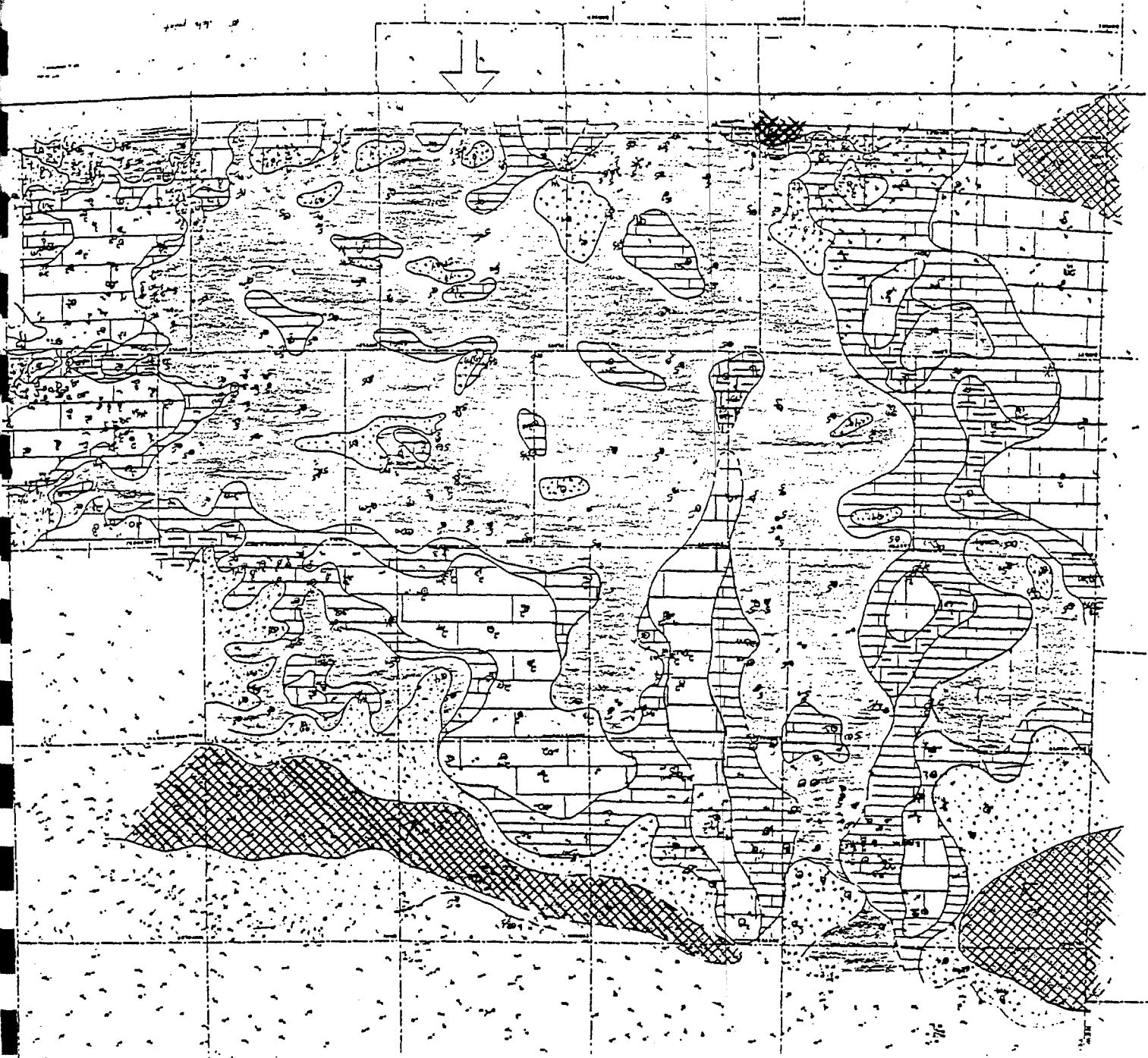
- >75% CO₃ Massive shelf & shelf margin carbonate (>100')
- Mixed shelf limestone & shale
- Thin shale (<100') under massive carbonate
- Clastic deposits, sand or granite wash & shale
- >75% shale - basinal
- Lower Wolfcampian absent
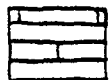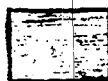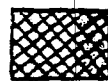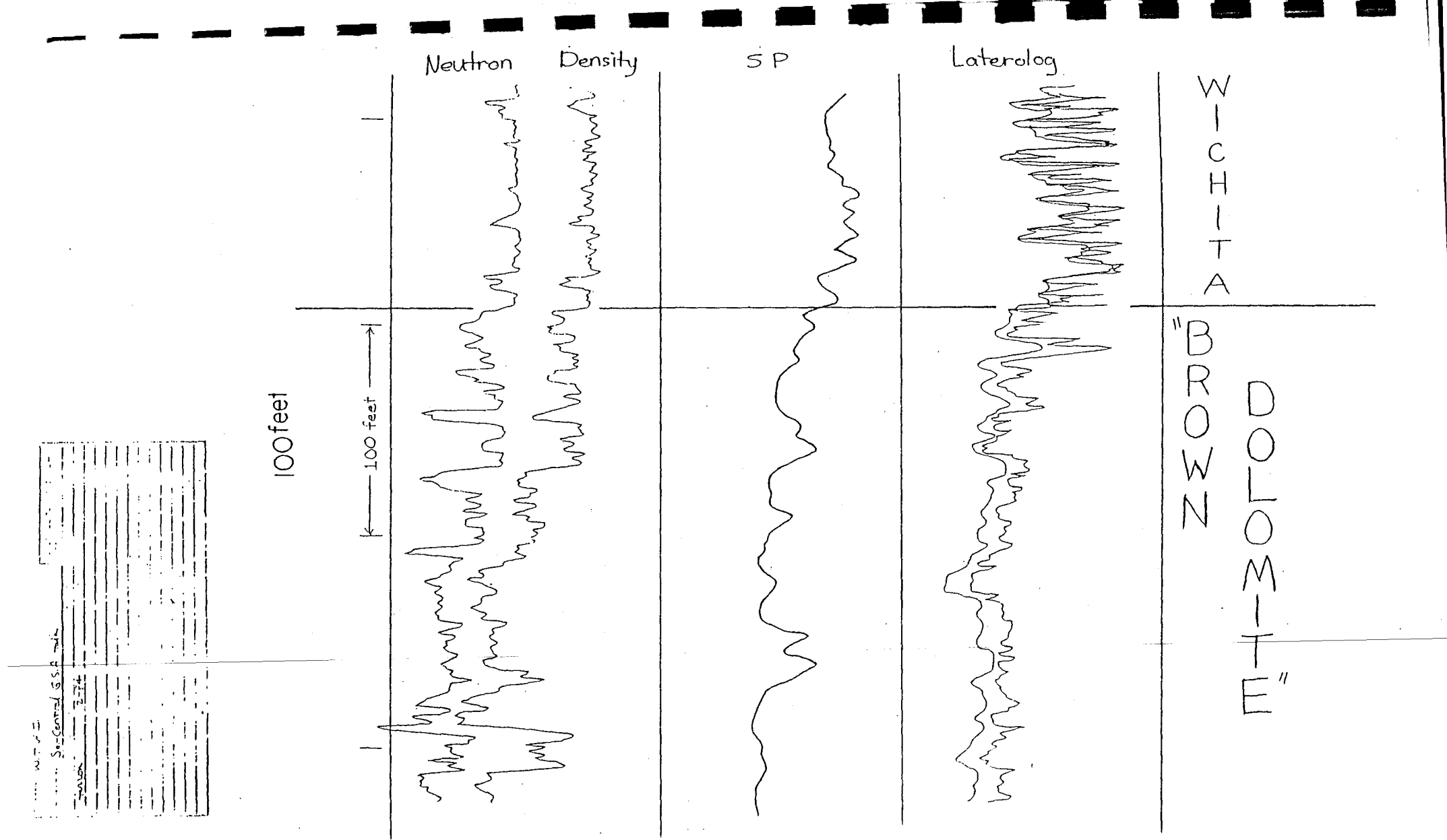
Figure 30. Typical electric log signatures at the top of the Wolfcampian, Palo Duro Basin.

FiG. 31.

ANHYDRITE
PRESENT

ANHYDRITE
ABSENT

NOT STUDIED
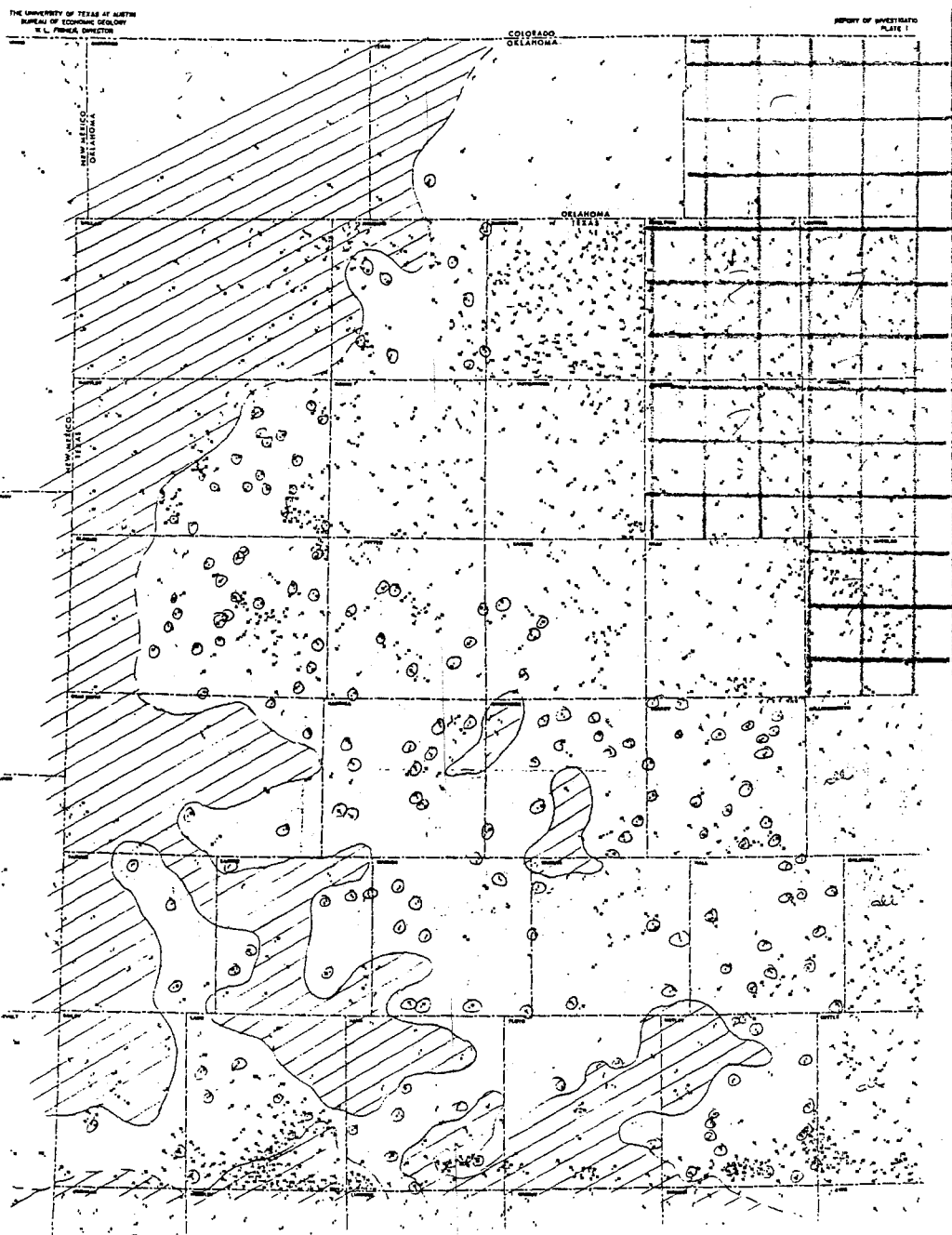
FIGURE 31.   DISTRIBUTION OF ANHYDRITE IN LOWER WICHITA.
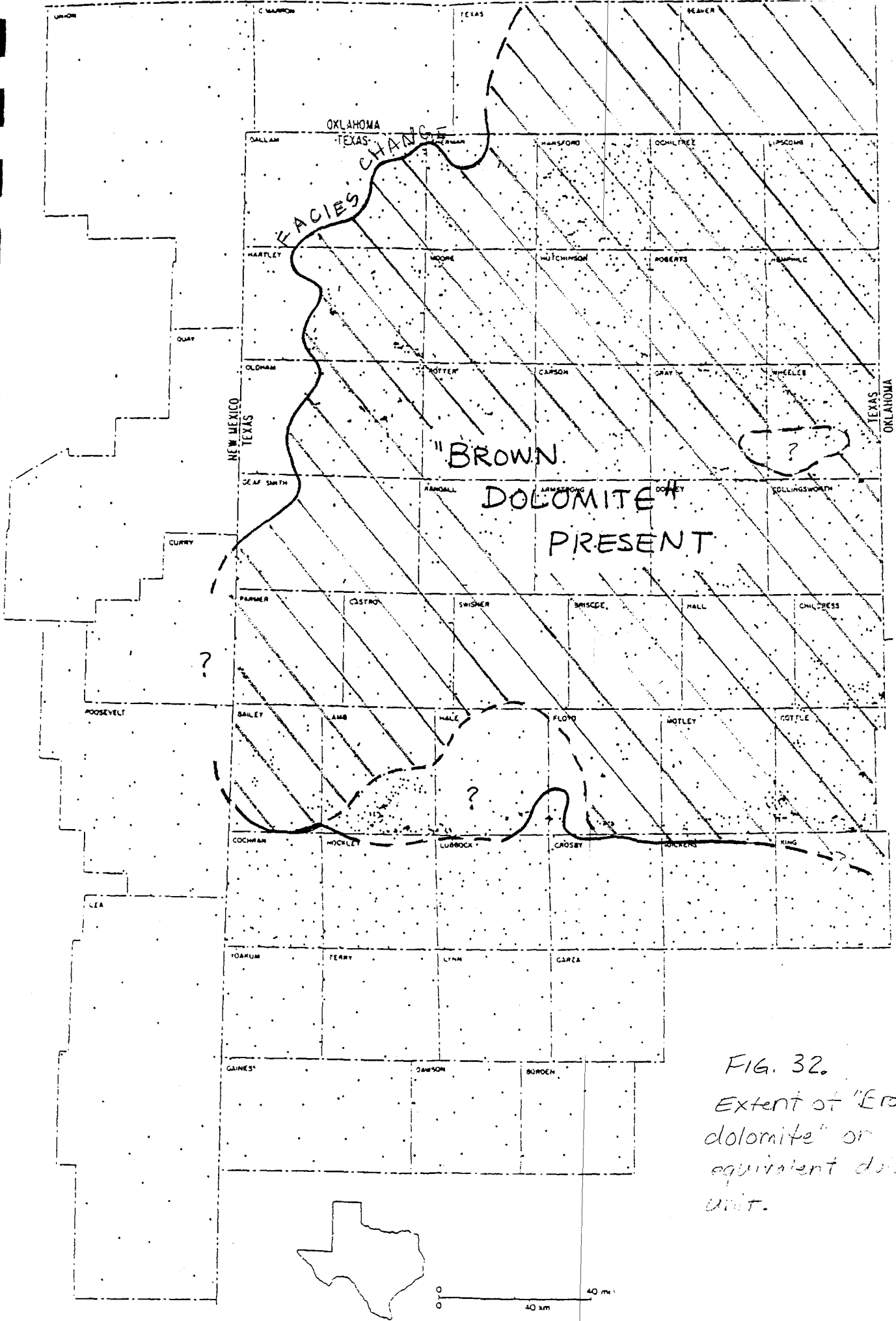
FIG. 32.

FIG. 32.
Extent of "Brown
dolomite" or
equivalent clastic
unit.
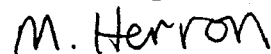
FIGURE 33. ISOPACH OF "BROWN DOLOMITE"

M. Herron

EARLY WOLFCA SHELF MARGIN

LATE WOLFCAN SHELF MARGIN

- ABSENT

400-600'

600-800'

800-1000'

>1000'

C.I.-200'
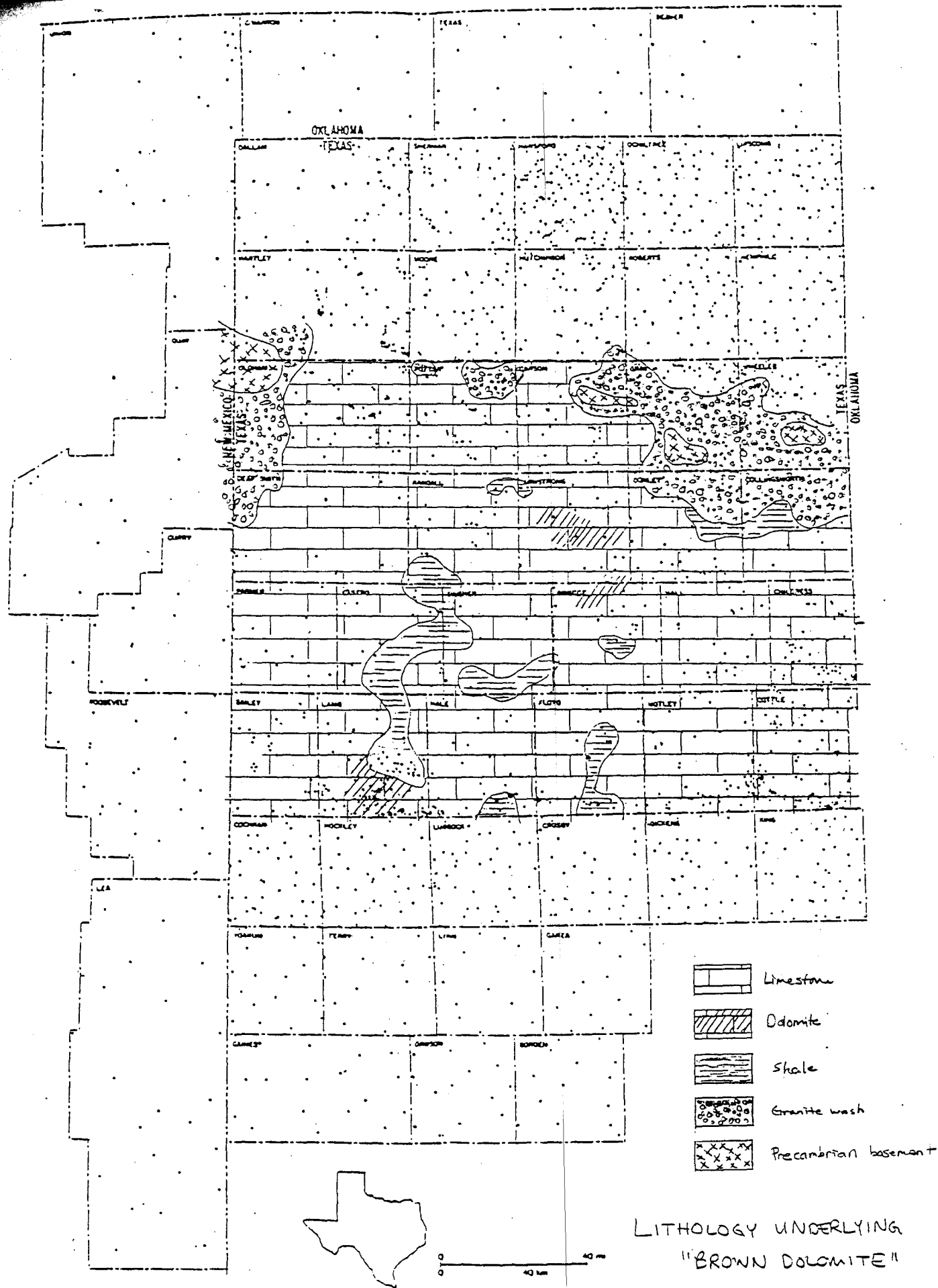
Figure 34. Lithology of unnamed unit underlying the "Brown Dolomite" in the Palo Duro Basin.
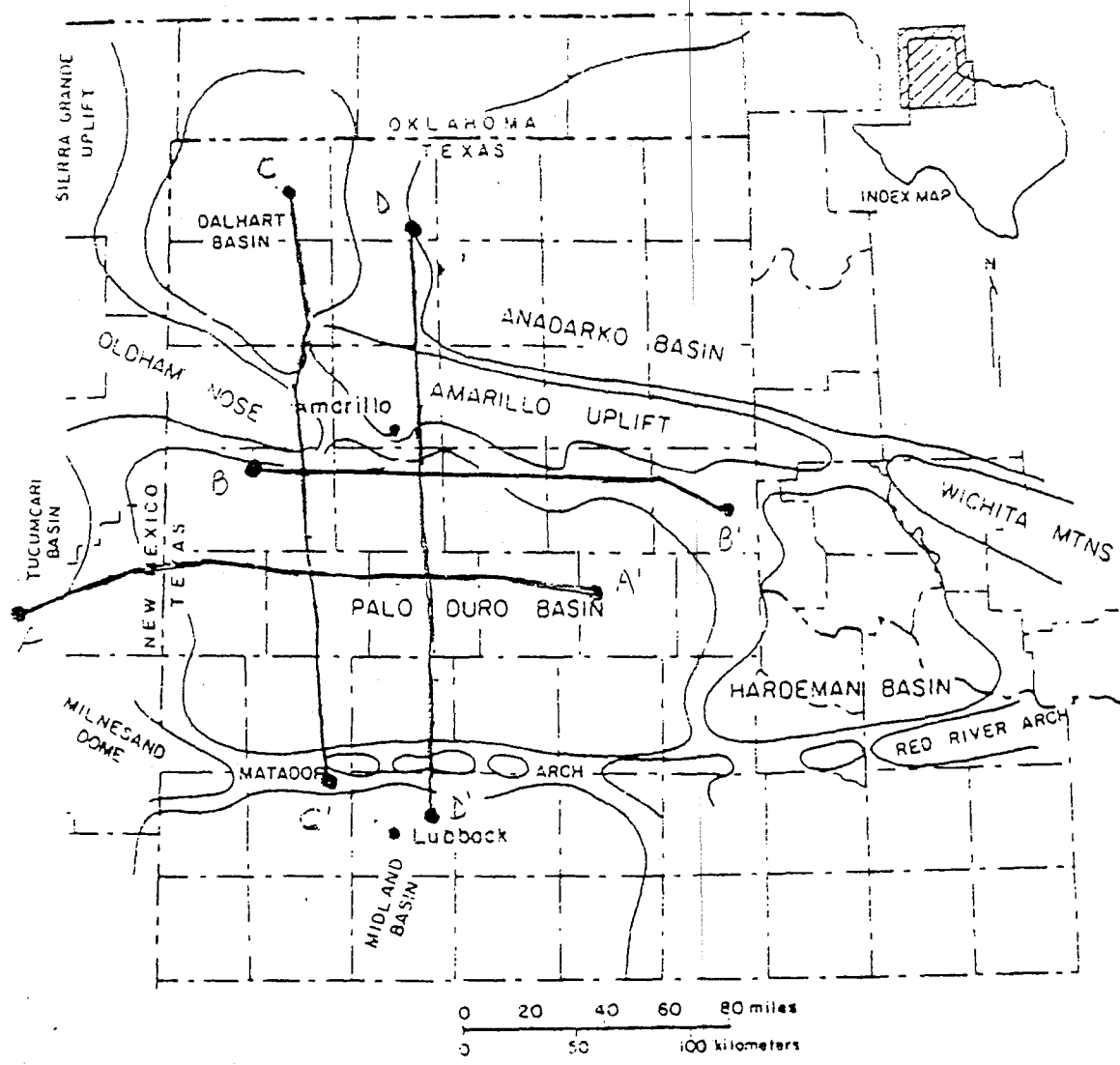
Figure 35. Basement structures and location of San Andres Formation cross sections and DOE wells, Texas Panhandle.
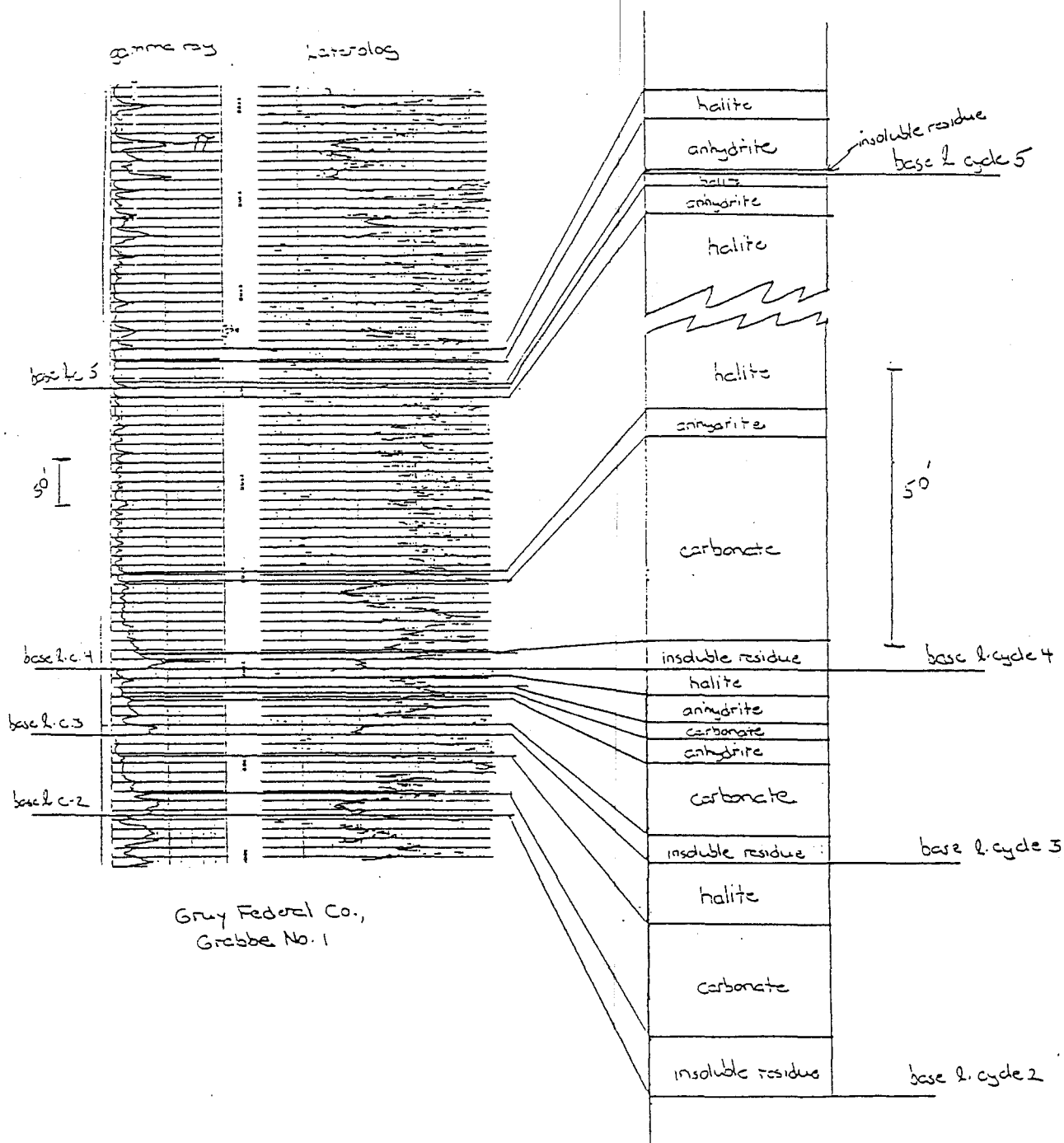
Figure 40. Ideal cyclic vertical facies sequence and gamma ray log pattern, San Andres Formation, Palo Duro Basin.

Figure 41. Depositional environments in lower San Andres unit 4 carbonate in Oldham and Deaf Smith Counties. The left column of each well shows percent lithology; the center column shows fabrics; the right column shows an interpretation of fabrics listed from right to left in interpreted order of increasing salinity. The limestone intervals show no pattern of salinity increase, and the fluctuation of facies is best interpreted as due to local migration of higher and lower energy facies in a carbonate shelf facies mosaic.
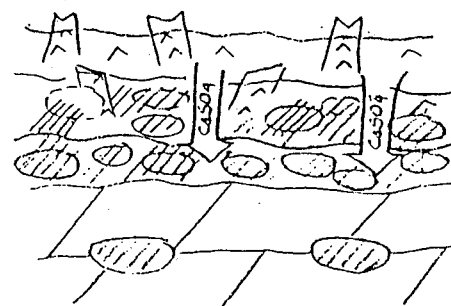
1

As salinity increases, gypsum is deposited above carbonate
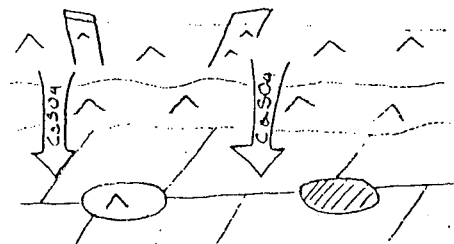
Sulfate-saturated brines penetrate unconsolidated carbonates and deposit replacive/displacive nodules of gypsum or anhydrite
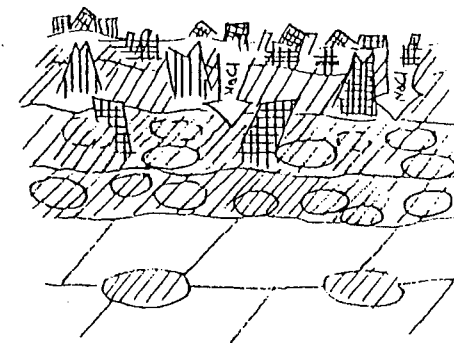
2

Gypsum deposition continues

Sulfate-saturated brines penetrating previously deposited gypsum at shallow burial depths dehydrates gypsum to anhydrite. During alteration nodular fabric develops

3

Increasing restriction increases salinity to halite saturation

Halite-saturated brines penetrating previously deposited gypsum at shallow burial depths replace remaining gypsum with halite but do not effect anhydrite. The halite replacement therefor effects the uppermost beds and large gypsum crystals which were slow to dehydrate

Figure 42. Model for the origin of the sequence of fabrics observed in the anhydrite parts of cycles. The salinity of the water in the brine pool influences the diagenesis of the previously deposited sediments.
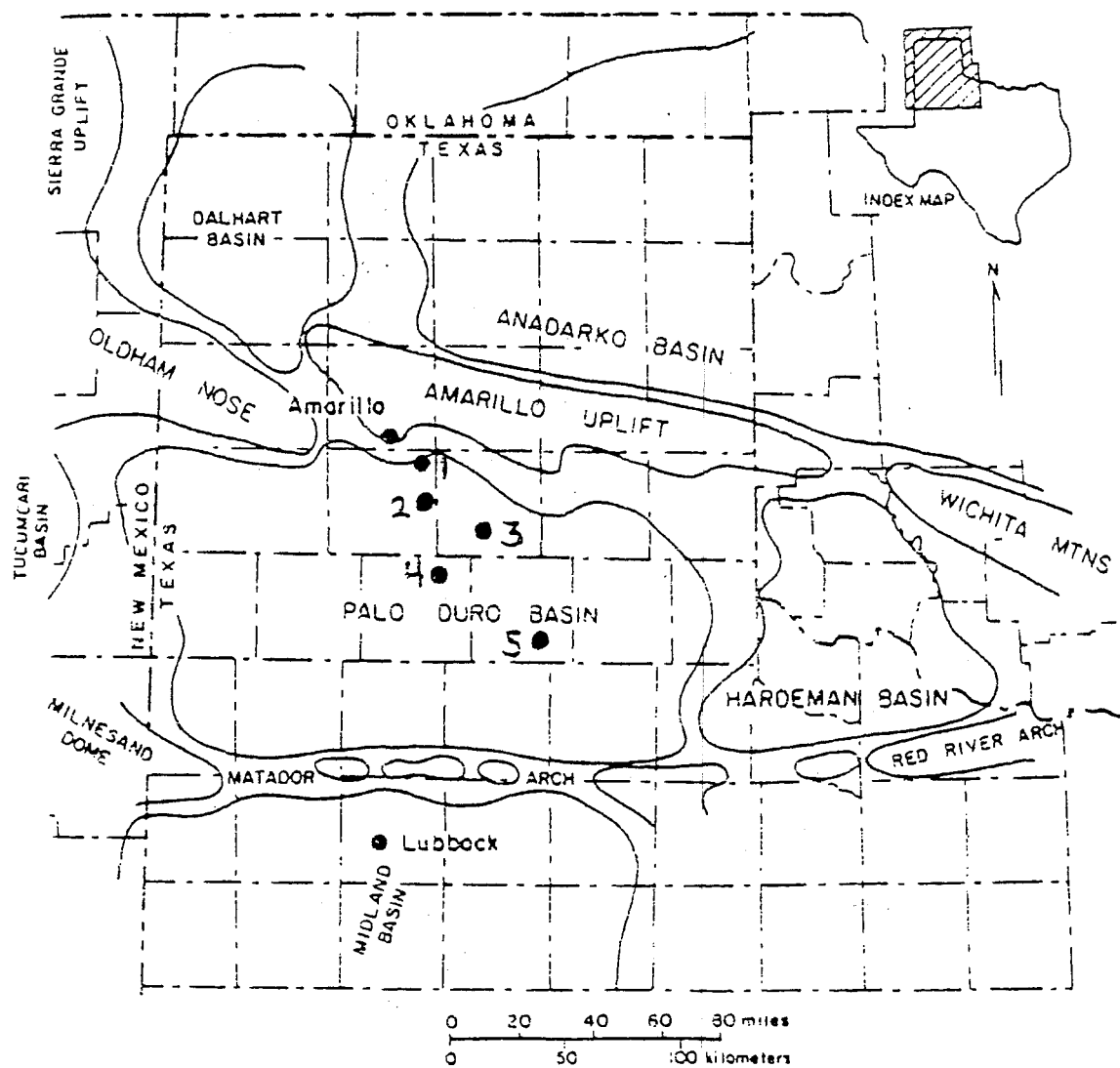
Figure 52. Structural elements in the Texas Panhandle Region (after Nicholson, 1960), and locations of measured sections and volcanic ash beds in the Quartermaster and Dewey Lake Formations. 1: DOE/Gruy Federal, Rex H. White #1; 2: Palo Duro Canyon State Park, section K-3-83; 3: Texas Highway 207/117 crossing Palo Duro Canyon, section K-4-83; 4: DOE/Gruy Federal, D. Grabbe #1; 5: Caprock Canyons State Park, sections K-1-83, K-2-83 and K-5-83.
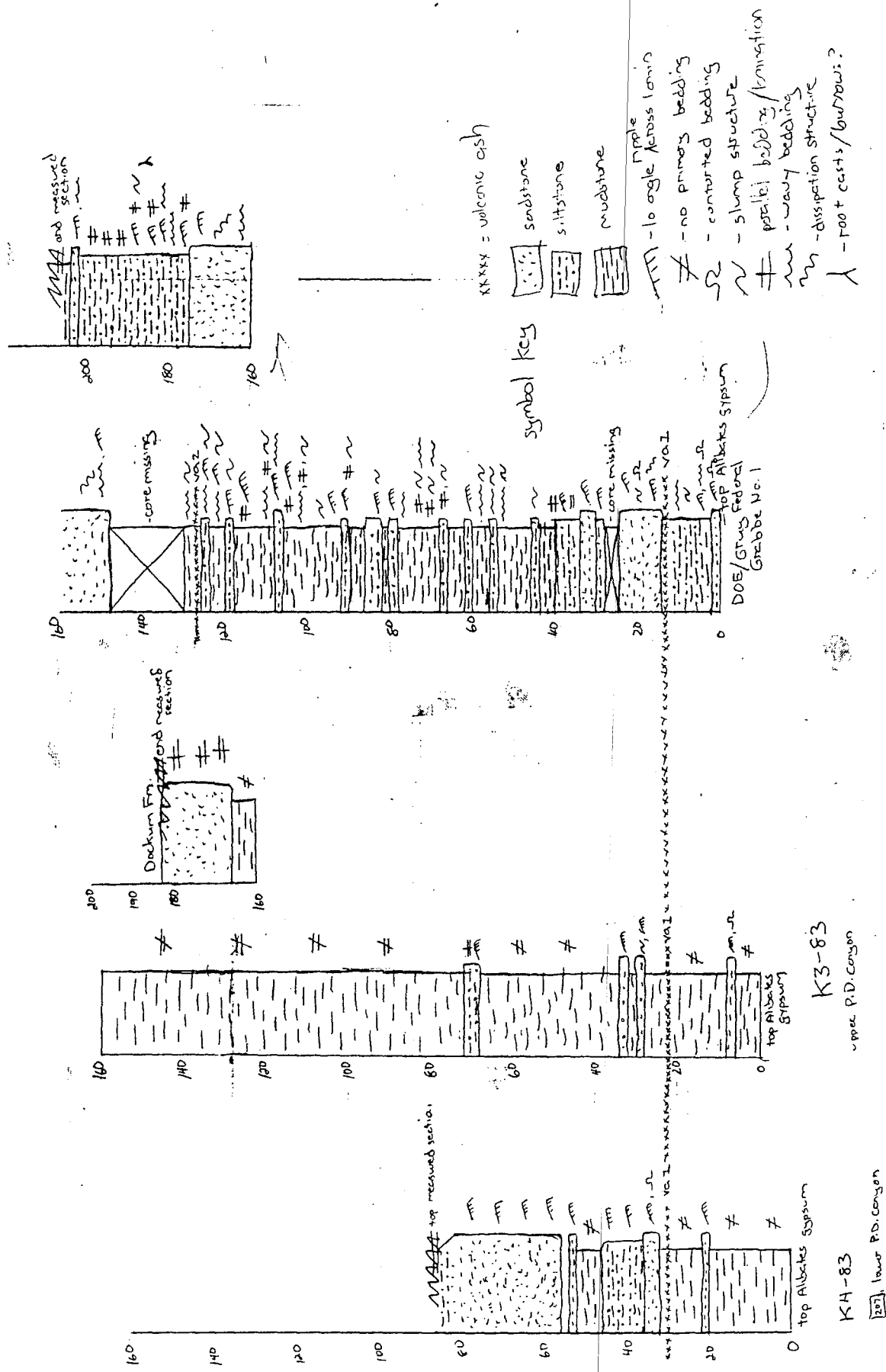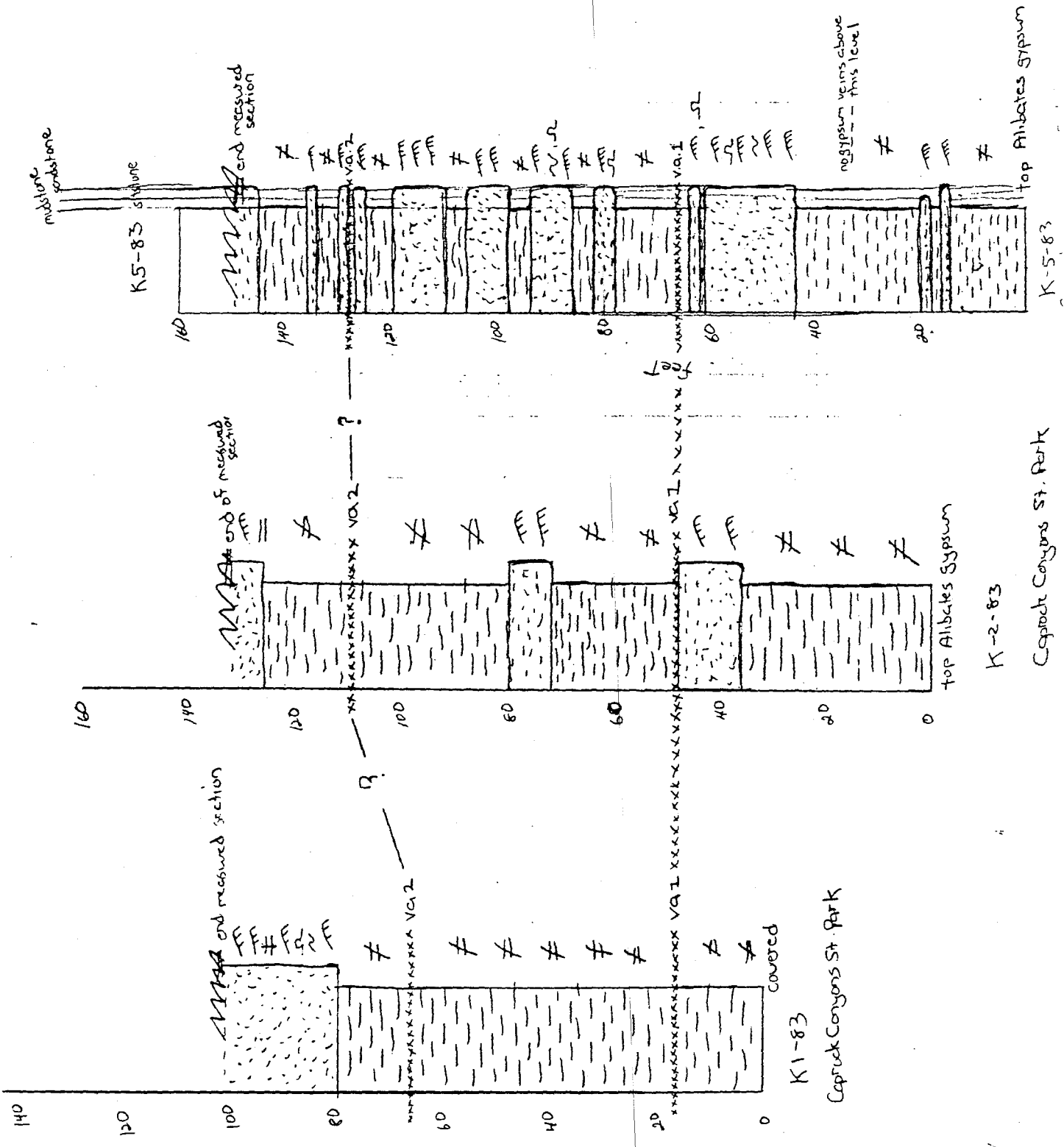
Figure 53

Symbol Key

KKKK = volcanic ash

sandstone
siltstone
mudstone

- lo angle ripple across lamina
- no primary bedding
- contorted bedding
- slump structure
- parallel bedding/lamination
- wavy bedding
- dissipation structure
- root casts/burrows?

Fig. 34.

K-5-83

mudstone
sandstone
end measured section

no gypsum veins above
— this level

top Alibates gypsum

Caprock Canyons St. Park

K-5-83

K-2-83

end of measured section

top Alibates Gypsum

Caprock Canyons St. Park

K-2-83

K-1-83

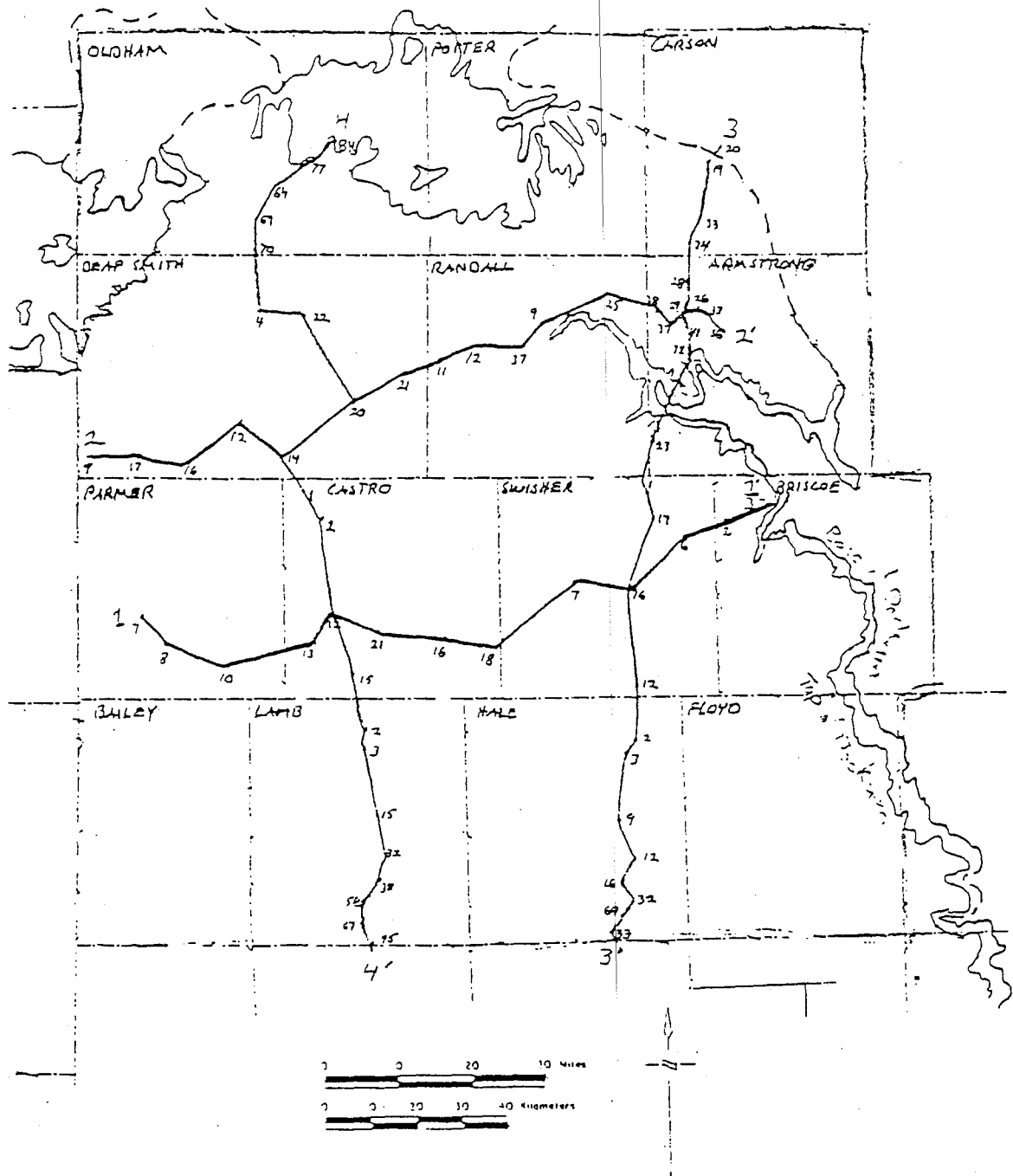end measured section

covered

Caprock Canyons St. Park

K-1-83

Figure 56. Outcrop areas of the Dockum Group and locations of principal cross sections in Palo Duro Basin used for this report.
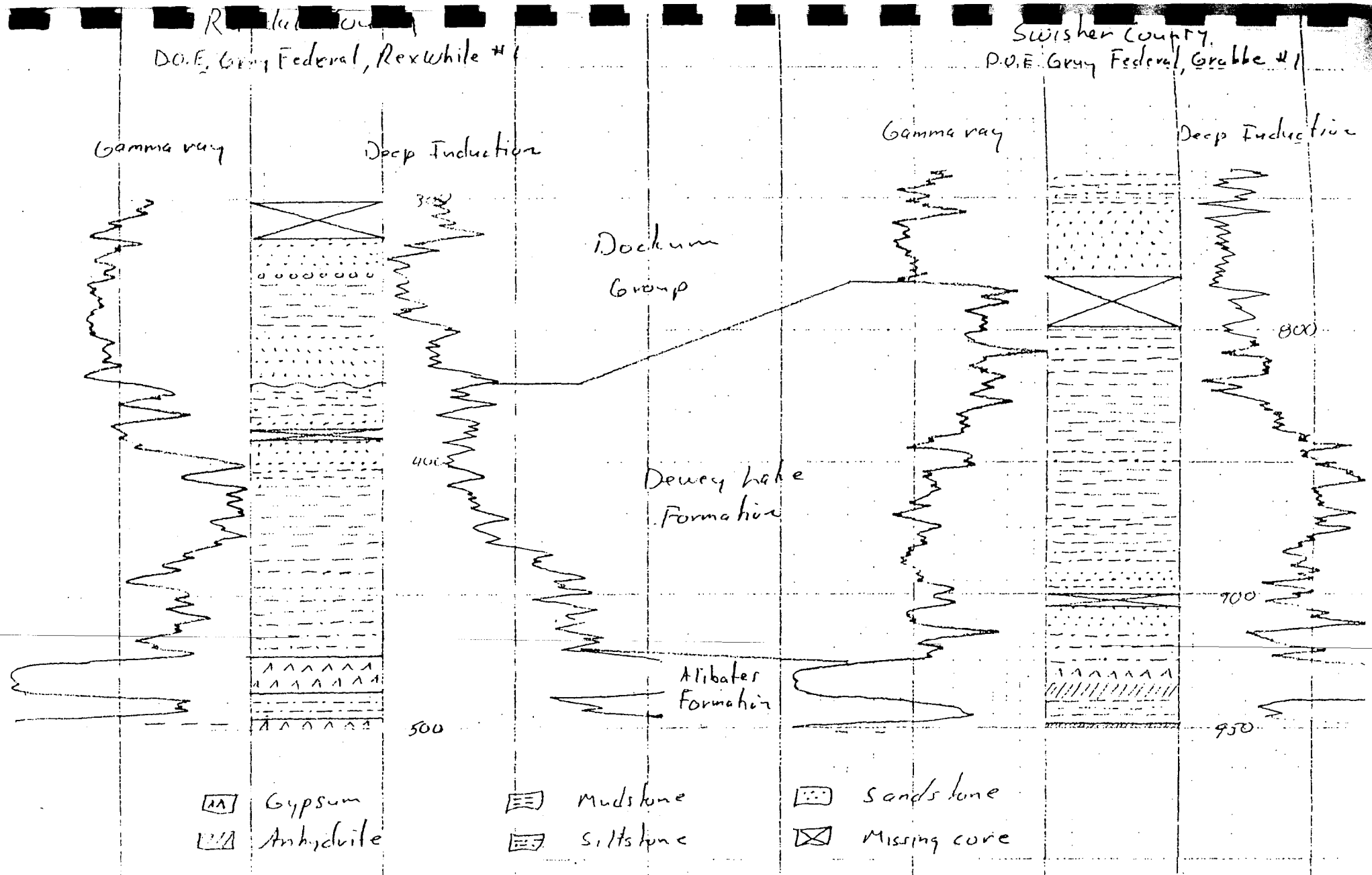
Figure 61. Correlation of the Dewey Lake Formation and Dockum Group based on lithology and geophysical well log patterns, Rex White #1 (Randall #25) and Grabbe #1 (Swisher #17).

1 - 776.5 ⎫
   751.8 ⎬ transition
   740.9 ⎭

   72.5.8
5 - 709.9
   658.8
   653.0
   627.0
   621.0
10 - 583.3
   578.8
   577.8
   572.9
   561.5
15 - 551.6
   537.7
   537.0
   530.8
   530.0
20 - 528.6
   526.0
   521.6
   520.0
   516.2
25 - 514.0
   509.0
   505.2
   504.2
   502.8
30 - 487.5
   482.0
   477.0
   477.0
   473.0
35 - 471.5
   467.8
   461.0
   456.9
   455.5

Dockum

40 4520
   443.0
   433.3
   419.8

51   872.9
56 1096.5
57 1176.0
56 1453.0
55 1516.0
54 1547.8
53 1613.0
52 1677.9
51 1726.1

Permian

Q

F.Q = 15·85

silt

litharenite

arkose

calclithite

fine and v.
medium &

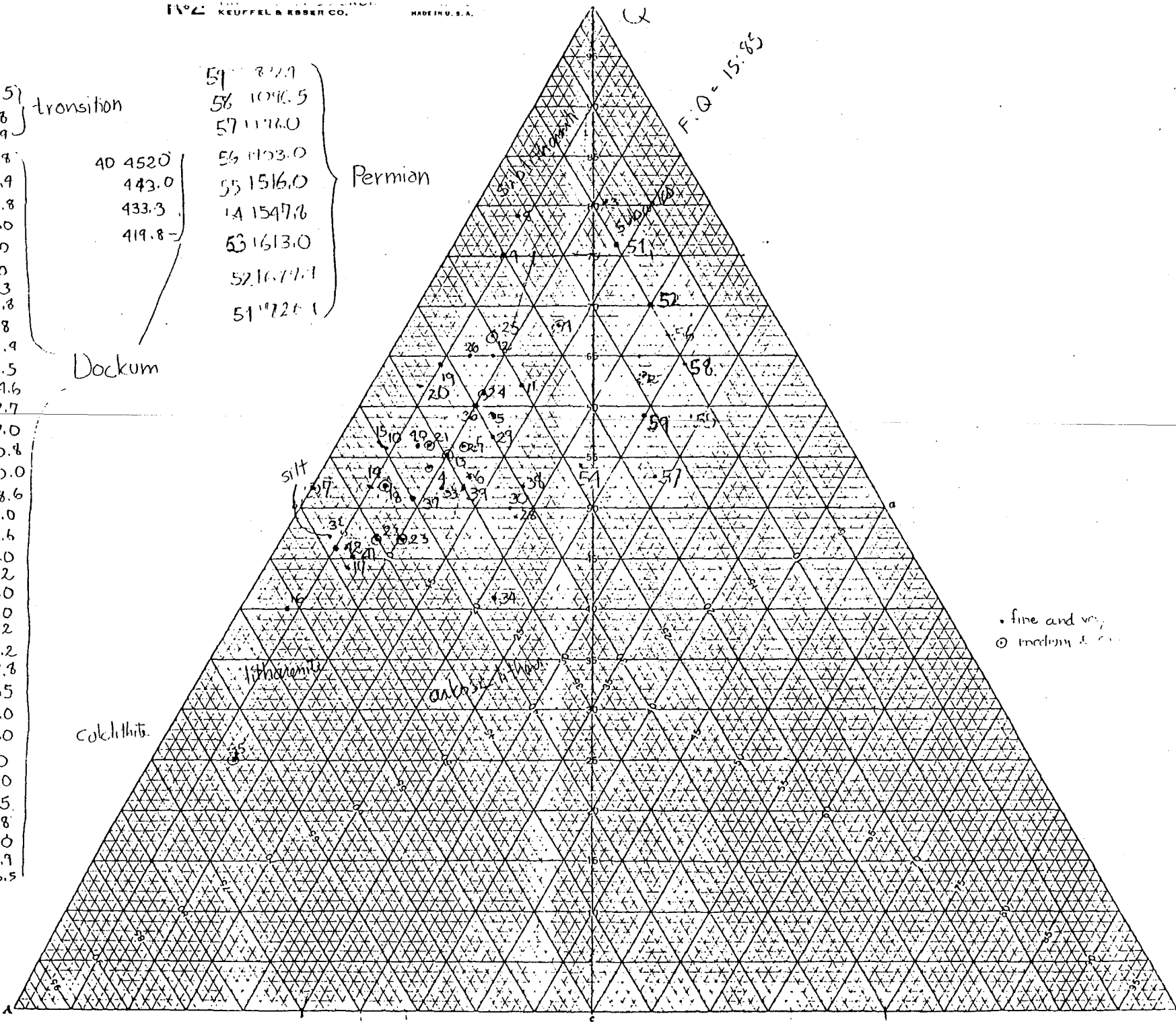R   F

Figure 62. Ternary plot (Quartz, Feldspar, Rock Fragments) of Dockum and Permian samples
from DOE/Gruy Federal #1 Grabbe well.